Implantable Neural Interfaces for Direct Control of Hand Prostheses

by

Alex Kikeri Vaskov

A dissertation submitted in partial fulfillment
of the requirements for the degree of
Doctor of Philosophy
(Robotics)
in the University of Michigan
2021

Doctoral Committee:

Associate Professor Cynthia A. Chestek, Co-Chair
Professor R. Brent Gillespie, Co-Chair
Associate Professor Robert D. Gregg, IV
Assistant Professor Elliot J. Rouse

Alex K. Vaskov

akvaskov@umich.edu

ORCID iD: 0000-0002-2336-9877

Dedication

I am dedicating this thesis to my cat, Delonte, who succumbed to cancer February 1st, 2021. He has been an integral part of my life over the past decade and his presence will be missed.

Acknowledgements

First and foremost, I would like to thank my immediate family for shaping into the person I am today. My wife, Nicole, who moved to Ann Arbor during my P.h.D. and made this town my home. I could not imagine accomplishing what I have without her support and that of my twin brother, Sean who has been with me my entire life. I would also like to thank my parents, Steve and Vinita, for raising me with love, and my younger brother, Ryan. You all constantly inspire me to pursue my passions and never doubt my dreams. There is a long list of extended family and friends I owe this to as well, but that list would take up a few pages. So, while I did not name everyone, know that I was thinking of you when I wrote this.

I would like to extend a particular thanks to my academic advisor Cindy Chestek. I will be forever grateful for this life-changing opportunity. I still vividly remember my first interview for grad school! Your mentorship over the years has been invaluable. While I cannot hope to retain all the advice, I hope that I will keep enough and pay it forward to the next generation of engineers, researchers, and scientists. I would also like to thank my co-advisor, Brent Gillespie, who always pushed me to think deeper. Finally, my other committee members, Elliott Rouse and Robert Gregg. Given the interdisciplinary nature of our work, your perspective has helped me approach problems in a unique and thoughtful way.

I would not have been able to reach this point without our many collaborators and colleagues. In particular, Alicia Davis and Deanna Gates, working with you has helped me connect and focus my research in a manner that will truly benefit people. Alicia, I also welcome

all the business and life mentorship. I would also like to thank Paul Cederna and his medical team. You all are just a passionate group that motivates me to do by best.

Lastly, I would like to thank all the members in Cindy and Deanna's labs. Philip Vu, who never made any of these years feel like work – even when we desperately needed to grind out a demo. Sam Nason and Paras Patel for literally always being willing to lend a hand or advice. Christina Lee and Michael Gonzalez for being the opposite of the horror stories I heard about shared labs and collaborations. Finally, for all the lab members I did not name, I am grateful for everything I have learned from you. I cannot wait to see what the future holds for all of us.

Table of Contents

List of Tables

s

List of Figures

Abstract

State-of-the art robotic hands can mimic many functions of the human hand. These devices are capable of actuating individual finger and multi-joint movements while providing adequate gripping force for daily activities. However, for patients with spinal cord injuries or amputations, there are few options to control these functions seamlessly or intuitively. A common barrier to restoring hand function to both populations is a lack of high-fidelity control signals. Non-invasive electrophysiological techniques record global summations of activity and lack the spatial or temporal resolution to extract or "decode" precise movement commands. The ability to decode finger movements from the motor system would allow patients to directly control hand functions and provide intuitive and scalable prosthetic solutions. This thesis investigates the capabilities of implantable devices to provide finger-specific commands for prosthetic hands. We adapt existing reasoning algorithms to two different sensing technologies.

The first is intracortical electrode arrays implanted into primary motor cortex of two non-human primates. Both subjects controlled a virtual hand with a regression algorithm that decoded brain activity into finger kinematics. Performance was evaluated with single degree of freedom target matching tasks. Bit rate is a throughput metric that accounts for task difficulty and movement precision. A state-of-the-art re-calibration approach improved throughputs by an average of 33.1%. Notably, decoding performance was not dependent on subjects moving their intact hands. In future research, this approach can improve grasp precision for patients with spinal cord injuries.

The second sensing technology is intramuscular electrodes implanted into residual muscles and Regenerative Peripheral Nerve Interfaces of two patients with transradial amputations. Both

participants used a high-speed pattern recognition system to switch between 10 individual finger and wrist postures in a virtual environment with an average completion rate of 96.3% and a movement delay of 0.26 seconds. When the set was reduced to five grasp postures, average metrics improved to 100% completion and a 0.14 second delay. These results are a significant improvement over previous studies which report average completion rates ranging from 53.9% to 86.9% and delays of 0.45 to 0.86 seconds. Furthermore, grasp performance remained reliable across arm positions and both participants used this controller to complete a functional assessment with robotic prostheses.

For a more dexterous solution, we combined the high-speed pattern recognition system with a regression algorithm that enabled simultaneous position control of both the index finger and middle-ring-small finger group. Both patients used this system to complete a virtual two degree of freedom target matching task with throughputs of 1.79 and 1.15 bits per second each. The controllers in this study used only four and five differentiated inputs, which can likely be processed with portable or implantable hardware.

These results demonstrate that implantable sensors can provide patients with fluid and precise control of hand prostheses. However, clinically translatable implantable electronics need to be developed to realize the potential of these sensing and reasoning approaches. Further advancement of this technology will likely increase the utility and demand of robotic prostheses.

Chapter 1 Introduction

The loss of hand function is a devastating injury that severely impacts a person's ability to interact with the world around them. Hands remain our primary mechanisms for tool use and are important components of social interaction. Advances in robotics have yielded electronic prostheses which can mimic anywhere from 5 to 30 degrees of freedom (DOF) of the human hand and provide adequate gripping force for functional tasks (Akhtar et al., 2016; Atzori & Müller, 2015; Resnik et al., 2014). For patients with spinal cord injuries (SCI) that have lost hand function, there are few existing options to control these devices since one must interface directly with the brain. A lack of prosthetic solutions means that patients cannot independently perform many activities of daily living. For patients with amputations, the peripheral nervous system remains intact up until the point of injury. The clinical standard is for patients to use muscle activity to control their devices with surface electromyography (EMG). Standard dual-site control schemes are cumbersome and unintuitive, requiring a substituted pair of easily accessible agonist-antagonist muscles to trigger switches between hand and wrist movements and modulate single degrees of freedom (DOF). For some patients, state of the art pattern recognition systems have eliminated the need for triggers or movement substitutions and targeted muscle re-innervation (TMR) surgery can expand these benefits to more proximal cases (Kuiken et al., 2009, 2016). However, a limited number of movements can be activated (Cheesborough et al., 2015) and a failure to meet functional expectations remains a common reason for prostheses abandonment (Østlie et al., 2012).

A common barrier to restoring hand function in both populations is a lack of high-fidelity control signals. The ability to extract or “decode” finger movements from the motor system would

allow patients to directly control hand functions and provide intuitive and scalable prosthetic solutions. Patients across both populations have a favorable view of surgical interventions that can restore hand function (Blabe et al., 2015; Engdahl et al., 2015; Lahr et al., 2015). This thesis will investigate the capabilities of implantable devices to provide finger-specific commands for prosthetic hands. We will adapt existing reasoning algorithms to two different sensing technologies: an intracortical electrode array applicable to SCI, and intramuscular electrodes implanted into residual muscles and Regenerative Peripheral Nerve Interfaces (RPNIs). In the latter, we will show that two patients can use this system to control existing robotic hands.

1.1 Sensing

1.1.1 Intracortical Recording

For patients suffering neurodegenerative diseases or severe SCI, the peripheral nervous system can be an unusable or poor source of control signals. The brain is the origin of movement commands for arm and hand control, and its somatotopy is understood well enough to target these functions. Electroencephalography (EEG) records electrical brain activity from the surface of the scalp. However, the activity of a single neuron is too small to be picked up remotely through the skull so EEG reflects a summation of thousands or millions of pyramidal neurons (Nunez & Srinivasan, 2006). The low conductivity of bone and exponential decrease of voltage gradients with recorder distance reduce specificity and lower signal to noise ratios (Nunez, 1988). These properties make EEG ill-suited for prosthetic control applications, which require algorithms to confidently decode movement intentions in real-time. Over the past two decades, BMI researchers have capitalized on the availability and development of surgically invasive techniques for neuroprosthetic control.

For motor control applications, intracortical electrodes have yielded the best performance in both non-human primate (NHP) and clinical studies (Collinger et al., 2013; Gilja et al., 2012; Shanechi et al., 2017). The Utah Electrode Array (Blackrock Microsystems) is clinically available in multiple configurations with electrode shanks that penetrate the surface of the brain and allow for simultaneous recording. When implanted into motor cortex, individual shanks capture single or multiple neuron activity tuned to movement kinematics and dynamics (Kennedy & Schwartz, 2019; Perel et al., 2013). Neural firing rates can be estimated by manually identifying individual wave-forms (Todorova et al., 2014), aggregating threshold crossings per channel (Christie et al., 2015; Fraser et al., 2009), or measuring power in specific frequency bands (Irwin et al., 2016; Nason et al., 2020; Stark & Abeles, 2007). Biological responses such as tissue scarring or cell death can reduce signal quality so the longevity of penetrating electrodes is under consideration (Chestek et al., 2011; Simeral et al., 2011; Suner et al., 2005). Novel electrode designs to mitigate these issues are an active area of research (Guido et al., 2020; Patel et al., 2016; Welle et al., 2020). Flexible electrode grids record Electrocorticography (ECoG) from the surface of the brain and alleviate concerns related to tissue scarring. However, less invasive recording techniques inherently lack temporal resolution. For example, gamma power bands from ECoG contain enough information to infer the occurrence of individual finger movements, but may not capture velocity changes in real time (Chestek et al., 2013; Volkova et al., 2019).

1.1.2 Peripheral Nerve Interfaces

For persons with amputations, peripheral motor activity can be monitored via surface EMG and used to command prostheses. However, this places limits on the functionality that myoelectric devices can provide. Intuitive grasp and fine motor control is of high interest to prostheses users (Engdahl et al., 2015), but is difficult to achieve with surface EMG since muscles responsible for

thumb and finger movements are either lost due to the level of amputation or obscured by more superficial muscles. TMR is a clinically practiced surgical innovation that creates motor control sites for lost muscles. TMR surgery transplants severed nerves to deinnervated muscles. The target muscles are superficial and signals can be recorded with surface electrodes (Zhou et al., 2007). These restored motor signals can be used to control lost elbow, wrist, and hand functions (Kuiken et al., 2009). Patients with TMR have been able to simultaneously control elbow flexion-extension and hand open-close to make coordinated multi-joint movements (Young et al., 2014). However, simultaneous control of individual fingers is difficult due to limitations on signal independence (Farina et al., 2017).

To acquire movement specific signals from surface EMG, researchers are using high density electrode grids and software techniques to decompose global activity into specific neural drives (Farina et al., 2017). Alternatively, individual muscles can be directly monitored with implantable electrodes (Birdwell et al., 2015). Muscle tissue provides a durable implant site and clinical studies have recorded stable EMG for months and years (Dewald et al., 2019; Salminger et al., 2019; Vu et al., 2020). Intramuscular EMG is often pre-processed for input into control algorithms by band-pass filtering, rectification, and integration. Bandwidths and processing windows vary across studies, but are similar to parameters used to isolate nearby muscle activity in surface EMG (Davis et al., 2016; Dewald et al., 2019; Vu et al., 2020). In a bipolar configuration, the mean absolute value of each filtered channel reflects a localized summation of motor unit activity specific to the implanted muscle. However, in the absence of other surgical interventions, intramuscular recording is entirely dependent on the muscles a patient retains after amputation.

In cases where intact muscles are lost due to the level of amputation, we have demonstrated Regenerative Peripheral Nerve Interfaces (RPNIs) can be paired with indwelling electrodes to

provide a stable neuromuscular interface. RPNIs are created by suturing autologous muscle grafts to the ends of severed nerves. The nerve reinnervates the muscle, which prevents the formation of neuroma and "bio-amplifies" efferent nerve signals into EMG (Frost et al., 2018; Santosa et al., 2020). RPNIs can be created at the time of amputation or retroactively. Furthermore, nerves can be dissected during the surgery to create multiple RPNIs per nerve. Under ultrasound, we've shown this dissection creates individual RPNIs that contract for specific finger movements (Vu et al., 2020). Recording surface EMG from RPNIs has proven difficult. However, the nature of RPNI surgery makes specific signals from nerve branches easily accessible to implantable devices, compared to TMR which transplants a whole nerve to a deinnervated muscle. Due to the flexibility of the surgery and resolution of control signals, RPNI is a promising technique to deliver high fidelity grasp control to a broad range of people with amputations.

1.2 Reasoning

1.2.1 Regression Algorithms

As described earlier, many patients have positive attitudes towards implantable devices if they provide high levels of performance (Blabe et al., 2015; Lahr et al., 2015). BMI can achieve dexterous reach and grasp performance with regression algorithms that model the intended position or velocity of individual DOF as continuous variables that are simultaneously predicted (Collinger et al., 2013; Gilja et al., 2012; Wu et al., 2004). The Kalman filter (KF) was first applied to BMI in 2004 to recursively estimate kinematic states at each time-step by modeling channel activity as a linear combination of kinematics (Wu et al., 2004). Velocity estimates are typically output to the prostheses regardless of whether or not neural activity is assumed to be tuned to position (Gilja et al., 2012; Vaskov et al., 2018), and is suspected to produce a simple physical

system for real-time control in the presence of noisy inputs (Marathe & Taylor, 2011; Zhang & Chase, 2015). Some neurons in motor cortex may be highly specific to individual movements (Aggarwal et al., 2008), although observing enough broadly tuned channels is often sufficient (Wodlinger et al., 2015). Following its use in BMI, the same algorithms have been applied to dexterously control multi-DOF hands using intramuscular EMG as an input. Patients have used this framework to simultaneously control three to six wrist and hand DOF using research hands or virtual reality environments (George et al., 2018; Vu et al., 2020).

In a clinical setting, BMI are calibrated similar to commercial pattern recognition systems. The patient mimics a computer animation or robotic hand to capture neural activity reflective of an intended movement. However, brain activity can change between observed, imagined, and attempted movements (Rastogi et al., 2020). Patients that lack peripheral motor abilities may have a difficult time consciously distinguishing between these brain states or precisely following movement cues in part due to broken feedback links. This can severely limit the quality of training data for fine finger and grasping movements (George et al., 2020). In able-bodied animal studies, finger kinematics can be directly measured to estimate decoding parameters. However, rich calibration data does not guarantee good decoding performance. Electrode arrays under-sample neurons in the motor cortex and some recorded units may not be tuned to the controlled movements. Adaptive calibration techniques can improve performance by reducing the effects of motor system noise during parameter estimation or rejecting interfering circuits (Fan et al., 2014; Shenoy & Carmena, 2014). They can also ease adoption by placing the learning burden on the algorithm, instead of relying solely on the patient to adjust their behavior (Dangi et al., 2013). State of the art techniques use supervised re-calibration sessions where online kinematic data is cleaned by adjusting the velocity vector to assume the user always intends to move towards a target

(Collinger et al., 2013; Gilja et al., 2012; Shanechi et al., 2017). These techniques have been shown to effectively double performance of BMI that decode arm reaches, however the extent to which they can improve grasp precision has not been investigated.

1.2.2 Real-Time Pattern Recognition

Pattern recognition allow persons with amputations to control their devices with intended movement commands and can reduce fatigue and mental effort compared to dual-site controllers (Deeny et al., 2014; Wurth & Hargrove, 2014). These systems use classifiers that detect movement states in real-time. Reducing the movement prediction problem to discrete states can be particularly useful in systems with fewer input channels (Li et al., 2010). For most patients, classifiers are capable of distinguishing wrist movements and a single DOF open-close hand signal from surface EMG. Commercial and research systems are beginning to offer grasp selection capabilities with multi-articulating robotic hands (Kanitz et al., 2018; Krasoulis et al., 2020; Kuiken et al., 2016). However performance may degrade across different physical contexts such as limb position changes (Betthauser et al., 2018). More robust classifiers, the addition of inertial measurements, enhanced calibration methods, or intramuscular recording electrodes have all been proposed to improve reliability (Betthauser et al., 2018; Krasoulis et al., 2020; Teh & Hargrove, 2020; Weir et al., 2009). Pattern recognition systems may also distinguish more hand movements when combined with surgical interventions. TMR re-routes the nerves that control hand movements to multiple control sites that can be read by surface electrodes. In similar virtual experiments, a multi-grasp pattern recognition system was more accurate in patients with proximal amputations and TMR than in transradial patients who retained extrinsic hand muscles (Kuiken et al., 2009; Li et al., 2010). Accessing finger specific signals with intramuscular electrodes can also increase the capabilities of pattern recognition algorithms. The previous studies with surface EMG

or other external sensors accurately distinguished anywhere between two and four grasp patterns. In one study, able-bodied subjects with intramuscular electrodes achieved accurate control of six grasps in a virtual environment (Birdwell et al., 2015).

In BMI, classifiers have used to detect multiple grasps for FES control (Colachis et al., 2018). In other implementations, classifiers have been used to improve the performance of continuous controllers by initiating stop or click states for virtual cursors (Kao et al., 2017; Pandarinath et al., 2017) or allowing controllers switch between regression models specifically tuned to different movements (Sachs et al., 2015; Wu et al., 2004; Yu et al., 2007). The Hidden Markov Model (HMM) is commonly applied to model transitions between movement states (Kemere et al., 2008). This framework allows a classifier to operate on rapid timescales without sacrificing stability. This is important because integration delays reduce controller responsiveness and decrease the user's ability to make fine adjustments. The HMM can also model the progression of several latent states per movement (Kemere et al., 2008). When paired with high resolution inputs, the HMM can capture activation patterns throughout grasp phases, whereas single-state classifiers require users to match a specific contraction for each movement.

1.3 Summary of Thesis

This thesis investigates the ability of implantable sensors to provide high fidelity grasp control for neuroprostheses.

Chapter 2 investigates the use of state-of-the-art BMI control algorithms for dexterous grasp control. Two primates were trained to move their index finger independently from their middle-ring-small (MRS) finger group. Utah electrode arrays were implanted into primary motor cortex and we were able to distinguish figer movements from neural activity. Precise single DOF

control of each finger group was achieved in a virtual environment using a ReFIT Kalman filter (Gilja et al., 2012). These results demonstrate that adaptive calibration techniques, previously used for endpoint control alone, can improve grasp precision.

In Chapter 3 we briefly show that Regenerative Peripheral Nerve Interfaces (RPNIs) can be used as motor control sites in patients with amputations. Two patients with transradial amputations had electrodes surgically implanted into RPNIs and residual muscles. We implemented a pattern recognition algorithm that allowed each patient to control a virtual prostheses with their RPNIs.

In Chapter 4, the same two patients use a combination of implanted RPNIs and residual muscles to control virtual and physical prostheses with a high speed pattern recognition system. We adapt a Hidden Markov Model to estimate movement states with low latency and high accuracy (Kemere et al., 2008). Classification performance remained robust to changes in arm position and both participants completed a functional assessment with robotic prostheses. These results indicate that indwelling electrodes provide stable input signals for accurate and reliable grasp control.

In Chapter 5, we build on the results of Chapter 4 to show that the same pattern recognition framework can be combined with a linear Kalman filter to provide simultaneous position control of a two-DOF grasp. These results demonstrate that an implantable device could use peripheral nerve interfaces to provide dexterous hand control of myoelectric prostheses.

Lastly, Chapter 6 will discuss the results of each study and future research directions while considering the clinical translation of implantable technologies.

Chapter 2 Decoding Individual Finger Movements from Intracortical Electrode Arrays

A version of this chapter "Cortical Decoding of Individual Finger Group Motions Using ReFIT Kalman Filter" was published in Frontiers in Neuroscience in 2018 (Vaskov et al., 2018).

2.1 Introduction

Recent clinical trials have demonstrated the use of neural prostheses to restore motor activity in individuals with severe paralysis (Willett et al., 2017; Wodlinger et al., 2015). Brain machine interfaces (BMIs) provide intuitive control signals that are particularly useful for focused upper-limb movements such as reaching tasks and tool use. These signals can last for years (Collinger et al., 2013; Gilja et al., 2012; Hochberg et al., 2012; Simeral et al., 2011) enabling, at minimum, long term feasibility studies. They are a natural choice for improving the control of functional electrical stimulation (FES) systems, which apply small electric pulses to muscles to produce movement. Indeed, restoring natural movement of the arm is more desirable to people with cervical level SCI than controlling a robotic prosthesis (Blabe et al., 2015). With existing FES systems, certain patients with spinal cord injuries can regain partial use of their paretic hands controlled via residual muscle signals (Kilgore et al., 2008). More recently, this has been demonstrated using BMIs, restoring a small number of functional movements during activities of daily living (Ajiboye et al., 2017; Bouton et al., 2016). These work demonstrate the immense progress that has been made in the field. However, performance limitations still persist, including the inability to activate joints simultaneously or command complex grasps.

Early studies demonstrated neural decoders, which translate neural signals from the motor cortex into motion commands, successfully gave NHPs online control of a robotic arm capable of whole arm movements and a basic grasp (Carmena et al., 2003; Lebedev, 2005; Serruya et al., 2003; Taylor et al., 2002; Velliste et al., 2008). While these studies represented major advances, they involved relatively rudimentary movements. Since these work, advances in experimental setups, implantation hardware and techniques, signal processing and control algorithm development have positioned the community to investigate whether decoders can account for more complex multi-joint movements. More recent clinical studies have demonstrated online control of a robotic prostheses in human patients with tetraplegia (Hochberg et al., 2012), with increasing degrees of freedom (DOF) (Collinger et al., 2013), and the ability to activate different grasp patterns (Wodlinger et al., 2015). The selection of multiple grasps has also been demonstrated in recent FES systems (Colachis et al., 2018). Although these studies are impressive demonstrations in a practical setting, grasps were limited to a simple open-close, a few gross motions, or discrete selections. In general, precision typically decreases as subjects are given control of more DOF. Neural prostheses will ultimately need to provide more dexterous hand functionality to allow users to fully interact with the world around them to gain broad acceptance. Newer upper-limb decoders continue to promise increased levels of performance and reliability (Shanechi et al., 2017; Sussillo et al., 2016). However, their application has been limited to decoding arm reaches and have yet to demonstrate improvements in grasp performance. Some studies have proposed using semi-autonomous control of a robotic arm to achieve more complex grasps (Downey et al., 2016; Hotson et al., 2016). While this may be a well-received solution for some users, it hands off a majority of fine motor control to an autonomous system, thereby limiting grasping capabilities to what the chosen algorithm can learn and execute. Here we will focus on direct control strategies, specifically

the challenge of decoding control signals for precise hand motions for eventual use in an FES system.

The human upper-limb is a high dimensional system: arm and wrist joints provide 7 DOF while the hand is a complex 23 DOF end-effector. Previous NHP studies have shown neural signals can be used to reconstruct 18 (Aggarwal et al., 2013), 25 (Vargas-Irwin et al., 2010), and even 27 (Menz et al., 2015) DOF offline during reach and grasp movements. However, these studies only demonstrate that DOF of the hand are well correlated with primary motor cortex (M1) activity during highly coordinated grasping movements. They do not demonstrate that motion in these DOF can be approximated or controlled individually. Principal component analysis or other forms of dimensionality reduction can be used to characterize the majority of hand motions in fewer well-separated DOF which have been shown to dramatically improve the performance of discrete offline classifiers (Schaffelhofer et al., 2015). Even though it is unclear if the principal dimensions are actually represented in the motor cortex (Mollazadeh et al., 2014), using them for decoding can theoretically provide more precise control over a large amount of hand configurations (Rouse & Schieber, 2015). Recent algorithms have successfully given NHPs the ability to actively select and continuously modulate 4 principal movement dimensions of a virtual hand (Rouse, 2016). Although such techniques have proven to be a promising and efficient way to process information, control is achieved through long periods of reward-based training and is not a reproduction of biomimetic motions. Furthermore, studies have yet to demonstrate precise control along these dimensions.

The body of previous work has successfully demonstrated that information relating to fine motions is well represented in M1. This begs the question if it is possible to use BMIs to control continuous motion at the level of individual fingers. Earlier NHP studies have established that M1

may contain enough information to distinguish between individual finger movements (Aggarwal et al., 2008; Hamed et al., 2007). In our previous NHP work, we characterized the flex-extend motion of all four fingers together as a single DOF, and used signals from M1 to provide subjects with online continuous control of a virtual hand (Irwin et al., 2017). Here we have developed a novel manipulandum to track and control movement of two separate finger groups. Furthermore, we seek to improve decoder performance with the use of the ReFIT (Recalibrated Feedback Intention-Trained) Kalman filter which has proven successful in reach tasks (Gilja et al., 2012). We use the manipulandum in combination with the ReFIT Kalman filter to provide our NHP subjects with continuous control of each finger group in a separate fashion. To our knowledge, this is the first systematic and biomimetic separation of digits for continuous online decoding in a NHP as well as the first demonstration of the ReFIT Kalman filter improving the performance of precise finger decoding.

2.2 Materials and Methods

2.2.1 Novel Manipulandum

All experimental tasks were performed in compliance with NIH guidelines as well as the University of Michigan's Institutional Animal Care & Use Committee and Unit for Laboratory Animal Medicine. We trained two male rhesus macaques, Monkey W and Monkey N, to use a novel manipulandum, designed to isolate finger movements (Figure 2.1B), in order to match fingertip position targets in the same virtual environment described in previous work (Irwin et al., 2017). The manipulandum consists of two "doors" with dividers to isolate index finger movements from MRP movements. The doors can be locked separately or together in different positions to

create a wide range of movement conditions. Here we used three configurations, each resulting in 1 DOF control:

- Index: MRP door locked to full extension, index finger allowed to move
- MRP: index door locked to full extension, MRP fingers allowed to move
- All: index and MRP doors are locked together to encourage simultaneous movement of all fingers

Switching between configurations can be done in a short period of time, allowing us to alternate between finger groups in a single session. Resistive flex sensors (FS-L-0073-103-ST, Spectra Symbol, Salt Lake City, UT) were attached to each door of the manipulandum and values were read from a 10 bit analog-to-digital converter (ADC) on a custom circuit board. At the beginning of each experiment day, ADC values corresponding to full flexion and extension of the active DOF were noted. The amount of flexion at any given time was then determined by centering and scaling the current ADC value such that a position of 0 corresponded to the recorded value for full extension and 1 corresponded to the value for full flexion. Each door also contained a torsional spring which was tuned to apply as little resistance as possible during flexion, but still allowed the door to follow the subject's fingers during extension.

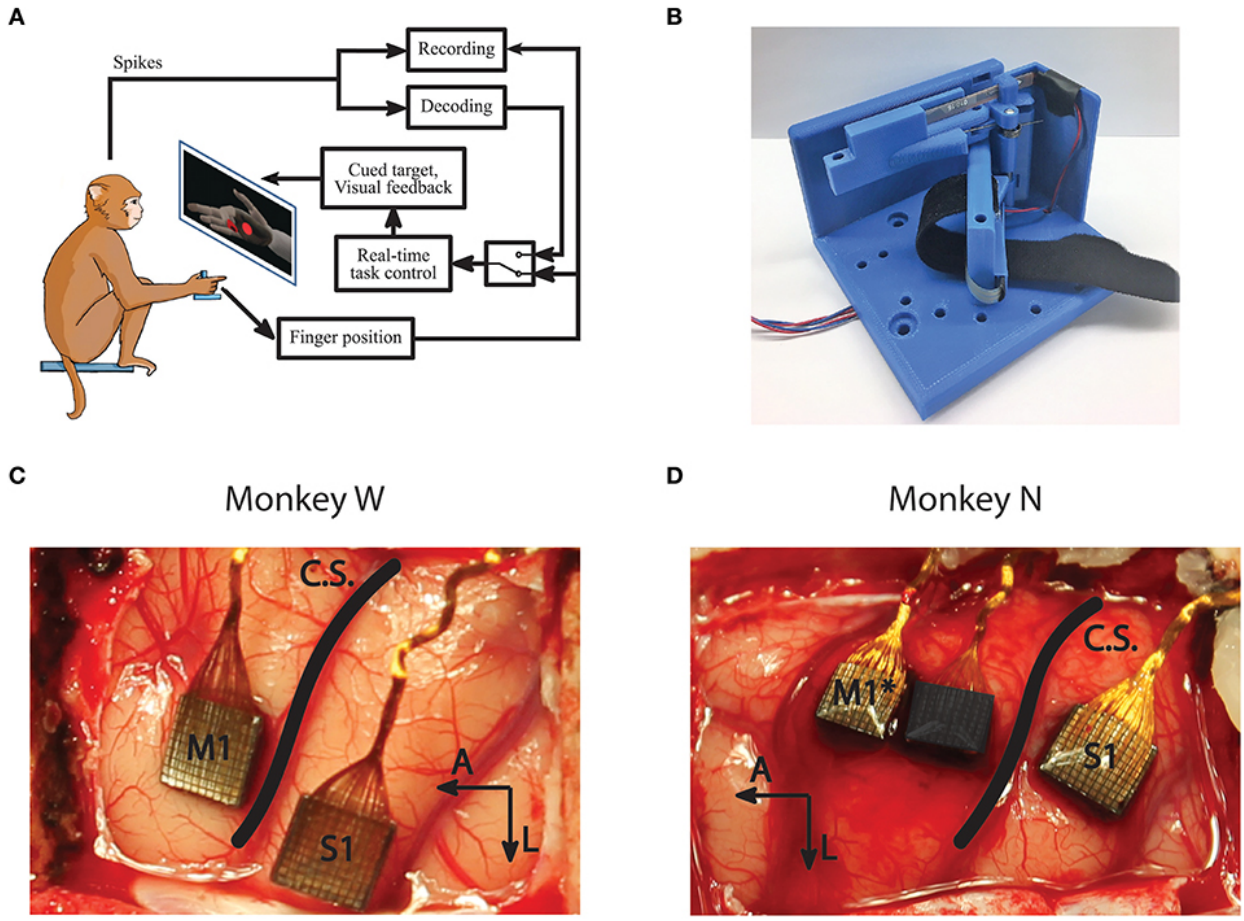

Figure 2.1 BMI Experiment setup and methods. (A) Subjects performed a target acquisition task using a virtual hand controlled either by flex sensors or neural decoder output. (B) A novel manipulandum was used to separate finger movements into three active configurations: index only; middle, ring, and pinky (MRP); or all fingers moving together. An unrestrictive stanchion (not pictured) that does not restrict finger movements was also used for sensory context experiments. (C,D) Array implants for Monkeys W and N. Only signals from the motor arrays were used in this study. *Monkey N was implanted with a split array, however 64 channels (darkened) were inactive for the study period.

2.2.2 Behavioral Task

Both subjects performed a target matching task in an electrically shielded room with their right forearm flexed 90 degrees, comfortably restrained inside of an acrylic tube. Their hand rested on a table and inserted into the manipulandum. Position data and neural data were acquired in real-time using xPC Target (Mathworks, Natick, MA, United States). The xPC received UDP packets with neural data marking threshold crossings on array channels. The specific thresholding scheme is described below in Signal Processing and Feature Selection. The real-time execution of the xPC ensured that neural and behavioral data were synchronized with millisecond precision. The

subjects viewed a virtual hand (MusculoSkeletal Modeling Software; (Davoodi et al., 2007)), with finger group animations controlled by the xPC to either measured flex sensor data or decoded finger position. The virtual hand was controlled via either the flex sensors for decoder calibration and offline analysis or the predictions from a decoding algorithm for online BMI control (Figure 2.1A). The experiments for this study only involved control of 1 DOF at any point in time. For future studies, the system is capable of animating trajectories for simultaneous control of multiple DOF.

At the start of each trial, a spherical target is placed along. the flex-extend arc and the subject must move the virtual fingertip inside and remain in the target for a given hold period. The range for a successful hold was considered to be within the visible edges of the spherical target and the required hold period varied between 500 and 750 ms depending on the subject and experiment. Successful trials were rewarded with apple juice. Figure 2.2 shows an example target sequence for each finger configuration. To encourage separation of finger movements, behavioral training was almost always done using either the index or MRP group to acquire center-out targets. Here, "center-out" means that targets appear in 1 of 7 positions along the flex-extend arc with every other target appearing at "center" (50% flexion). At the time of this study, Monkey W was an experienced BMI user, previously trained to move all four fingers together with his hand positioned in a stanchion that did not impede or restrict finger movement in any way. Monkey N was a new user who had only been trained with the manipulandum restricted to index or MRP movements. The first time Monkey N performed the task with the unrestrictive stanchion was during the sensory context experiments described later.

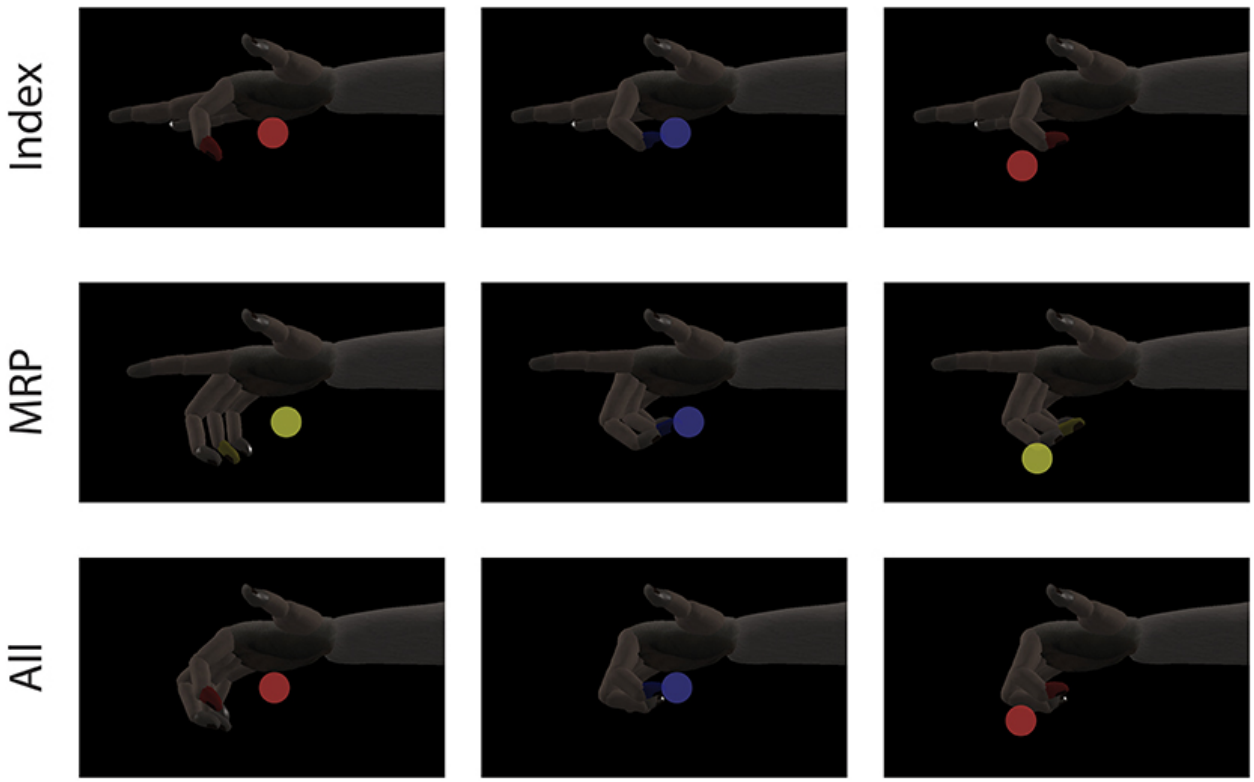

Figure 2.2 Single DOF target tasks. Each row shows a target sequence for a different finger configuration. For Index and MRP configurations, both the display and manipulandum of the inactive group were fixed to extend. A single trial consists of a target being presented (first column) and the subject moving his active finger group to the target (second column). After the subjects satisfies the required hold time or the trial times out, a new target is presented immediately to begin the next trial (third column).

2.2.3 Surgical Procedure

The surgical procedure was performed in compliance with NIH guidelines as well as the University of Michigan's Institutional Animal Care & Use Committee and Unit for Laboratory Animal Medicine. We implanted each monkey with intracortical electrode arrays targeting the hand area of left primary motor cortex (M1), as identified by surface landmarks (Figures 2.1C,D). After the craniotomy, the genu of the arcuate sulcus was identified and a line was traced posteriorly to central sulcus. Arrays were then implanted along this line just anterior to central sulcus, as allowed by vasculature. Both subjects were implanted with Utah arrays (Blackrock Microsystems, Salt Lake City, UT, United States) targeting M1 as well as the left primary sensory cortex (S1). The arrays implanted in both subjects had 1.5 mm long electrodes spaced with 400 μm pitch. Monkey W received 96-channel arrays in both M1 and S1, while Monkey N received a 96 channel

array in S1 and a 128 channel split array covering M1 with one array potentially overlapping with pre-motor cortex (PMd). Note that only the motor arrays were used for analysis and decoding in this study. Due to wiring damage, Monkey N only had 64 channels of neural input available for this study (Figure 2.1D). The active array was the one implanted on the rostral edge of the M1 area, so it is possible that units recorded from his array are located in PMd. Similar studies for arm reaches have used signals from both M1 and PMd for continuous decoding (Gilja, Nuyujukian, Chestek, Cunningham, Yu, Fan, Ryu, et al., 2012).

2.2.4 Signal Processing and Feature Selection

During experiment sessions, neural data was recorded and processed via a Cerebus neural signal processor (Blackrock Microsystems, Salt Lake City, UT, United States). Neural spikes were detected online by a threshold of –4.5 times the RMS voltage on each channel, after applying a 250 Hz high-pass filter to the broadband signal. The signals used here were the voltage difference between each channel and a common ground. Software referencing techniques such Common Average Referencing (Ludwig et al., 2009) were not used in this study but could be explored in future work to provide cleaner signals. Broadband data was sampled and recorded at 30 kHz, while the thresholded spikes were also recorded for offline analysis and sent to the xPC for real-time decoding. On each experiment day, channel selection for analysis and decoding was done simply by retaining all channels with an average firing rate >1 spike/s determined by threshold crossings during a training run. Some high-impedance (> 1 MOhm) channels repeatedly showed threshold crossings of large disturbances not reflective of neural activity. Therefore, an additional 13 channels for Monkey N and 3 for Monkey W with no visible information content were excluded regardless of whether or not they met the activity cutoff on experiment days. The cutoff threshold was chosen empirically by visually comparing waveforms to impedances. Although daily

impedance measurements were taken, the excluded channel list was determined at the start of the study and not updated. While electrode impedances may vary in-vivo, the excluded channels almost always remained above the 1 MOhm threshold, ranging from 19.03 to 23.16 MOhm for Monkey W and 0.98 − 23.19 MOhm for Monkey N.

For offline analysis and online decoding, we compared the summed threshold crossings in 50 ms time bins to the averaged kinematic data recorded from the flex sensor. Previous work demonstrated processing bin widths in the 50 − 100 ms range produces an accurate decoder that is sufficiently responsive for online control (Kim et al., 2008). We selected a 50 ms bin width empirically in both subjects while they were being familiarized with BMI control, using a standard Kalman filter. In both subjects, we first tested a 100 ms bin width and observed online performance as we decreased the bin width. Anecdotally, we found that 50 ms produced a more responsive online decoder without a noticeable trade-off in stability and smaller widths performed inconsistently. For offline analysis and parameter estimation, the raw 1 kHz flex sensor data was passed through a moving average filter with a 50 ms span before being averaged into time bins. Velocity measurements were then computed by taking the difference between successive position bins and scaling according to bin width.

2.2.5 Decoding Algorithm

A linear Kalman filter was used to predict kinematics of the selected finger group during each session. For this study, we predicted the motion of a single DOF at a time. At the beginning of each experiment day, all parameters for the initial Kalman filter were estimated from a training run of approximately 300 center-out trials with a hold time of 750 ms scaled to take up 15% of the flex-extend arc. To reduce the effects of sensor noise during parameter fitting, velocities with magnitude below an empirically chosen threshold (0.2%flex/s) were set to 0.

$$X_t = [pos\ vel\ 1]^T \text{ (1)}$$

$$Y_t = [y_1\ y_2 \dots y_n]^T \text{ (2)}$$

Equation 1 details the state vector for the Kalman filter. It describes the estimated kinematics of the active DOF and contains an additional offset term to account for baseline firing rate of each of the *n* active channels shown in Equation 2.

$$X_t = AX_{t-1} + w \text{ (3)}$$

$$A = \begin{bmatrix} 1 & dt & 0 \\ 0 & a_{v,v} & 0 \\ 0 & 0 & 1 \end{bmatrix} and\ W = \begin{bmatrix} 0 & 0 & 0 \\ 0 & \sigma_v^2 & 0 \\ 0 & 0 & 0 \end{bmatrix} \text{ (4)}$$

Equation 3 is the physical model of a linear Kalman filter. The evolution of the kinematic states over time is modelled by the *A* matrix and estimation errors are assumed to have gaussian noise, *w*. Equation 4 describes our implementation. The active finger group's position is explained perfectly by velocity integration, which matches the decoder output to the virtual environment. Velocity estimates are assumed to be contaminated by zero mean Gaussian noise with the covariance matrix, *W*. The velocity damping coefficient $a_{v,v}$ and variance σ^2_v were determined each day via maximum likelihood estimation using measured hand kinematics from the training run. On average, the estimation yielded $a_{v,v} = 0.855 \pm 0.01$ for index sessions and $a_{v,v} = 0.869 \pm 0.04$ (mean ± s.t.d) for MRP sessions. Here dt is equal to the 50 ms bin width selected for use.

$$Y_{t-lag} = CX_t + q \quad \text{(5)}$$

$$C = \begin{bmatrix} c_{1,p} & c_{1,v} & c_{1,o} \\ c_{2,p} & c_{2,v} & c_{2,o} \\ \vdots & \vdots & \vdots \\ c_{n,p} & c_{n,v} & c_{n,o} \end{bmatrix} \quad and\ Q = \begin{bmatrix} \sigma_1^2 & \dots & \sigma_{1,n}^2 \\ \vdots & \ddots & \vdots \\ \sigma_{1,n}^2 & \dots & \sigma_n^2 \end{bmatrix} \quad \text{(6)}$$

Equation 5 is the measurement model for a linear Kalman filter. It assumes the firing rate of each active channel is a linear combination of each of the kinematic state variables. Equation 6 describes our implementation, where $c_{i,p}$, $c_{i,v}$, and $c_{i,o}$, are the respective coefficients for finger

position, velocity, and a baseline firing rate for channel i. The additive noise q is drawn from a multivariate gaussian distribution with covariance matrix Q. Parameters for C and Q were chosen daily via maximum likelihood estimation. Similar to previous work (Irwin et al., 2017), an optimal time lag parameter (0, 1, 2, or 3 bins) was also chosen from the same training dataset (Figure 2.3A). The time lag is an offset to temporally align bins of neural data with the ideal kinematic measurement.

$$pos_{t|t} = pos_{t-1|t-1} + vel_{t|t} \times d_t \quad (7)$$

Drawing from previous work (Gilja et al., 2012), we used integrated velocity for the virtual fingertip position control signal instead of the predicted position at each time step. We assume the subject modulate their neural activity in response to both the position and velocity of the virtual fingertip. During online control, the position after each time step is set to match the controller output in preparation for the next decode, shown in Equation 7.

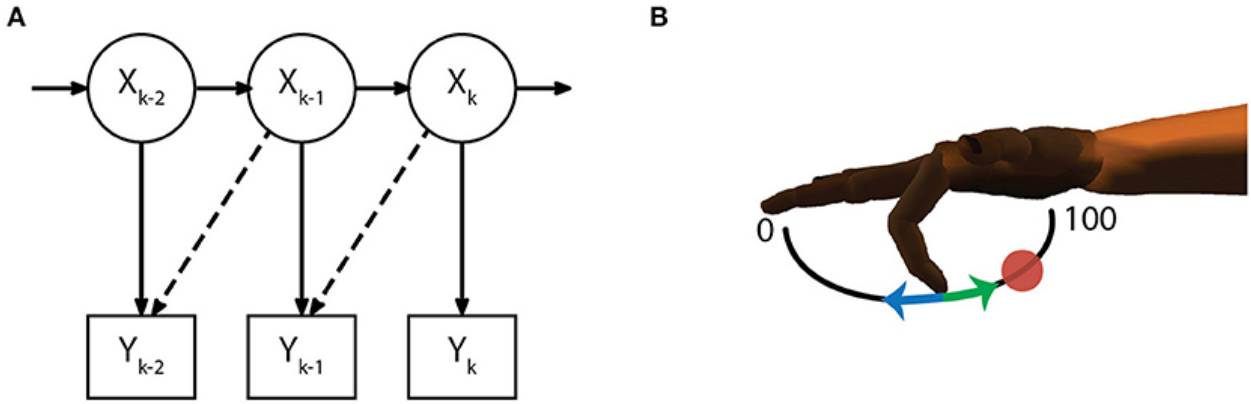

Figure 2.3 Decoding methods. (A) The initial Kalman filter estimates fingertip kinematics based on summed threshold crossings from either the current 50 ms time bin or an optimally chosen time lag (dashed lines show 50 ms lag). (B) Finger motion was characterized in 1 DOF per finger group such that a position of 0 corresponds full extension and 100 corresponds full flexion. Intention estimation was applied to the online kinematics of the initial Kalman filter by taking incorrect decoder velocities (blue arrow) and flipping them (green arrow) to point toward the desired target (red circle), on-target velocities are set to zero. Intention estimation is only applied to estimate parameters for the ReFIT decoder, no knowledge of target locations is used during online control.

2.2.6 Measurement Model Selection

Many algorithm implementations have successfully relied on models that only relate neural activity to velocity states (Collinger et al., 2013; Kim et al., 2008; Shanechi et al., 2017). However, neural activity has been observed to also vary with position changes during arm movements, possibly due to differing muscle activation required to maintain postures (Scott & Kalaska, 1997). Previous ReFIT implementations on reach tasks (Gilja et al., 2012) as well as our earlier Kalman filter implementation for finger motions (Irwin et al., 2017) used a measurement model that included both position and velocity states.

$$y_i = c_{i,p} \times pos + c_{i,o} \quad (8)$$

$$y_i = c_{i,v} \times vel + c_{i,o} \quad (9)$$

$$y_i = c_{i,p} \times pos + c_{i,v} \times vel + c_{i,o} \quad (10)$$

After implantation we performed initial testing with, three measurement models: position only, velocity only, and position + velocity. These are shown in Equations 8-10 where y_i is the expected number of threshold crossings in a 50 ms time bin for channel i. For finger motions, the position-only and velocity-only models did not provide satisfactory online control, so we opted to

continue experiments only with the position + velocity model (Equations 6,10). We conducted a post-hoc analysis to determine the amount of active channels (average firing rate > 1spike/s) that were "well tuned" to finger activity and showed decent encoding performance with the position+velocity model (cross-validated Pearson's correlation coefficient between predicted and actual firing rate of $\rho > 0.05$). We also compared the offline decoding performance of the Kalman filters used for decoding days (cross-validated ρ between predicted and actual kinematics) to examine how indicative reconstructions were of our online results.

2.2.7 ReFIT Process

The ReFIT Kalman filter was implemented at the beginning of each experiment day using the same two stage process described in previous studies (Gilja et al., 2012). After performing the task with online brain control with an initial Kalman filter for approximately 200 center-out trials, new measurement model coefficients were determined by regressing recorded neural activity against the intention-estimated online kinematics of the initial decoder (Figure 2.3B). Intention-estimation alters the training data used for parameter re-estimation by flipping the direction of the predicted velocities to always point toward the target (and setting velocities to zero when the predicted position was inside the target). This process "corrects" velocities with the assumption that the subject always intends to move the virtual hand toward the target, regardless of the direction that was predicted by the initial decoder. The online trials used for retraining were performed with the most challenging center-out targets the subject was able to acquire with the initial Kalman filter. For Monkey W, this was typically smaller targets (15.75% of the flex-extend arc) with longer hold times (750 ms), whereas Monkey N required a mixture of reduced hold times (500 ms) or larger targets (16.5% of the flex-extend arc). Note that intention estimation was only

used during the parameter re-estimation; no knowledge of the target locations was used during online control.

$$P_{t|t-1} = \begin{bmatrix} 0 & 0 & 0 \\ 0 & 1 & 0 \\ 0 & 0 & 0 \end{bmatrix} \left(AP_{t-1|t-1}A^T + W \right) \begin{bmatrix} 0 & 0 & 0 \\ 0 & 1 & 0 \\ 0 & 0 & 0 \end{bmatrix} (11)$$

Finally, during online processing for the ReFIT filter, we assumed the subjects perfectly internalize the position of the virtual fingertips and adjust their neural activity accordingly. Therefore, in Equation 11, we implement our assumption of zero a priori position uncertainty before calculating the Kalman gain.

2.2.8 Individuated Finger Analysis

Each subject performed one day of experiments to collect offline data to assess the viability of a 2 DOF decoder. On these days, the subject performed the center-out target task (1 s hold time, targets take up 16.5% of the flex-extend arc) with hand control of the index or MRP fingers in alternating blocks of approximately 200 trials for 2 sets (approximately 400 total trials per finger group). To determine whether information regarding individuated finger motions was present in M1, we attempted to distinguish between index and MRP movement onset, defined as the 100 ms surrounding the time the subject's finger(s) began to flex. Similar to earlier studies that classify individual finger movements (Aggarwal et al., 2008), we used a sliding window which updated every 20 ms with the summed threshold crossings of the last 160 ms as our neural feature. A support-vector machine with a Gaussian kernel function and L1 regularization was chosen as the classifier and tested using 10-fold cross validation.

$$X = [pos_{index} \quad pos_{mrp} \quad vel_{index} \quad vel_{mrp} \quad 1]^T (12)$$

$$A = \begin{bmatrix} 1 & 0 & d_t & 0 & 0 \\ 0 & 1 & 0 & d_t & 0 \\ 0 & 0 & a_{v,v}^{index} & 0 & 0 \\ 0 & 0 & 0 & a_{v,v}^{mrp} & 0 \\ 0 & 0 & 0 & 0 & 1 \end{bmatrix} and\ W = \begin{bmatrix} 0 & 0 & 0 & 0 & 0 \\ 0 & 0 & 0 & 0 & 0 \\ 0 & 0 & \sigma_{v\ index}^2 & 0 & 0 \\ 0 & 0 & 0 & \sigma_{v\ mrp}^2 & 0 \\ 0 & 0 & 0 & 0 & 0 \end{bmatrix} (13)$$

$$yi = c_{i,pi} \times pos_{index} + c_{i,pm} \times pos_{mrp} + c_{i,vi} \times vel_{index} + c_{i,vm} \times vel_{mrp} + c_{i,o} \ (14)$$

A 2 DOF linear Kalman filter was also trained and tested offline across all trials using the same training protocol described earlier. To discourage co-contractions in the predicted output, the physical model described in Equation 13 was constrained to keep each finger group completely independent. The measurement model shown in Equation 14 was approximated in a similar manner as the single DOF case.

2.2.9 Online Experiments

The first group of online experiments was designed to test performance across a variety of target styles and hand configurations. For these, a total of 12 experiments were conducted over 10 days for Monkey W while 8 experiments were conducted over 5 days for Monkey N (Table 2.1). On each day, subjects were given 1 DOF control over a specific group of fingers (index or MRP). After the ReFIT algorithm was fully trained using center-out targets, the subjects performed the task using online brain control and one of three target styles:

- Center-out (C-O): same as training, targets appear in one of 7 positions along the flex-extend arc with every other target occurring halfway (50% flexion)
- Random (Rand): targets appear in random positions along the flex-extend arc
- Flex-Extend (F-E): targets alternate between flexed (95% flexion) and extended (5% flexion)

The alternate target styles were chosen to test decoder controllability. The random style is not predictable and requires the decoder navigate untrained trajectories. On the other hand, the flex-extend style is entirely predictable, but exclusively contains difficult targets.

Monkey	Finger Group			Target Style		
	Index	MRP	ALL	C-O	Rand.	F-E
W	6	6	2	6	4	4
N	4	4	2	6	4	-

Table 2.1 Number of online BMI sessions performed. Sessions are grouped by either finger group or target style. Monkey W performed a total of 14 online experiments while Monkey N performed 10. Subjects performed sensory context experiments with "All" four fingers, while target acquisition sessions were performed with either "Index" and "MRP" finger groups.

No limits were placed on decoder output so predictions were capable of hyper-extending or over-flexing during online control. To maintain usable feedback during such adverse events a visual limit of −50% to 150% flexion was placed on the virtual fingertips. Otherwise, a disturbance or series of particularly poor predictions could place the virtual hand in state that the subject cannot interpret and correct. The subjects performed the novel task with both the ReFIT and initial Kalman filter in alternating blocks of approximately 50 trials for 3 sets (approximately 150 total trials per decoder). Including the full ReFIT training process and block testing, subjects completed between 826 and 1,252 trials on these experiment days, depending on whether or not multiple target styles were tested. Experiments usually lasted 2–4 h including time for rig setup and decoder calibration. Monkey W performed two sessions for each of the three target styles with a 750 ms hold time and the targets taking up 15.75% of the flex-extend arc. Monkey N performed two sessions of center-out and random target styles with a 500 ms hold time and the targets taking up 16.5% of the flex-extend arc.

2.2.10 Sensory Context

Previous work has shown that sensory signals from fingertip stimulation are well represented in motor cortex (Schroeder et al., 2017). Although the springs on each door of the manipulandum were selected to provide minimal resistance, the subjects still had the tactile sensation of their fingers pushing on the door. To make sure most of the neural information used by our decoder is primarily a product of motor activity and not a sensory reaction, which may not be a reliable input for SCI patients, subjects performed 2 daily sessions each in which the sensory cue of touching the manipulandum doors was removed. In these sessions, subjects performed these experiments with the manipulandum doors locked together (encouraged to move all fingers together). A ReFIT filter trained with the manipulandum was then used to acquire center-out targets after the manipulandum was replaced with a stanchion that did not interfere with or restrict finger movements, and therefore introduced no additional sensory feedback during movements. Including the initial training period, subjects completed a total of 905–1,063 trials during these experiment days. Performance was compared across decoders and sensory contexts using center-out targets that took up 16.5% of the flex-extend arc and a 500 ms hold time.

2.2.11 Online Performance Metrics

In an attempt to ignore initial adjustments to the decoder, the first 5 BMI trials from each trial block were excluded from performance analysis. To compare performance across experiment sessions while accounting for variations in target difficulties, we used bit rate as our primary performance metric (Thompson et al., 2014). Random trials that required minimal movement to complete (target center appearing within 10% flexion of fingertips) were excluded from this analysis. We did not attempt to draw direct comparisons between the subjects as Monkey W had more experience at the time of these experiments. Furthermore, targets with longer hold times are

considerably more difficult to acquire in BMI mode due to orbiting, a phenomena in which the controller oscillates around the desired position and is unable to stop. This increase in difficulty is not fully captured in the metric, despite the hold time itself being excluded from the calculation.

We compared the average acquisition time and average orbiting time for each decoder over all of the center-out decoding sessions. Acquisition time was defined as the time taken to complete a trial from the start to the beginning of a successful hold time. Orbiting time was defined as the time between first target contact and successful acquisition, again excluding the target hold time. Unsuccessful trials are counted as the time between first target contact and the end of the timeout period. Since these metrics can count close to the entire timeout period for unsuccessful trials, they penalize failure more heavily than bit rate. The center-out task was the most conducive for this analysis as it was performed by both subjects and consistently produced targets that were far enough apart to induce orbiting.

2.3 Results

2.3.1 Neural Tuning and Finger Separation

We first evaluated whether finger kinematics were well represented in the neural units we recorded. Excluding channels due to low firing rate, artifact activity, or low correlation with finger kinematics as described in the Methods, an average of 48 ± 9 channels from Monkey W and 10 ± 2 channels from Monkey N (mean ± s.t.d) were “well tuned" to finger activity on a given day. Offline Kalman filters from active channels across all training days yielded an average correlation coefficient between predicted and actual position of 0.807 ± 0.074 for Monkey W and 0.655 ± 0.035 for Monkey N (mean ± s.t.d). Example offline decodes are shown in Figure 2.4A. The average correlation between predicted and actual velocity was 0.618 ± 0.093 for Monkey W and

0.421 ± 0.050 for Monkey N (mean ± s.t.d). Between the two subjects, Monkey W had better offline results and was able to achieve better online performance metrics (see Online Decoding below) while performing a significantly more difficult task (longer hold times, smaller targets) than Monkey N. We suspect that higher quality neural signals, potentially due to a better array location, contributed to Monkey W's better performance. In both subjects, the encoding performance of an active channel was positively ($\rho = 0.594$ Monkey W and $\rho = 0.849$ Monkey N) and significantly correlated with its value to the offline decode (Monkey W, $p < 1 \times 10^{-9}$, $n = 92$ channels; Monkey N, $p < 1 \times 10^{-14}$, $n = 52$ channels; Student's t-test). The value of a specific channel was determined each day by comparing the initial Kalman filter's ability to predict velocity to an offline decoder without that channel (Wahnoun et al., 2006). Across days, we noticed positive but statistically insignificant correlations between offline predictive power and online bit rate, consistent with other studies which note that one is not necessarily indicative of the other (Cunningham et al., 2011; Ganguly & Carmena, 2010; Kim et al., 2008). We also did not uncover any significant correlations between either the quantity of active channels or the number of "well tuned" channels and daily online performance, so we cannot rule out subject motivation and experience as additional performance factors.

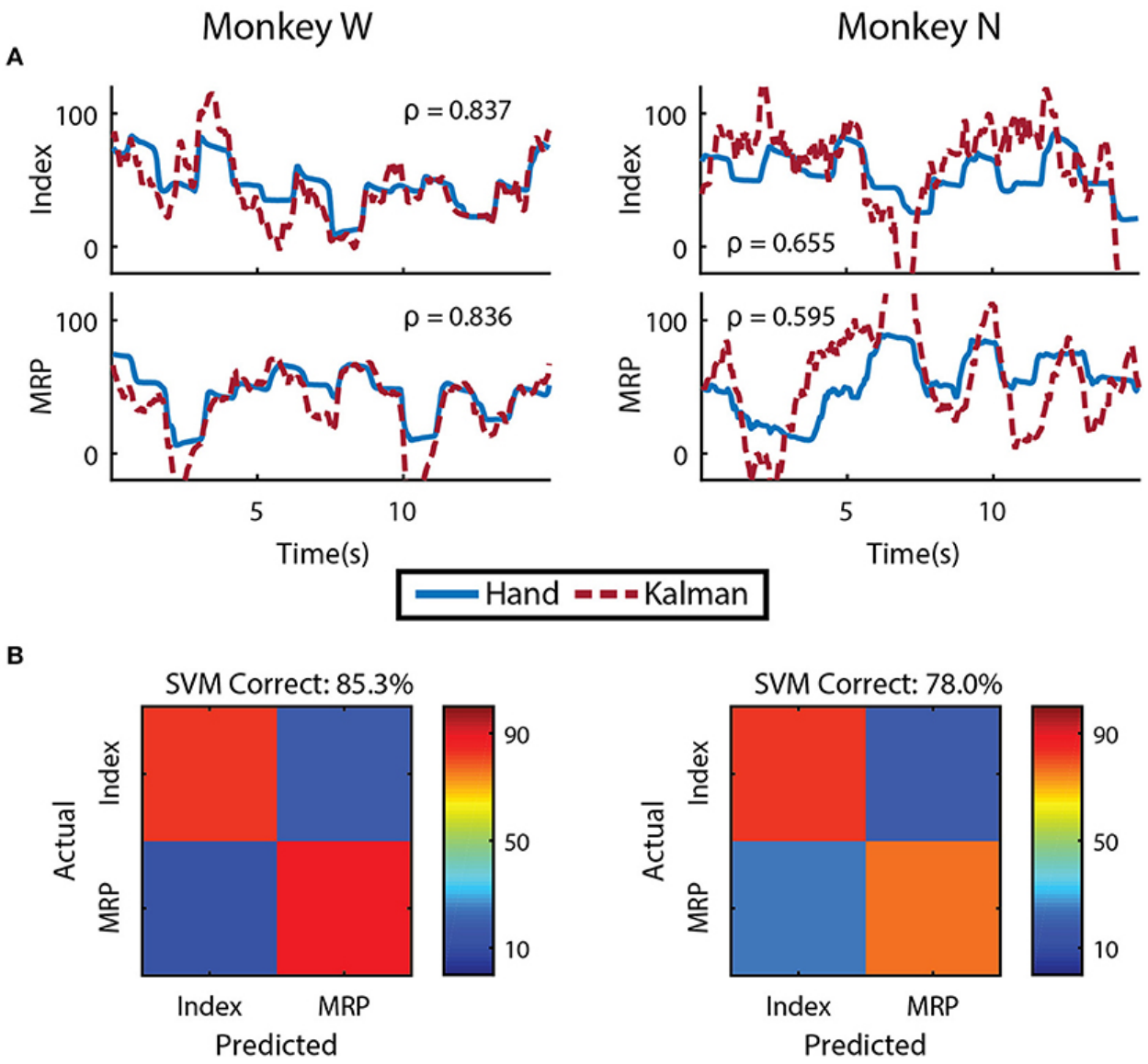

Figure 2.4 Offline decoding performance. **(A)** Single DOF reconstructions representative of average error on separate training runs for each DOF and subject. Correlations across the entirety of each training run using 5-fold cross validation are shown. **(B)** Cross validated classification of finger group during onset of flex movements using a support-vector machine. Threshold crossings were binned in a sliding window that was updated every 20 ms. The feature vector was formed from multiple time bins for all available channels.

To determine if the separate DOFs in our task are well represented in our neural units, we had each subject run an additional offline session in which they alternated between trial blocks of index and MRP target acquisition. Similar to techniques used in (Hamed et al., 2007) and (Aggarwal et al., 2008), we restricted our analysis to the onset of flex movements from the center position and used a sliding window that was updated every 20 ms to including summed threshold

crossing over the preceding 160 ms. The feature vector used for classification contained all time bins during the movement onset period for every available channel. A support-vector machine, tested with 10-fold cross validation, was able to distinguish between index and MRP flexion with 85.29% accuracy for Monkey W and 78.03% accuracy for Monkey N (Figure 2.4B). Classification performance suffered when using non-overlapping 20 ms bins (71.01% Monkey W and 68.20% Monkey N) or a larger 100 ms bin (65.97% Monkey W and 61.98% Monkey N). The poor classification performance with the single 100 ms bin suggests that the majority of neurons we recorded were broadly tuned. However supplying the classifier with temporal history at a high resolution appeared to alleviate this issue. Therefore, consistent with previous work (Aggarwal et al., 2008; Hamed et al., 2007), these two finger movements could be distinguished from motor cortex activity.

2.3.2 Online Decoding

Both subjects were able to achieve some level of online control of the virtual hand with the initial Kalman filter as shown in Figures 2.5A, 2.6A for index finger and MRP fingers, respectively. Across all sessions, Monkey W achieved an average bit rate with the initial Kalman filter of 1.32 ± 0.29 bps, while Monkey N achieved a bit rate of 1.07 ± 0.16 bps (bits-per-second; mean ± s.t.d.). The Kalman filter was generally responsive to each subject's input. However, similar to center out literature, sometimes the decoder was unable to stop on-target for the required hold time. Examples of longer trial times, often due to orbiting, are highlighted in orange in Figures 2.5A, 2.6A. In some cases, particularly with the initial Kalman filter, orbiting was so severe that the subjects were unable to acquire targets within the timeout period. While using the ReFIT filter, orbiting was generally less frequent and less severe for both index and MRP decoding, resulting in improved performance metrics (example sessions shown in Figures 2.5B, 2.6B).

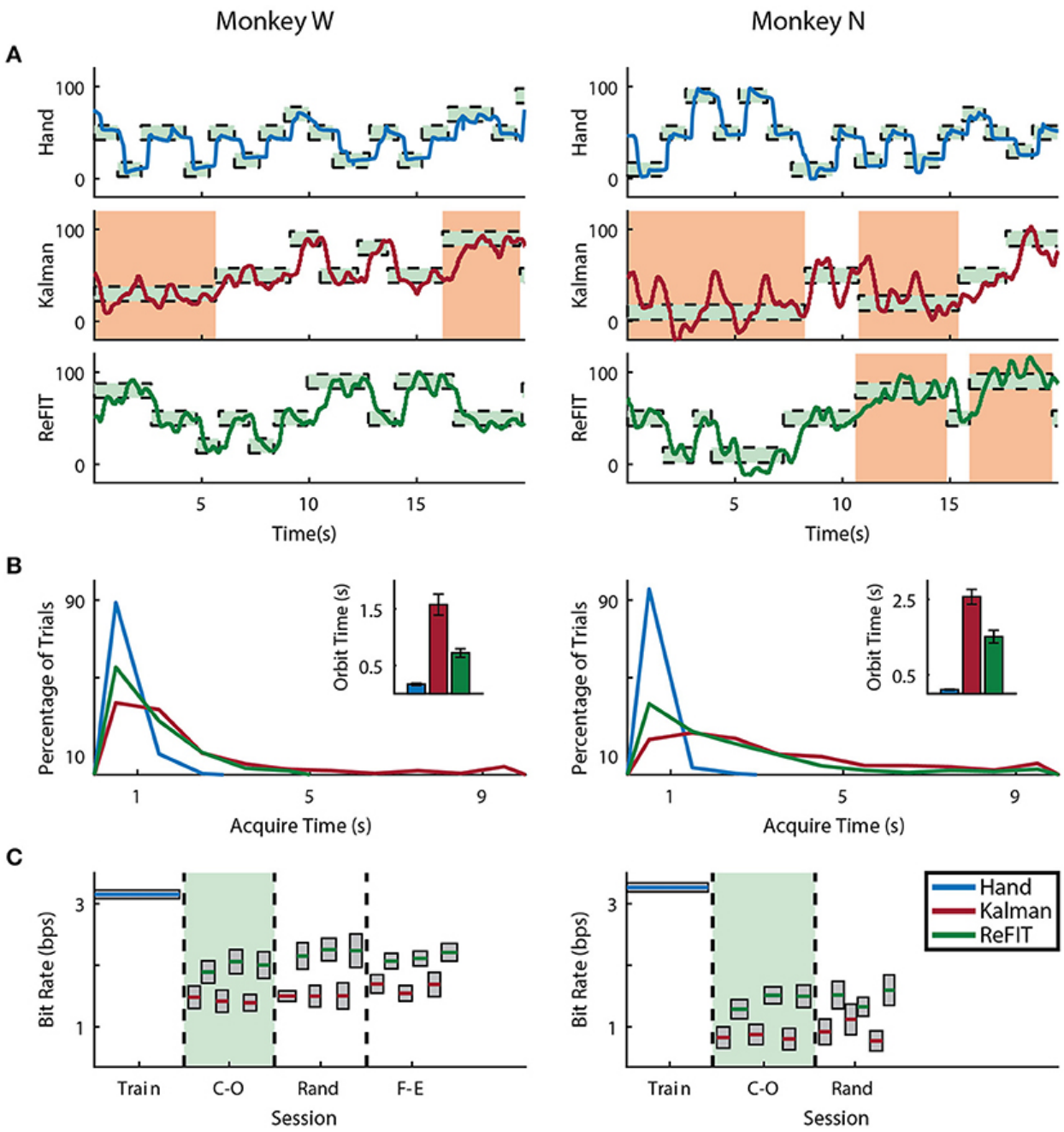

Figure 2.5 Online index finger decoding performance. **(A)** Traces of the center-out trials closest to session average (session shaded in green below), orange shading indicates trials with > 3 s acquisition time. **(B)** Acquisition times from the same center-out session binned in 1s intervals shown along with average orbiting times (mean ± s.e.m.). **(C)** Decoding performance across trial blocks for each target style (mean ± s.e.m.). Dashed lines indicate separate experiment sessions, with a center-out training session shown for a comparison to hand performance. Within each session, the initial Kalman filter trials used to train the ReFIT filter are not shown.

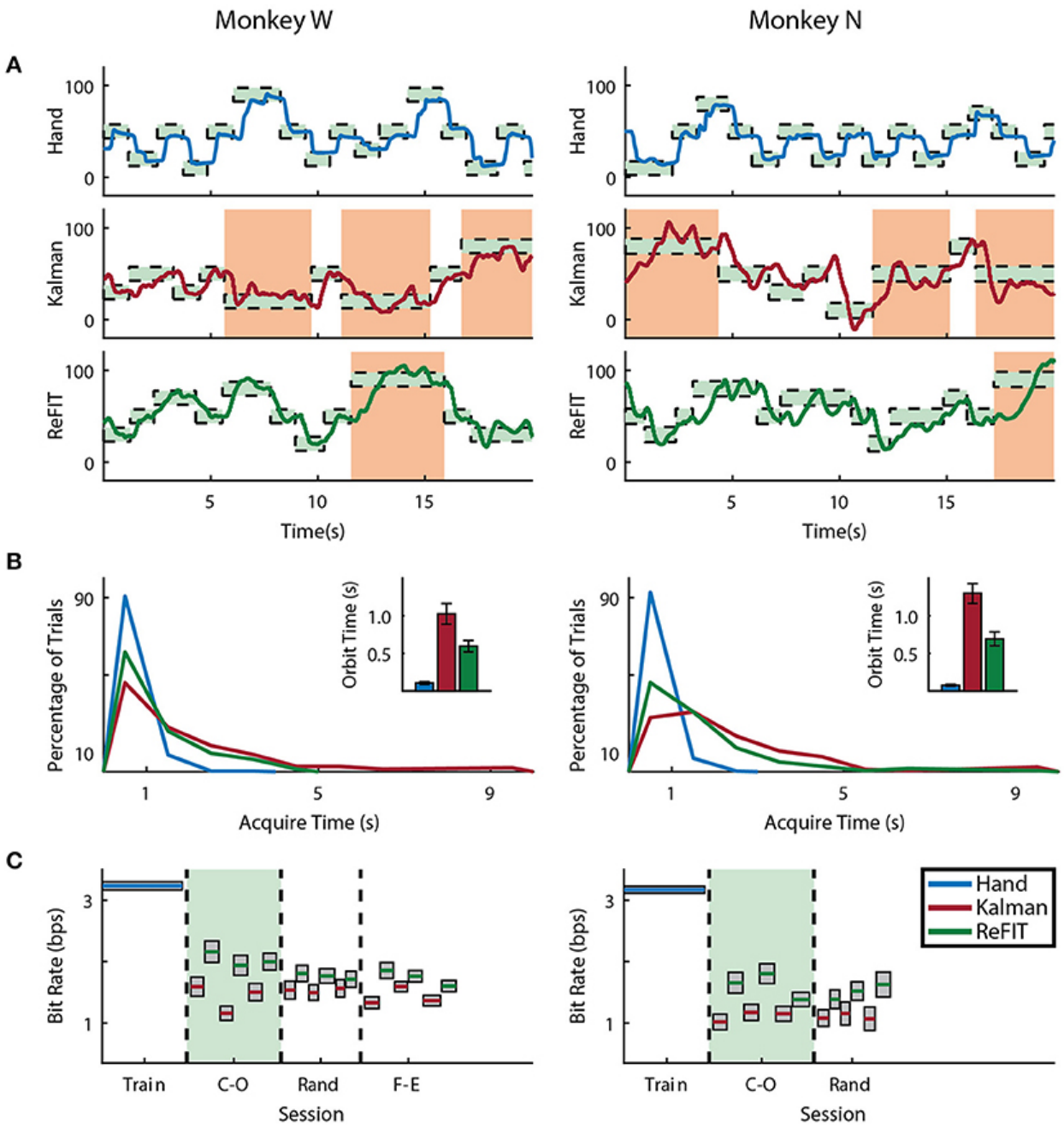

Figure 2.6 Online MRP finger decoding performance. **(A)** Traces of the center-out trials closest to session average (session shaded in green below), orange shading indicates trials with > 3 s acquisition time. **(B)** Acquisition times from the same center-out session binned in 1s intervals shown along with average orbiting times (mean ± s.e.m.). **(C)** Decoding performance across trial blocks for each target style (mean ± s.e.m.). Dashed lines indicate separate experiment sessions, with a center-out training session shown for a comparison to hand performance. Within each session, the initial Kalman filter trials used to train the ReFIT filter are not shown.

Consistent with previous studies (Fan et al., 2014; Gilja et al., 2012), subjects were able to achieve their best online performance with the ReFIT algorithm, which always outperformed the initial Kalman filter throughout the day (Monkey W, $p < 1 \times 10^{-7}$, n = 38 trial blocks; Monkey N,

$p < 1 \times 10^{-5}$, n = 26 trial blocks; one-sided Wilcoxon sign-rank test). Example target acquisition sessions for both subjects are shown in Figures 2.5C, 2.6C. Figure 2.7 shows the online success rate averaged across trial blocks for the tasks performed by each subject. Overall, the ReFIT decoder improved success rate by 4.33 ± 7.19% for Monkey W (mean ± s.t.d; $p < 1 \times 10^{-4}$, n = 38 trial blocks; one-sided Wilcoxon sign-rank test) and 5.78 ± 7.35% for Monkey N (mean ± s.t.d; $p < 1 \times 10^{-5}$, n = 26 trial blocks; one-sided Wilcoxon sign-rank test). Across all experiment sessions, the ReFIT algorithm improved the average bit rate by 31.04 ± 2.78% for Monkey W (mean ± s.e.m; $p < 1 \times 10^{-36}$, n = 2114 KF trials and 2010 RF trials; one-sided two sample t-test) and 35.17 ± 4.44% for Monkey N (mean ± s.e.m; $p < 1 \times 10^{-20}$, n = 1558 KF trials and 1607 RF trials; one-sided two sample t-test). See Supplementary Material for individual session statistics. Furthermore, improvements in bit rate when using the ReFIT decoder were not limited to a particular finger group (Table 2.2) or target style (Table 2.3). Overall, while the improvement was robust and reliably present, the increase was not as large as was previously observed in upper limb center out studies (Gilja et al., 2012).

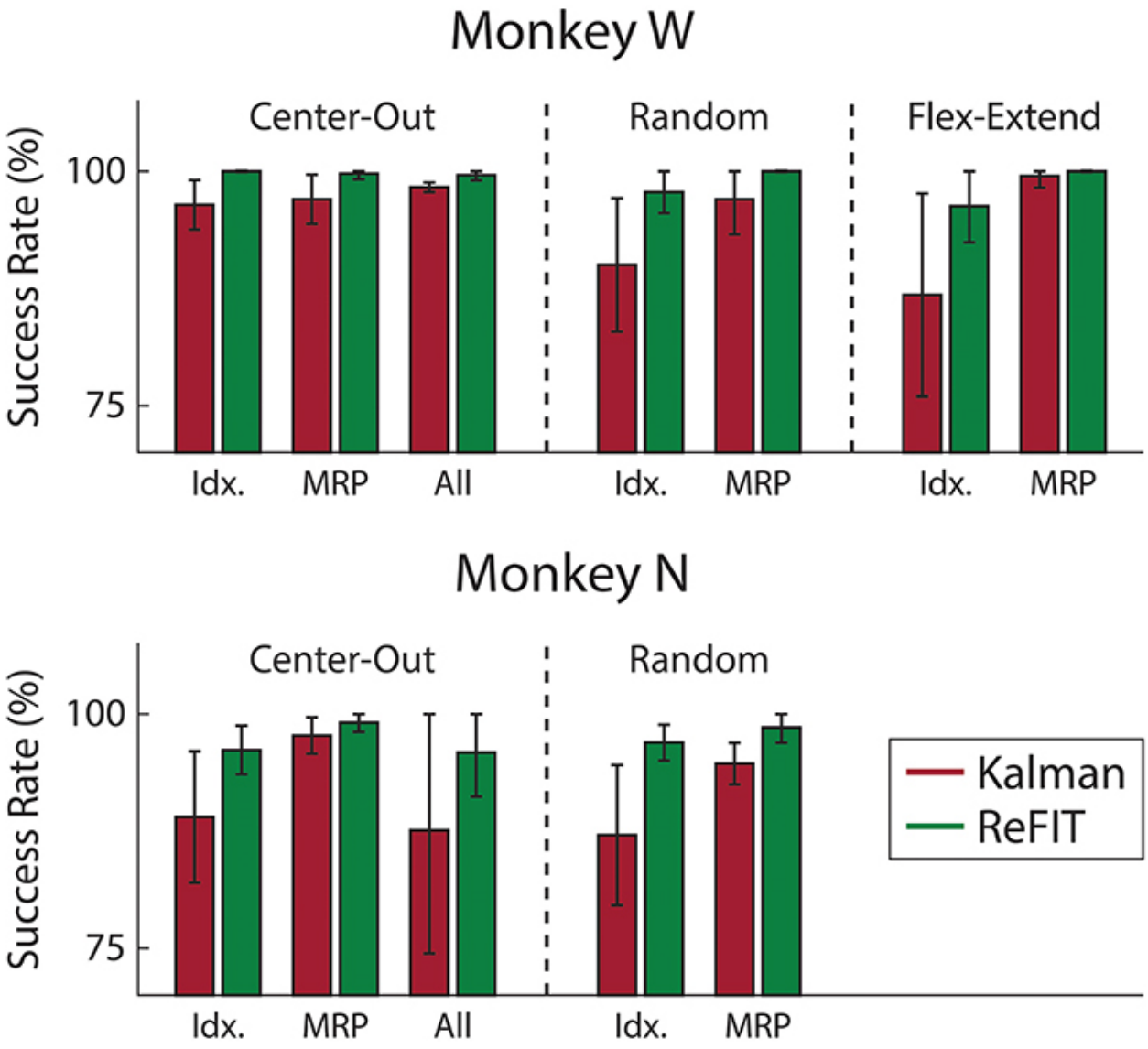

Figure 2.7 Online success rates across two sessions. Average success rate of trial blocks for each subject (mean ± std). Overall, the ReFIT decoder improved success rate by 4.33 ± 7.19% for Monkey W ($p < 1 \times 10^{-5}$, n = 38 trial blocks; one-sided Wilcoxon sign-rank test) and 5.78 ± 7.35% for Monkey N ($p < 1 \times 10^{-4}$, n = 26 trial blocks; one-sided Wilcoxon sign-rank test).

Monkey	Finger Group (% Improvement)		
	Index	MRP	All
W	38.21±5.04****	28.97±3.56****	18.38±6.76*
N	55.60±10.43****	33.97±6.07****	17.08±7.04*

Table 2.2 ReFIT performance improvements across finger groups. Finger groups are listed such that "Index" is the improvement to average bit rate (% mean ± s.e.m) across all sessions and target styles performed with the Index finger active. Total number of sessions for each group is shown in Table 2.1. Starts indicate a significant improvement of ReFIT over the initial Kalman filter (one-sided two sample t-test with *$p < 0.05$ and ****$p < 1 \times 10^{-6}$)

Monkey	Target Style (% Improvement)		
	C-O	Rand	F-E
W	35.28±4.33****	30.20±6.04****	24.92±4.18****
N	31.61±4.95****	43.74±9.43****	-

Table 2.3 ReFIT performance improvements across target styles. Target styles are grouped such that "C-O" is improvement to average bit rate (% mean ± s.e.m) across all sessions and finger groups acquiring center-out targets. Total number of sessions of each type is shown in Table 2.1. Stars indicate a significant improvement of ReFIT over the initial Kalman filter (one-sided two sample t-test with ****$p < 1 \times 10^{-6}$)

Figure 2.8 shows the average acquisition time performing the center-out target task along with the average fraction of each trial spent orbiting. Metrics between both subjects were similar when viewed as percentages. Across all finger groups, using the initial Kalman filter, subjects spent an average of 45.95 ± 0.81% (mean ± s.e.m.) of each trial orbiting the target. Using the ReFIT filter, the average fraction of trial time spent orbiting dropped by 28.21 ± 2.12% (mean ± s.e.m; $p < 1 \times 10^{-37}$, n = 1994 KF trials and 1929 RF trials; one-sided two sample t-test). The reduction in orbiting time helped improve average center-out acquisition time by 33.43 ± 2.02% (mean ± s.e.m; $p < 1 \times 10^{-37}$, n = 1994 KF trials and 1929 RF trials; one-sided two sample t-test). Consistent with its application in decoding center-out arm reaches (Gilja et al., 2012), ReFIT significantly increased target acquisition rate primarily due to improved stopping behavior.

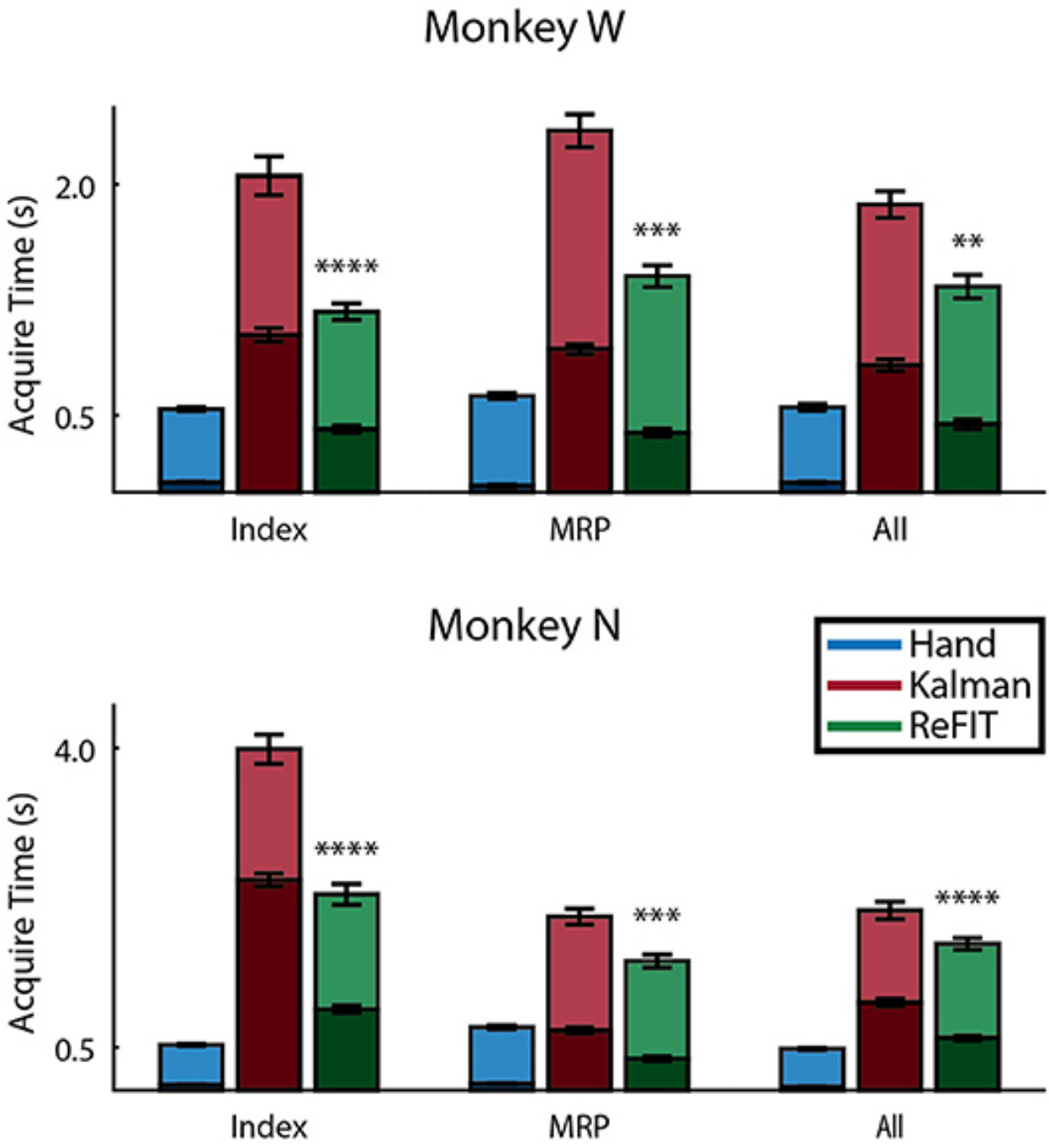

Figure 2.8 Acquistion and orbiting time metrics of center-out target task. Bar graphs indicate average acquisition time (mean ± s.e.m.), with the darkened region scaled to represent the average fraction of each trial spent orbiting (mean ± s.e.m.) across two sessions for each subject. Stars indicate a significant improvement in the orbiting behavior of ReFIT over the initial Kalman filter (one-sided two sample t-test, $n \approx 300$ trials; with $^{**}p < 0.001$, $^{***}p < 1 \times 10^{-4}$, and $^{****}p < 1 \times 10^{-6}$).

2.3.3 Modulation Analysis

Most of the improvement of ReFIT for upper-limb movements has been attributed to the sharpening of directional velocity tuning by intention estimation (Fan et al., 2014). Since we

characterize finger motions in 1 dimension, velocity tuning is simply represented as the difference in firing rate between flexion and extension. The absolute value of this difference is referred to as modulation. We looked at the change in modulation when intention estimation is applied to the native center-out training data across each monkey's experiment days. Many channels are not well tuned, and therefore are neither expected to benefit or worsen from intention estimation. Therefore, we limited this analysis to "high quality" examples defined as channels on any day that were velocity modulated before applying intention estimation (Mod. >1 spike/s), had good encoding performance ($\rho > 0.1$ Monkey W, $\rho > 0.05$ Monkey N), and were valuable to the decoder. Specifically, the value of a specific channel was determined as described in the Neural Tuning and Finger Separation section above. Here, a negative result indicates the channel is valuable since performance is worse when it is removed. In both subjects, the majority of the high quality channel examples (33 out of 37 channels Monkey W, 12 out of 16 channels Monkey N) chosen for analysis benefited from intention estimation, meaning they showed a raw increase in modulation after intention estimation was applied (Figure 2.9). Monkey W had an average raw improvement of 3.34 ± 0.51 spikes/s (mean ± s.e.m.; $p < 1 \times 10^{-5}$, one-sided Wilcoxon sign-rank test). Monkey N had an average raw improvement of 1.54 ± 0.54 spikes/s (mean ± s.e.m.; $p < 0.01$, one-sided Wilcoxon sign-rank test). Monkey W had more significant results overall, likely due to the fact that he had more high quality channels available at the time of the study. The positive response to intention estimation suggests that ReFIT may improve performance for finger motions via similar mechanisms observed in upper-limb studies.

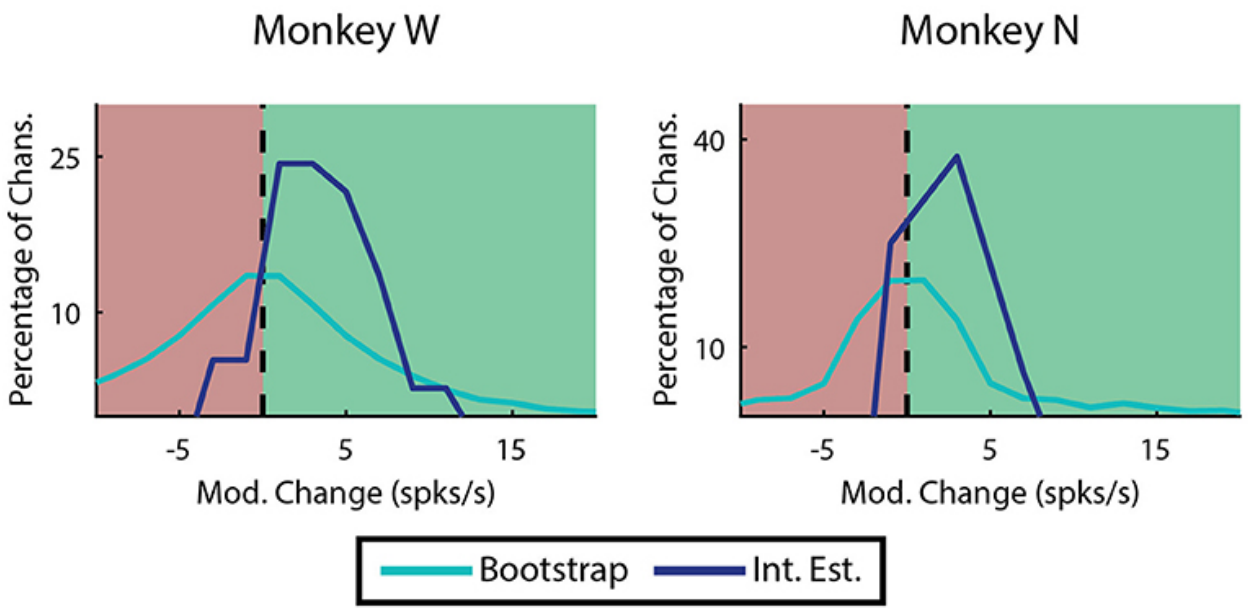

Figure 2.9 Effects of intention estimation on velocity modulation. Analysis was restricted to channels that were originally velocity modulated, had a well correlated linear model, and were valuable to offline decoder performance (n = 37 channels over 12 days, Monkey W; n = 16 channels over 7 days, Monkey N). The raw change in modulation after intention estimation is applied to the original velocities is shown binned in 2 spike/s intervals. In both subjects intention estimation improved modulation compared to a randomized bootstrap analysis ($p < 1 \times 10^{-7}$ Monkey W, $p < 0.01$ Monkey N; one-sided two sample t-test).

2.3.4 Sensory Context Results

Each subject also performed two days of sensory context experiments. In these sessions, online performance with the manipulandum moving all fingers was compared to performance after the manipulandum was removed in favor of a stanchion that provided no restrictions on finger movement or tactile finger sensations. To compare performance across subjects, data was normalized across animals by centering around initial Kalman filter performance at 1 bps. Across both subjects and sessions, the ReFIT Kalman filter improved performance over the initial Kalman filter ($p < 1 \times 10^{-4}$, n = 747 RF trials and 781 KF trials; one-sided two sample t-test). However, there was no statistically significant change using the ReFIT filter across sensory contexts ($p > 0.9$, n = 747 manipulandum trials and 780 stanchion trials; two sample t-test; Figure 2.10A). At the minimum, this suggests that the neural information used by the decoders is largely a product of motor activity and subjects are able to adjust to sensory context shifts. Furthermore, we noticed that sometimes subjects will stop moving their active fingers while performing the task in online

BMI mode. An example of Monkey W voluntarily holding his MRP fingers still during an online center-target acquisition session is shown in Figure 2.10B. The subject is still able to control the virtual hand to acquire MRP targets even after electing to hold his MRP fingers still. This indicates that decoding performance is not purely dependent on proprioceptive feedback.

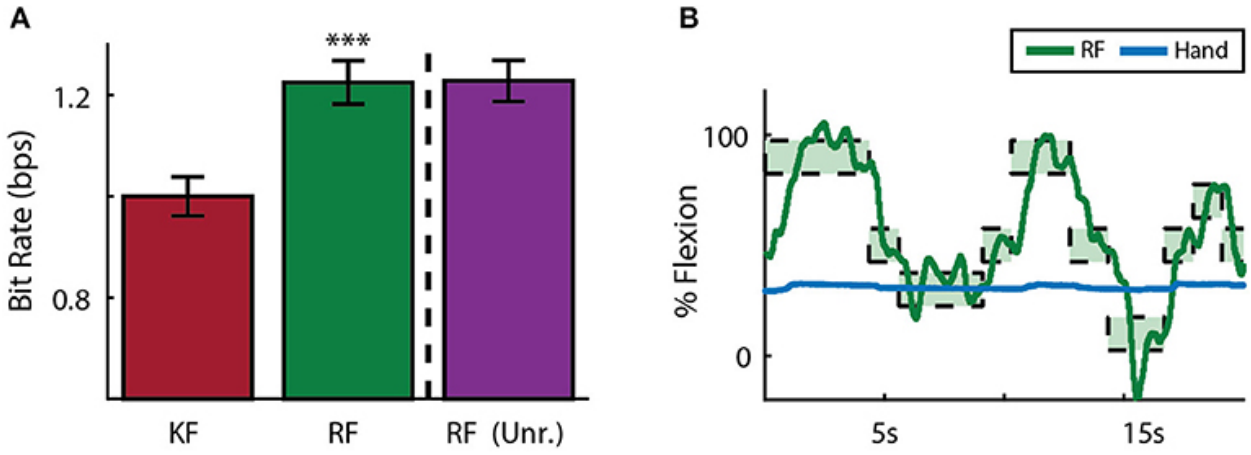

Figure 2.10 Online decoding under various sensory contexts. **(A)** A ReFIT decoder was trained with the manipulandum to control flexion of all 4 digits. At the dashed line, the manipulandum was removed and subjects continued online control with the same ReFIT decoder (Unr.). Bars represent average bit rate (mean ± s.e.m.) across all sessions for both subjects. For each day and subject, data was normalized by centering such that the average bit rate for the initial Kalman filter was 1 bps. Stars indicate a significant improvement of ReFIT over the intial Kalman filter ($p < 1 \times 10^{-4}$, n = 747 ReFIT trials and 781 Kalman filter trials; one-sided two sample t-test). **(B)** Target trace of Money W performing center-out target acquisition in BMI mode while voluntarily holding his active MRP fingers still. Green rectangles represent the displayed target ranges the subject successfully acquired.

2.3.5 Multiple DOF Analysis

As an initial test of decoding multiple fingers simultaneously, the animals both performed a four block set of alternating datasets (A-B-A-B) for index and MRP fingers. This was decoded offline with cross validation using a Kalman filter state vector that simply included position and velocity for both fingers. As shown in Figure 2.11, the moving finger had similar decodes to those shown above, however, the motionless finger was usually incorrectly decoded as moving as much or more as the active finger, as shown with example traces in Figure 2.11. As the physical model (i.e., the A matrix) explicitly decouples the fingers, this correlation apparently results from the neural observation model. This is consistent with the modulation depths listed above, in which almost all of the modulated neurons had significant correlations with both index and MRP motion.

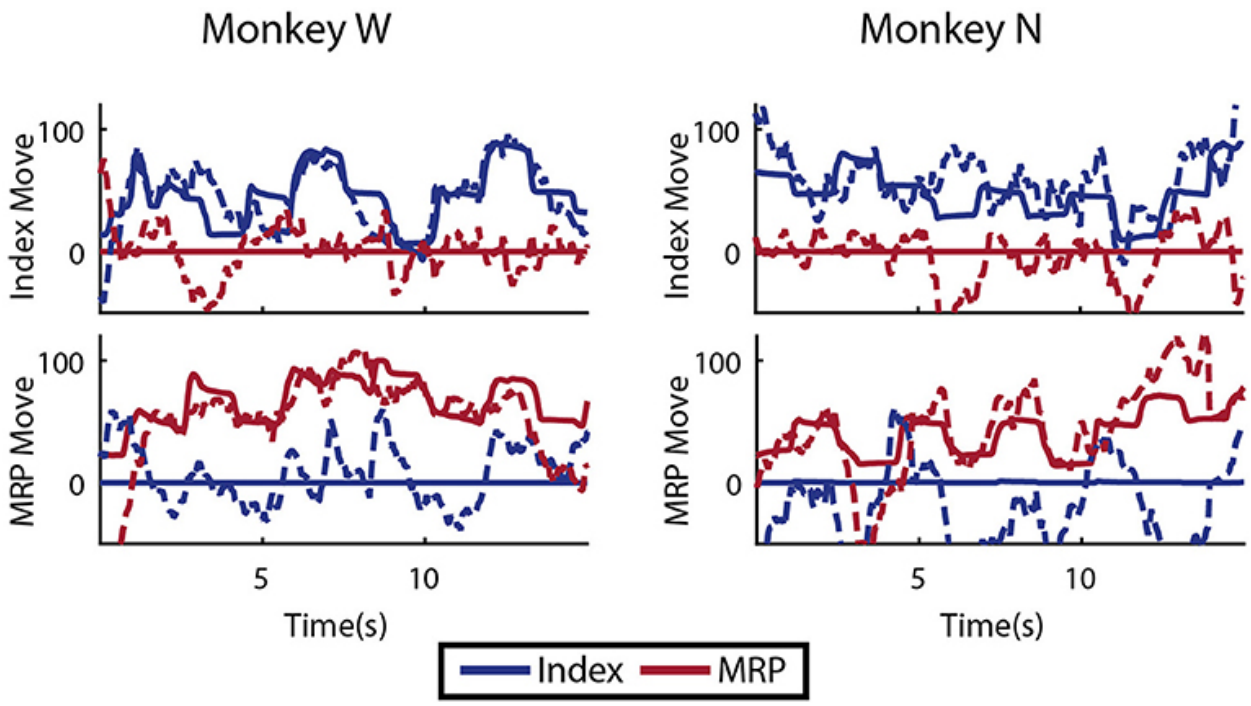

Figure 2.11 Offline traces of two DOF decoding. Dashed lines are the Kalman filter prediction, while solid lines are the actual finger group position. Training data for this decoder was created by combining multiple training runs, each with a single active DOF. For each subject, intervals where each DOF is active and the other is restricted are shown.

2.4 Discussion

Here we showed that NHPs are able to use a ReFIT Kalman filter to acquire fingertip targets using multiple finger groups. The decoder appears controllable in a variety of target configurations and responsive to the subject's intent, as judged by their ability to maneuver to random and unpredictable positions along the finger arcs. Consistent with previous studies, the ReFIT process improved performance over the standard Kalman filter with a substantial improvement in stopping behavior. This was not a given, since the mechanism of improvement is not fully understood, and there is no obvious cosine tuning model (Georgopoulos et al., 1986) for finger movements. However, the performance improvements observed for finger motions are less dramatic than those observed in upper-limb studies (Gilja et al., 2012). If we consider a purely biomimetic perspective, the increase in modulation via intention estimation shown here and in previous work may result from a reduction in motor noise (Fan et al., 2014). Since fingers are

smaller lever arms with actuators designed for precise movements, it stands to reason that there may be less motor noise to eliminate in an able-bodied subject. Secondly, this study and previous work have observed a significant positional tuning element to finger movements. However, our implementation only assumes and corrects noise from velocity measurements. If we look at performance discrepancy from a perspective of decoder adaptation, the task complexity may affect the intention estimation process. The subjects in this study were only given control of 1 DOF at a time: a simple task where a naive decoder has a relatively high chance level of choosing the correct direction at any timepoint. In other words, the chance of false positives with the initial decoder is higher in our 1 DOF task. It is possible that intention estimation techniques may be more impactful when attempting to control multiple degrees of freedom simultaneously, as in a 2 DOF center out task.

In earlier studies, intention estimation was noted as the primary mechanism by which the ReFIT Kalman filter improved performance (Gilja et al., 2012). The second training stage serves as a closed-loop adaptation period during which the user is presented with visual feedback from the initial Kalman filter and is able to issue corrections in real time which are later processed via intention estimation. Initial decoder parameters may be suboptimal due to poor training data, a shift from physical control to BMI control, or both. Poor training data may be the result of noise in the motor system - discussed earlier, or inconsistent physical behavior. In this context, signal availability and noise from the electrode array is associated with the shift from physical to BMI control. An optimal adaptation to BMI control could be a synergy in which the brain is able to learn a particular decoder and the decoder adapts to better execute commands (Shenoy & Carmena, 2014). Indeed, the brain may identify neurons critical BMI performance and modulate them accordingly (Orsborn et al., 2014a). In this view, ReFIT then improves performance by

highlighting and better executing commands from these important neurons. In this study and earlier work (Gilja et al., 2012), a separate re-training step was used, although online learning techniques can potentially update decoder parameters recursively on a shorter timescale (Dangi et al., 2013; Orsborn et al., 2012). Newer adaptive decoders have leveraged more accurate encoding models, improved intention estimation transformations, and assistive training to further optimize parameter convergence (Shanechi et al., 2017). Assistive training strategies combine the output of an initial decoder with an optimal trajectory or enforce constraints along an ideal path during the adaptation phase, typically with decreasing levels of assistance as performance improves. Such techniques incorporate a similar assumption of intention estimation with the addition of online visual feedback of the ideal decoder in a graded fashion. Assistive strategies have successfully provided a paralyzed human subject with high DOF control of a prosthetic arm and hand (Collinger et al., 2013; Wodlinger et al., 2015), and may prove useful as we increase task complexity beyond 1 DOF.

For individual finger control to ultimately be available using neuroprostheses, we must provide control of multiple finger groups simultaneously in an online setting. Decoders that leverage a linear encoding model have been shown to simultaneously control four distinct hand motions in a human subject (Wodlinger et al., 2015). This study is remarkable because it demonstrates that the combination of a well-chosen basis and simple decoder can provide BMI users with modulated control of different grasps in a clinical setting. In the future we aim to provide our NHP subjects with precise online control in a 2 DOF target matching task with the index and MRP finger groups. However, the offline results in this study suggest that linear decoders may not be able to achieve high precision for heavily interdependent finger motions, potentially due to co-contraction. It would be interesting to examine a linear decoder's performance on a subset of the

full range of motion we tested. Not only is a reduced range more likely to remain in an area of linearization, but a well chosen range where the subjects can comfortably modulate each DOF with limited natural co-contraction may produce better initial results. It would then be interesting to see if ReFIT or other training techniques allow subjects to generalize to the full range of motion. If the combination of various online linear decoders and intention estimation or adaptation techniques does indeed prove insufficient, there are multiple design directions which may be fruitful. One could develop a more accurate classification scheme to account for and suppress unwanted finger movements, similar to work in reach tasks (Aggarwal et al., 2013; Sachs et al., 2015) and cursor control (Kao et al., 2017). Another study effectively reduced the numbers of DOF of the hand using dimensionality reduction (Rouse, 2016). However, ultimately we need to control multiple fingers at the same time for a hand to be truly useful. We could also seek a more accurate model of the natural muscle synergies that may enable more generalization to multi-finger movements (Ethier et al., 2016; Nazarpour et al., 2012; Oby et al., 2013). These can be incorporated into more general non-linear machine learning approaches, for example including neural networks (Gao et al., 2016; Sussillo et al., 2012). Finally, we could explore contributions from additional information sources (Aflalo et al., 2015) to augment these approaches.

In this study we demonstrated that online finger decoders can be robust to changes in sensory context and proprioception in able-bodied subjects. We hypothesize that had we introduced a context change via increasing spring tension during training, the subjects would be able to compensate with the ReFIT decoder much like they did to other sensorimotor input shifts. As described earlier, the online adaptation of ReFIT may be creating a decoder that is optimal for BMI control of the virtual hand irrespective of existing forward motor path. However, BMIs that promise complex grasps will have to perform under dynamic conditions and disturbances during

object manipulation. So while we believe that subjects can compensate for global changes, the rate of environmental adaption may not be sufficient for many realistic conditions. In the future, non-visual feedback mechanisms for BMIs may become available (Flesher et al., 2016), which can greatly improve motor performance provided they are well integrated into the sensorimotor system. Other studies that have examined finger control in able-bodied subjects have observed that the precision of finger control in response to physical disturbances can vary with naturally occurring or induced input noise (Mendez-Balbuena et al., 2012). The authors of that study found that for different individuals introducing a mechanical stochastic noise at different levels produced optimal performance. BMI systems are novel sensorimotor systems where select neurons in the brain interface with either the natural periphery or robotic devices through decoders and encoders. Studying the effects of different types of input noise may be a step toward characterizing and optimizing fine motor control of BMI-FES systems with different feedback modes.

In clinical settings, recent FES systems have provided human patients with the ability to modulate previously paralyzed joints (Ajiboye et al., 2017; Bouton et al., 2016). These implementations show immense potential and represent an amazing convergence of technology and knowledge of the human motor system. As this technology becomes more advanced and transitions further into clinical and ultimately commercial use, further systems level experiments will be required to achieve higher levels of performance in terms of activities of daily living. The everyday functionality of such systems will be limited by both our ability to extract meaningful control signals as well as our ability to actuate multiple joints. It has recently been shown in human subjects that commanding many degrees of freedom simultaneously introduces more error (Ajiboye et al., 2017). In that study, grasp failures with the muscle controller often occurred when the BMI command was generally correct, but small oscillations triggered large swings in other

joint movements. While the FES efficacy could be improved with better implantable devices and physical therapy, some of the problem with multiple degrees of freedom will likely require different algorithms. The able-bodied NHP model enables the development of these algorithms with simultaneous knowledge of the complex plant that these neural signals are driving, including significant co-contraction of the muscles. It is not immediately obvious whether the most effective system for individuated finger control will involve directly extracting muscle activation commands from motor cortex or a more agnostic machine learning approach. In a practical setting, the amount of training data required impacts this decision as well, and may favor muscle based decoders. Ultimately, further systems level brain-controlled FES experiments could focus on dynamic motions to answer these equations and continue advancing the state of the art for neuroprostheses.

2.5 Acknowledgements

The following colleagues contributed to this work: Zach Irwin developed the original real-time application as well as base code which I then modified to apply intention estimation to train ReFIT parameters. Sam Nason, Philip Vu, Chrono Nu, and Autumn Bullard assisted with monkey training, fixed issues with the real-time application and experiment set up and helped develop automated criteria to exclude channels for decoding. Mackenna Hill developed the novel manipulandum with an undergraduate project team and assistance from Samuel Nason and Chrono Nu. Naia North assisted with offline metrics for modulation analysis. Parag Patil performed the implant surgery on both subjects and helped shape experiment goals. Cynthia Chestek was the principal investigator for this study, providing oversight and advice throughout the entire experiment and writing process. Eric Kennedy managed primate care and training, Matthew Willsey provided surgical assistance with Monkey N, and Paras Patel helped maintain

rig electronics. This work was supported by the Craig H. Neilsen Foundation, A. Alfred Taubman Medical Research Institute, NIH grant R01 GM111293, and DARPA grant N66001-16-4006. I was supported by fellowship from the Robotics Graduate Program at University of Michigan. Philip Vu, Chrono Nu, and Autumn Bullard were supported by NSF-GRFP.

Chapter 3 Clinical Validation of the Regenerative Peripheral Nerve Interface

This chapter briefly explains my key contribution as second author on the manuscript "A regenerative peripheral nerve interface allows real-time control of an artificial hand in upper limb amputees", published in Science Translational Medicine in 2020 (Vu et al., 2020)*. The same two patients participated in this study and Chapters 4 and 5. This work focused specifically on RPNIs. The pattern recognition system used only RPNI signals as inputs to demonstrate their control capabilities. In later chapters, we use mixtures of RPNIs and residual muscles depending on the functional goals of those experiments. The figure shown here is from the above manuscript, while the text summarizes the results as they relate to this thesis.*

3.1 Introduction

Commercial myoelectric control systems using surface electromyography are unable to obtain consistent control signals for finger-specific motions because the desired signals are either obscured by more superficial muscles or non-existent due to the level of amputation. Intramuscular recording techniques and Regenerative Peripheral Nerve Interfaces (RPNIs) can potentially resolve these issues. RPNIs consist of free autologous muscle graft that are sutured to the end of severed nerves. The host nerves reinnervate the grafts which prevents the formation of neuroma (Kubiak et al., 2019; Woo et al., 2016) and creates a stable biological interface to extract movement commands for prosthetic devices. Implanted electrodes can safely record large amplitude and highly specific EMG from RPNIs (Frost et al., 2018; Vu et al., 2018, 2020). In this clinical study, we demonstrated the capability of RPNI signals for real-time prosthetic control.

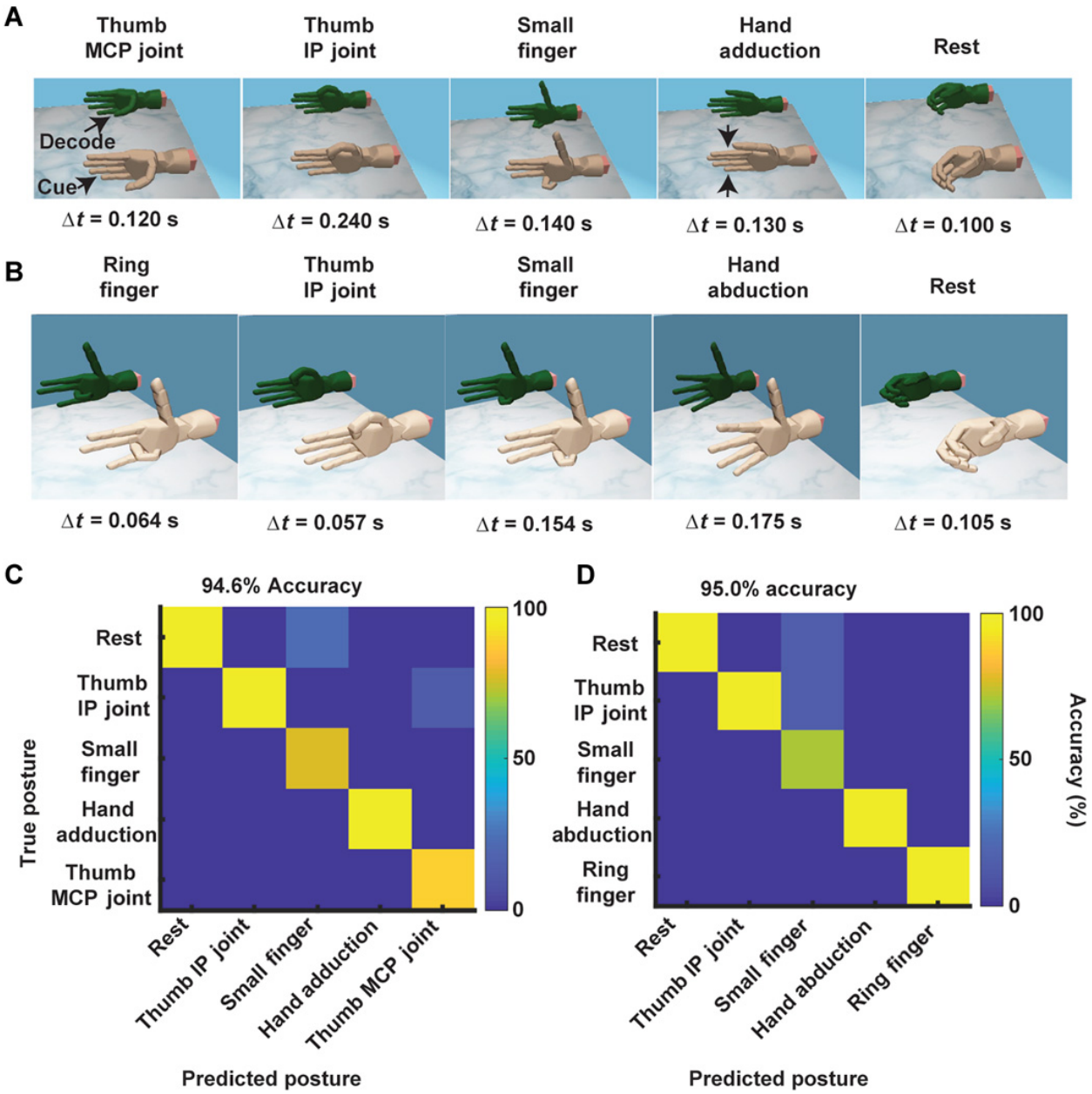

Figure 3.1 Real-time classification of finger movements with RPNI. **(A and B)** P3 and P4's discrete control of thumb MCP joint (opposition), thumb IP joint (flexion), small finger, adduction, and rest for P3, and ring finger, thumb IP joint, small finger, abduction, and rest for P4. The fastest motion selection times are shown for each posture. **(C and D)** Offline confusion matrix of the postures used in (A) and (B), respectively. The y axis represents the true posture, whereas the x axis represents the predicted posture. The color map indicates the accuracy (%) of the classifier's prediction. (Vu et al., 2020)

3.2 Results

Two patients with transradial amputations, P1 and P2 (listed as P3 and P4 in the published manuscript), had RPNIs created on the Ulnar, Median and Radial nerves. Eight pairs of bipolar recording electrodes (Synapse Biomedical, Oberlin, Oh) were implanted into the Ulnar and

Median RPNIs as well as residual muscles. In this study, signals from the RPNIs were used to control virtual prostheses (Kumar & Todorov, 2015) with a Naïve Bayes classifier. The experiment setup was similar to the posture switching task detailed in Chapter 4. P1 used the two electrode pairs in his Ulnar and Median RPNIs to distinguish the five postures in Figure 3.1A. P2's Ulnar nerve was dissected to create two RPNIs which she used along with her Median RPNI to distinguish the five postures in Figure 3.1B. These movements are anatomically consistent with Median and Ulnar nerve motor functions past the level of amputation. Offline results in Figures 3.1C and 3.1D indicate that the movements could be distinguished with high accuracy. Both participants were able to control the virtual hand in real-time with low latency indicated by the fastest movement times in Figure 3.1A and 3.1B.

3.3 Discussion

This study demonstrated that RPNIs can be used to control hand prostheses. A pattern recognition algorithm was used to reliably distinguish five movement states using two and three RPNI control signals in P1 and P2, respectively. In practice, some movements such as finger adduction may not be actuated depending on the robotic prostheses. Most multi-articulating hands have a single motor to flex each finger and a sixth motor to control thumb opposition. For patients with wrist disarticulations, RPNIs can be thought of as augmenting prosthetic control. Notably, they provide valuable control signals for intrinsic thumb movements (Vu et al., 2020). RPNIs also serve as additional inputs for movements such as small finger flexion which are also controlled by extrinsic muscles. Patients with more proximal amputations may be missing some or all of their muscles that control finger movements. In these cases, RPNIs will be critical to restoring hand function with robotic prostheses.

3.4 Acknowledgements

The following colleagues contributed to these experiments: Philip Vu, Cynthia Chestek, and helped design this study. Zach Irwin and Philip Vu developed the virtual reality environment for the task and assisted with development of real-time control software. Philip Vu helped gather data and develop analysis techniques. Paul Cederna and Theodore Kung. developed and performed the surgical implantation procedure. Kelsey Ebbs managed regulatory compliance and clinical trial coordination. This work was supported by the Defense Advanced Research Projects Agency (DARPA) Biological Technologies Office (BTO) Hand Proprioception and Touch Interfaces (HAPTIX) program through the DARPA Contracts Management Office grant/contract no. N66001-16-1-4006 and by the National Institute Of Neurological Disorders And Stroke of the National Institutes of Health under Award Number R01NS105132. Philip Vu was supported by the National Science Foundation Graduate Research Fellowship Program under Award Number DGE 1256260

Chapter 4 High Speed Pattern Recognition with Peripheral Interfaces

A version of this chapter has been submitted to IEEE Transactions on Robotics and was posted as "Surgically Implanted Electrodes Enable Real-Time Finger and Grasp Pattern Recognition for Prosthetic Hands" in pre-print on MedRxiv in 2020 (Vaskov et al., 2020)

4.1 Introduction

Hands are incredibly important to people because they provide the opportunity to handle tools, operate machines, and are essential components of social interaction and communication. The loss of an upper extremity can severely impact a person's ability to interact with the world around them. Unsurprisingly, some of the earliest documented examples of upper extremity prostheses produced in the sixteenth century mimicked the human hand. However, these devices were heavy, lacked active actuation, and were not practical for use in daily life (Romm, 1989). In the twentieth century, the development of the split hook body powered prosthesis provided a more functional solution that addressed many of these concerns (Belter et al., 2014). Body-powered hook prostheses are cable-driven devices that are controlled by exaggerated movements of residual joints. Unfortunately, they have very limited range of motion limiting their capacity to provide functional restoration (Chadwell et al., 2020; Hichert et al., 2018; Smit et al., 2012). Myoelectric prosthetic hooks can mitigate some of these issues but still lack dexterity and fine motor control. Advanced robotic prosthetic devices have been developed which can provide 5 to 30 degrees of freedom (DOF) of the human hand and provide adequate gripping force for functional tasks (Akhtar et al., 2016; Atzori & Müller, 2015; Resnik et al., 2014). Control of these devices is achieved by recording surface electromyography (EMG) signals from innervated muscles in the

residual limb, allowing users to leverage more natural motor pathways to control the device. However, current control schemes are either cumbersome, unintuitive, or unreliable, leading many users to abandon their devices (Biddiss & Chau, 2007). In spite of these issues, myoelectric hands are still an attractive approach for prosthetic rehabilitation following limb loss due to their high grip strength and potential for intuitive control (Biddiss et al., 2007; Engdahl et al., 2015).

Commercial EMG control systems typically rely on a mode selection scheme, where the user first selects between different movements and then secondarily activates them. In systems with an active wrist, users typically toggle between wrist and hand control with a pre-defined muscle contraction. Grasp selection is often done sequentially with muscle co-contraction or gesture control (Franzke et al., 2019). A more fluid control strategy is pattern recognition in which the intended movement is classified from the users' recorded EMG signals and can be proportionally activated based on signal amplitude (Kuiken et al., 2016). Most pattern recognition systems can independently activate wrist rotation, wrist flexion, or a general hand open-close signal. Grasp distinction is not common, even amongst persons with transradial amputations where extrinsic flexors and extensors are still present in the residual limb (Li et al., 2010). Commercially available systems that are capable of activating a multiple grips have only recently become available. Classifiers require a rich set of distinct inputs to accurately interpret movement intentions. Existing systems, that use surface EMG, record a spatiotemporal summation of motor unit action potentials from a distant location which is complicated by cross-talk between channels (Farina et al., 2017) and reduced signal strength (OrtizCatalan et al., 2020). Furthermore, signals from deep finger flexors (i.e. flexor digitorum profundus to the index finger), are obscured by more superficial muscle activity in the forearm (i.e. flexor digitorum superficialis to the middle finger) or lost entirely in more proximal amputations. In addition to these factors, the reliability of

commercial surface electrodes is limited by impedance and position alterations due to sweating or contact shifting (Farina et al., 2014). Hence, distinguishing grasps is challenging for pattern recognition systems that use surface EMG because finger-specific signals are hard to capture and sensitive to environmental changes.

Over the past decade, researchers have investigated software and sensing techniques to improve the reliability of pattern recognition systems and expand their capabilities to include grasp distinction. In earlier work, participants with transradial amputations used surface EMG and pattern recognition to select between 6 and 7 randomly cued hand postures with average movement completion rates of 53.9% (Li et al., 2010) and 77% (Cipriani et al., 2011), respectively. Other groups have used alternate machine learning approaches to distinguish up to 10-12 hand and wrist postures with greater than 90% offline accuracy (Atzori et al., 2016; Khushaba et al., 2012). The classifiers in these studies accurately distinguished more movements by adding information in the form of multiple input features per channel, or increasing modeling capabilities with deep networks. However, offline simulations alone are not sufficient to characterize online performance as real-time control is heavily influenced by the quality of feedback and individual experience levels (Krasoulis et al., 2019). Pattern recognition algorithms can also struggle to generalize to new contexts. For example, classifiers often issue incorrect predictions while supporting the prosthesis weight in untrained arm positions (Teh & Hargrove, 2020). One study found that more robust classifiers can mitigate this issue (Betthauser et al., 2018). However, this study did not include multiple grasp distinctions. Another study modelled transitions to show that three grasps could be distinguished in a variety of static arm positions and used in a functional task (Kanitz et al., 2018). Alternatively, another group used sensor fusion of EMG and inertial measurements to control four grasps and hand open. They found that it could improve performance across the

workspace (Krasoulis et al., 2020), but required context-specific training. In addition to software innovations, previous studies that quantified multiple grasp control improved signal consistency with adhesive research grade electrodes or captured more information with alternate sensing modalities.

Surgical interventions can more directly access the peripheral nervous system and improve the quality and fidelity of motor control signals. For users with more proximal amputations (i.e. above elbow amputation), EMG-based systems are limited due to the fact that the muscles used to generate EMG signals for hand control are missing. In these cases, a pattern recognition system would rely on subtle co-activations of remaining musculature, which is inherently difficult. Targeted muscle reinnervation (TMR) is a surgical procedure in which transected peripheral nerves are used to reinnervate surgically denervated areas of muscle. The target muscles are typically superficial and after reinnervation produce functional control signals that can be recorded via surface EMG (Zhou et al., 2007). TMR patients with transhumeral amputations or shoulder disarticulations equipped with adhesive electrodes selected four hand postures in a virtual reality environment with an average completion rate of 86.9%. Some patients have been able to control multiple grasps of robotic prostheses in laboratory environments (Kuiken et al., 2009; Piazza et al., 2020) and home trials (Kuiken et al., 2016). In combination with TMR, decomposition algorithms can estimate independent nerve signals from global surface recordings (Farina et al., 2017). This approach requires high-channel electrode grids and real-time control studies have focused on separation of wrist and gross hand movements to date (Kapelner et al., 2020). Implantable electrodes have also been proposed to record efferent motor commands directly from individual nerves. However, these electrodes are limited by low amplitude efferent motor action potentials (Davis et al., 2016) or lack of chronic stability. Conversely, electrodes implanted into

muscle tissue can record strong and stable EMG signals. In one study, indwelling electrodes eliminated the need to re-calibrate a regression controller in a virtual reality environment for months (Dewald et al., 2019). Intramuscular electrodes have also been shown to improve signal strength and control precision independent of changes to the mechanical interface or control strategy (OrtizCatalan et al., 2020). In another study, electrodes with multiple contacts were implanted into individual muscle bellies, enabling 6 degree of freedom (DOF) dexterous control including individual fingers of a robotic hand (Davis, et al., 2020). However, the ability for intramuscular electrodes to capture finger movements requires a sufficient amount of residual innervated musculature or other surgical interventions.

At the University of Michigan, we have developed the Regenerative Peripheral Nerve Interface (RPNI) which consists of a free muscle graft sutured to the end of a divided peripheral nerve. The muscle graft regenerates and becomes reinnervated by the regenerating peripheral nerve axons. RPNIs have been shown to effectively prevent and treat neuroma pain and phantom pain (Kubiak et al., 2019; Woo et al., 2016). Most importantly, RPNIs serve as a stable biological amplifier for efferent motor signals, retaining anatomical consistency between the host nerve and RPNI functions (Frost et al., 2018; Santosa et al., 2020; Vu et al., 2018). In a clinical trial, high resolution control signals recorded from electrodes implanted into RPNIs remained stable for up to 300 days (the duration of observation)(Vu et al., 2020). Vu et al. also used a pattern recognition algorithm in a virtual environment to validate RPNI control capabilities (Vu et al., 2020). Pattern recognition is the state of the art for intuitive device control and a natural match for most multi-articulating hands that are designed to switch between grip patterns. Therefore, it is both an easily comparable and immediately applicable control paradigm for implantable technologies.

In this study, we continue experiments with two persons with transradial amputations and electrodes surgically implanted into RPNIs and residual innervated muscles. Vu et al. focused specifically on each participant's RPNIs, here we investigate the signal quality and control capabilities of the full set of RPNIs and residual innervated muscles. We demonstrate that indwelling electrodes captured stable EMG control signals from both RPNIs and residual muscles with a highly favorable Signal-to-Noise ratio (SNR) in both participants. In addition to large amplitude recordings, the EMG was also highly specific for motor decoding. Real-time control with classifiers often presents a trade-off between responsiveness and stability when determining the length of the EMG processing window (Smith et al., 2011). Here we find a more optimal solution to this dilemma and utilize a Hidden Markov Model (HMM-NB) which learns transitions between latent states to make rapid predictions without sacrificing temporal stability (Kemere et al., 2008). We demonstrate online performance in a virtual posture switching task designed to reflect real-time finger and grasp control. To our knowledge, this is the fastest and most accurate signal acquisition and pattern recognition system that can switch directly between individual finger movements. We quantified performance for two posture sets: a 10 class set including extrinsic and intrinsic individual finger and hand movements and wrist flexion, and a five class set of functional grasps. To demonstrate robustness across physical contexts, we quantified stability of a grasp classifier in one participant across novel static arm postures with a prosthesis donned. Finally, both participants completed a functional assessment where they used robotic prostheses to move differently shaped objects that required the use of multiple hand grasps.

4.2 Results

4.2.1 Speed and Accuracy of Finger and Grasp Classifications

Two persons with transradial amputations (P3 and P4 from Vu et al., labelled P1 and P2 here), underwent surgery to have eight pairs of bipolar electrodes (Synapse Biomedical, Oberlin OH) implanted into RPNIs and residual innervated muscles. Differentiated signals from each electrode pair were filtered and the mean absolute value (MAV) was extracted with a sliding window. A Hidden Markov Model (HMM-NB) was trained by instructing participants to mimic 5-7 repetitions of each posture with their phantom limb. In offline simulations, the HMM-NB distinguished the same individual finger and wrist movements, known as the "1 of 10" posture set in P1 and P2 with 95.4% and 94.1% accuracy (Fig. 4.1A,D). Additionally, both participants controlled a virtual hand in real-time with the HMM-NB to complete a fast-paced posture switching task between each of the 10 postures. In one experiment session, P1 successfully maintained a one second hold within the 10 second timeout period on 100% of his trials. Online classifier accuracy measured real-time control errors during the first second of transition to the cued postures. P1 achieved an online accuracy of 93.0% in his experiment session (Fig. 4.1B). As shown in Fig. 4.1C, P1 used the HMM-NB to rapidly switch between postures with an online latency of 159±237 ms (median±i.q.r.). P2 performed the same calibration and decoding routine for three single day experiment sessions for the 1 of 10 posture set. Across all sessions, she achieved an online accuracy of 80.0% with a latency of 344±924 ms (Fig. 4.1D,F). P2 was able to make corrections and maintain successful holds on 89.3% of her trials. She had the most difficulty performing finger adduction, thumb opposition, and relaxing to rest with the virtual hand.

Unsurprisingly, online performance improved with a reduced number of postures (Fig. 4.2). Both P1 and P2 completed the same set of experiments using the HMM-NB to rapidly switch

between five postures: three functional grasps, finger abduction, and rest. Offline accuracy was relatively low for P2, notably the HMM-NB issued incorrect predictions of rest during simulated holds. However, when controlling the virtual hand in real-time, P1 and P2 achieved online accuracies of 99.5% and 96.3% across one and three experiment sessions respectively. Both participants were able to recover from errors and maintain successful holds on 100% of their trials. The HMM-NB was also able to distinguish the grasps posture set with even lower median latencies of 96±30 ms and 173±151 ms (median±i.q.r.) for P1 and P2 respectively. To compare to previous studies that classified finger and hand postures, movement completion metrics were calculated ignoring wrist flexion and rest trials (Table A.2.1).

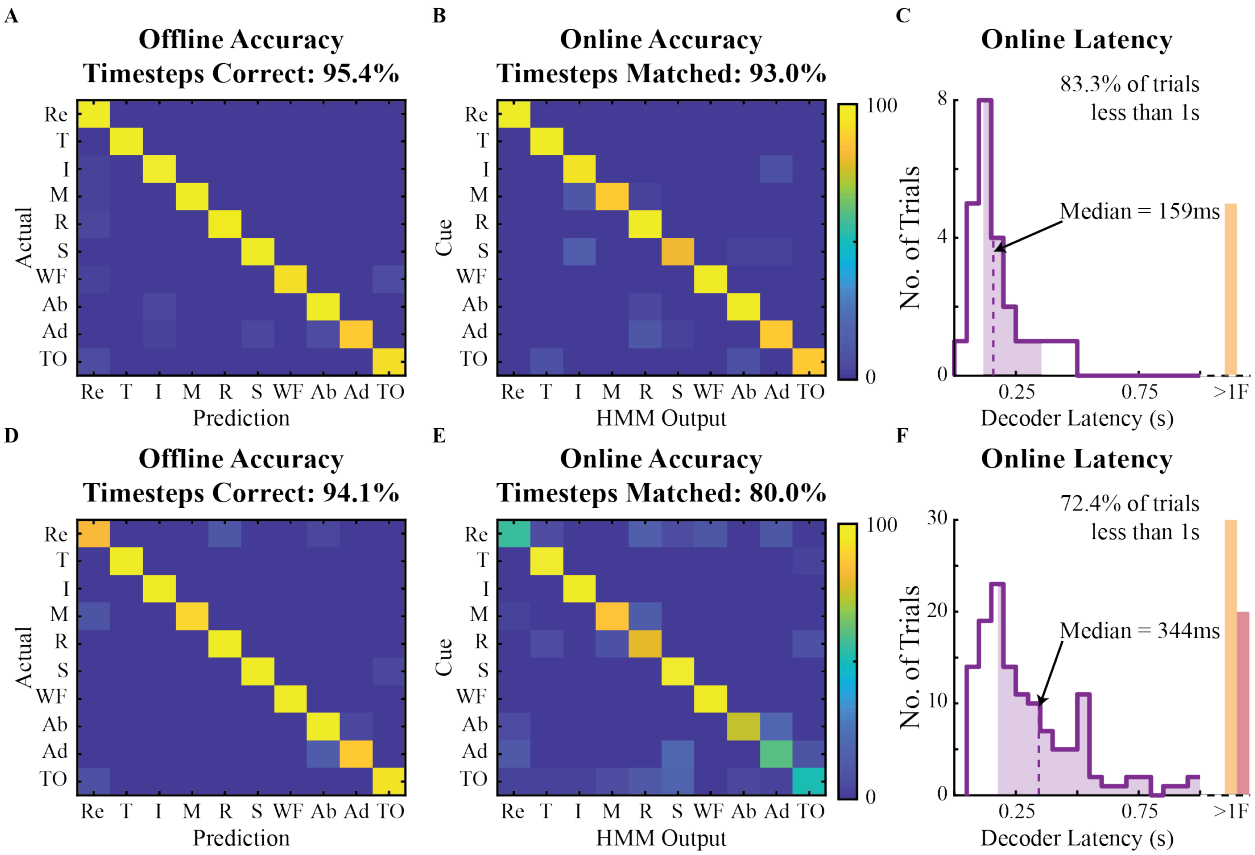

Figure 4.1 Online metrics of individual finger and wrist posture decoding. Participants controlled a virtual hand with the Hidden Markov Model (HMM-NB) to match 10 postures: flexion of all five fingers (T,I,M,R,S), wrist flexion (WF), finger abduction (Ab), finger adduction (Ad), thumb opposition (TO), and rest (Re). **(A)** Simulated offline performance of the HMM-NB during rest and hold periods for P1's training data (5-fold cross validation, 5-6 repetitions per movement). **(B)** An online confusion matrix captures transition errors to cued postures while P1 controlled the virtual hand in real-time. **(C)** Decoder latency was measured as the time difference between the onset of new EMG activity and a successful posture. The median (dashed line) and middle 50% (shading) is overlaid on histograms binned in 50 ms increments (n = 30 trials). Trials with latency greater than a second (>1) are aggregated in the orange rectangle. **(D)** Offline confusion matrix for P2 using training data from one experiment session. **(E-F)** Same as above for P2 across three single day experiment sessions (n = 181 trials). Trials where a one second continuous hold could not be maintained are marked as failures (F) and aggregated in the red rectangle

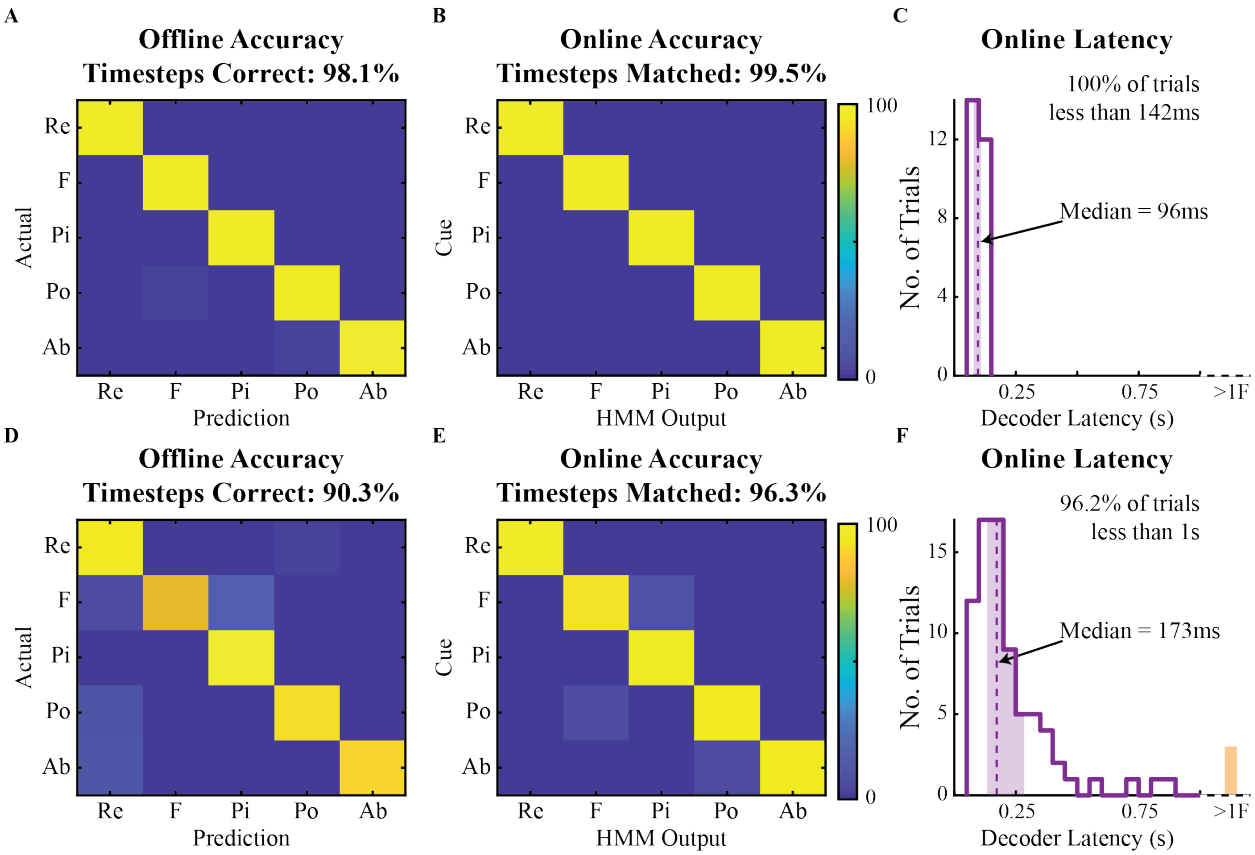

Figure 4.2 Online metrics of grasp decoding. A fewer number of functional grasps could be predicted in real-time with higher online accuracy and lower latency. **(A)** Simulated offline performance of the HMM-NB output distinguishing fist (F), pinch (Pi), point (Po), finger abduction (Ab), and rest (Re) for P1 (5-fold cross validation, seven repetitions per movement). **(B-C)** Online accuracy and decoding latency for P1 measured as in Fig. 4.1 (n = 26 trials). **(D)** Offline confusion matrix for P2 using training data from one experiment session (5-fold cross validation, five trials per movement). **(E-F)** Same as above for P2 across three single day experiment sessions (n = 79 trials). Trials with latency greater than a second (>1) are aggregated in the orange rectangle.

4.2.2 Robustness Across Arm Positions

In order to be of practical use for patients with upper limb amputations, decoders must be reliable to different physical contexts. P2 donned an i-Limb Quantum™ XS (Ossur, Reykjavik, Iceland) and was able to switch between functional grasps in eight different arm orientations. P2 had limited elbow range of motion, described in Supplementary Materials and Methods, and was asked to match arm postures to the best of her ability. The virtual reality environment was again used for cues and visual feedback to quantify decoding performance across 20-22 trials per arm position (Fig. 4.3A). The HMM-NB used for this exercise was trained with her arm and prosthesis resting on the table. Classifier performance remained robust across the majority of the arm

positions where transition errors were infrequent and quickly corrected (Fig. 4.3B,C). In six of the eight arm positions, P2 was able to control the virtual hand with online accuracy never dropping below 96% and a decoding latency of 173±113 ms (median±i.q.r). In two arm positions, arm raised and behind the back, there was a noticeable increase in transition errors to the cued posture, which occurred 7 and 6 times respectively. These positions at the superior and posterior extremes of her workspace had lower classification accuracy and a higher decoding latency of 301±299 ms. Even though there were more frequent errors in these two positions, the classifier did not completely fail and P2 was able to recover and achieve a successful one second hold within the timeout period on 100% of trials. In the same session. P2 used the same decoder to activate grips with her robotic prostheses following verbal instruction in five of the arm positions. During preliminary testing and demonstrations, P1 was able to activate the same set of postures using the LUKE arm (Mobius Bionics, Manchester NH) in three arm positions. P2 also activated individual flexion of fingers on the i-Limb in three arm positions, correctly executing 14 out of 15 flexion attempts.

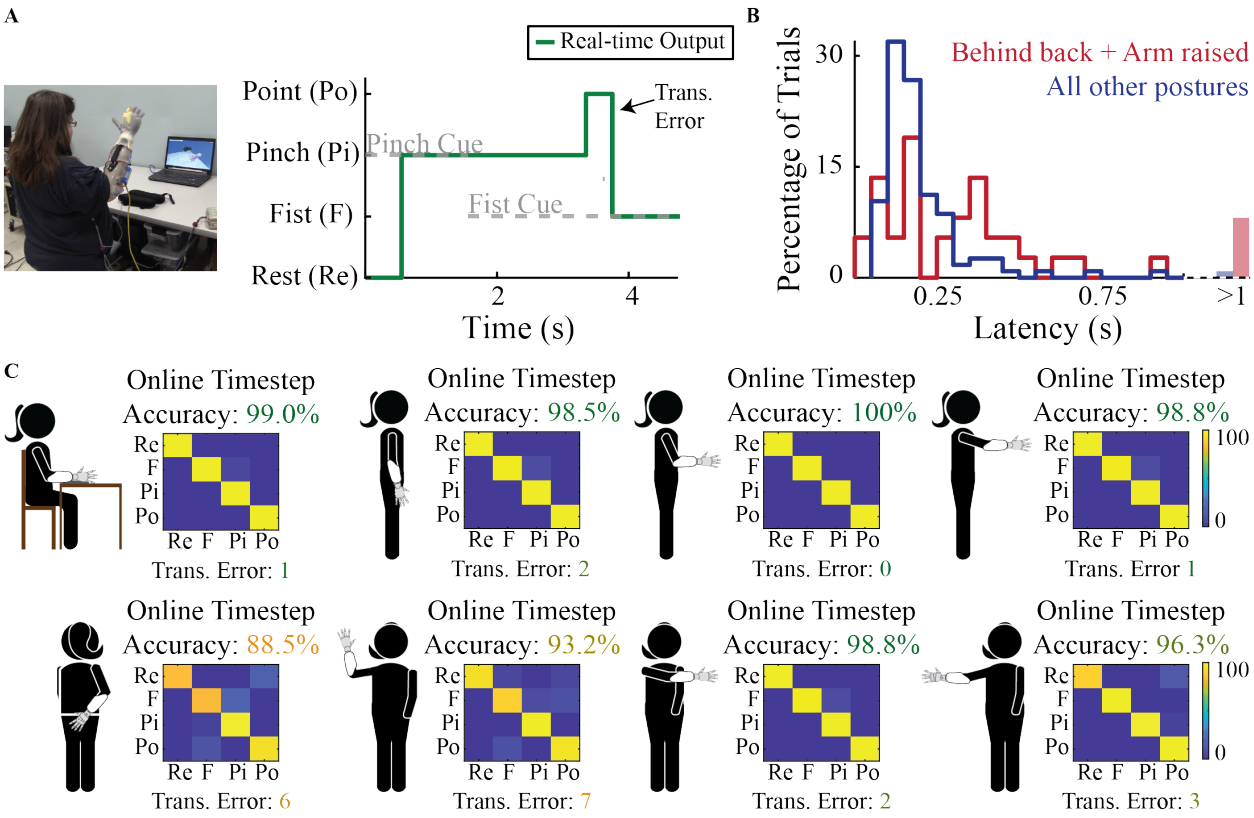

Figure 4.3 Decoder performance across eight different arm positions. P2 performed control experiments in the virtual reality environment to quantify decoder performance across eight different arm positions. **(A)** P2 donned her prostheses, but used the virtual reality environment to switch between fist (F), pinch (Pi), point (Po) and rest (Re). **(B)** P2 calibrated the HMM-NB with her arm resting on a table. Latency histograms binned in 50 ms increments for the majority of positions aggregated (blue, n = 116 trials), as well as the two positions with more frequent and longer transition errors (red, n = 37 trials). **(C)** In addition to online accuracy, the number of transition errors was also reported for each of the 8 positions.

4.2.3 Functional Prostheses Use

Both participants used the functional posture set to complete five trials of a Southampton Hand Assessment Procedure (SHAP)-inspired task (Fig. 4.4). Each trial consisted of five object interactions and required the activation of three different grasps. Participants were instructed to use specific grasps for the timer and each SHAP object. P1 used the LUKE arm to move SHAP heavy objects and completed the task with an average time of 18.75±3.42s (mean±s.t.d.). P2 used the i-Limb Quantum™ to move SHAP light objects and completed the task in 36.60±7.66s on average. P2 completed the objects in the reverse order. This made it easier for experimenters to assist with manual wrist adjustment for the power object. Both participants were largely successful,

performing 23 out of 25 interactions without dropping an object or failing to press the button. Additionally, P1 and P2 performed the instructed grasp during their first EMG activation attempt on 20 and 19 out of 25 interactions. The main issue P1 encountered was an inability to use point for timer stop. Interestingly, this error never occurred at trial start indicating the point could be activated under the right conditions. Both participants had instances where they led with a pinch to pick up the sphere. P1 seamlessly corrected and engaged the instructed fist grasp in all but 1 trial, while P2 needed to perform additional EMG activations for correction. The i-Limb took longer to switch between grips, so a state machine was coded that required P2 to issue a rest command before activating a grasp. This and the need for manual wrist adjustment contributed to the variation in completion times between participants.

A

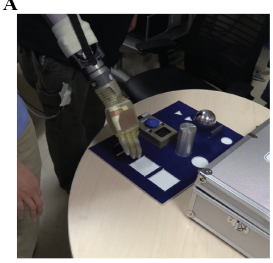

Trial Completion Time: 18.75±3.42s

	Button Start	Sphere	Power	Extension	Button Stop	**Total**
Sub-task Complete	5/5	4/5	4/5	5/5	5/5	**23/25**
Correct Grasp	5/5	4/5	5/5	5/5	1/5	**20/25**

B

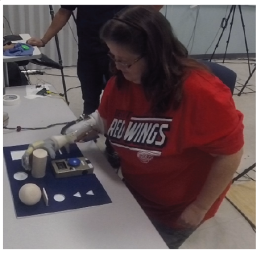

Trial Completion Time: 36.60±7.66s

	Button Start	Extension	Power	Sphere	Button Stop	**Total**
Sub-task Complete	5/5	5/5	5/5	3/5	5/5	**23/25**
Correct Grasp	5/5	3/5	4/5	3/5	4/5	**19/25**

Figure 4.4 SHAP inspired grip switching task. Both participants used their prostheses with the functional posture set to perform a task in which they were instructed to use specific grasps to interact with three objects and a timer. Sub-tasks were counted as complete if the participant succeeded on their first attempt, and correct grasps were counted when the instructed grasp was achieved on the first EMG activation attempt. **(A)** P1 used the LUKE arm and was instructed to use point to start the timer, fist for sphere, fist for power, and pinch for extension objects, before using point to stop the timer. **(B)** P2 used an i-Limb Quantum XS and completed the object trio in the reverse order. Completion time (mean±s.t.d, n = 5 trials) included manual wrist adjustments for P2.

4.2.4 Signal Strength and Specificity

The bipolar intramuscular electrodes recorded specific and spatially segregated EMG activity particular to individual finger movements. To visualize posture segregation, we used linear discriminant analysis (LDA) to define the top two discriminating dimensions for the 1 of 10 posture set (Fig 4.5). For this analysis, MAV from the 8 bipolar electrode pairs were processed with time history parameters that were input to a standard Naive Bayes classifier for successful real-time control (Table A.2.3). Rest data was excluded to maintain focus on movement distinctions. Overall, posture holds were well separated in the low dimensional space on both real-time and trial-averaged timescales. For P1, thumb movements were the most distinguished from other postures and separated along the first discriminant axis. For P2, wrist flexion was the best separated posture, along with flexion of the thumb or index finger in the first two discriminant dimensions. These movements were amongst those explicitly targeted by electrode implantation and were well represented by individual channels (Fig. A.2.3 and Fig. A.2.4). Additional discriminating dimensions would further separate movements, with 4-D embedding capturing approximately 90% of the variance in training data.

In addition to high specificity, the implanted electrodes also recorded large amplitude responses with a low noise floor (Fig. 4.6). For P2, we compared the SNR of five intramuscular channels to simultaneously recorded surface signals. Bipolar surface recordings were acquired using adhesive gelled electrodes (Biopac, Goleta, CA) connected to the same signal processing equipment. Across the compared channels, the average SNR for implanted electrodes was 105.4±82.6 and 152.5±138.6 (mean±s.t.d) gain for P1 and P2. P1 did not participate in a surface session, while P2's surface signals averaged an SNR of 8.5±6.6. A high surface SNR of 19.6 was observed during finger abduction which prompted a full splay of the hand. We recorded this

movement with surface electrodes targeting extensor pollicis longus (EPL) as described in Supplementary Materials and Methods. However, it is possible we also recorded activity from extensor digitorum communis (EDC) or other nearby muscles. Deep muscles that control individual finger movements were more difficult to capture from the surface. Gelled electrodes targeting flexor digitorum profundus of the index finger (FDPI) recorded signals with an SNR of 2.26 during index finger flexion. The SNR for simultaneously recorded implanted electrodes was 244 for EPL and 66 for FDPI. We also measured SNR for electrodes implanted into RPNIs, however attempts to accurately target and record matching surface EMG were unsuccessful. By nature, RPNIs also do not have a direct functional correspondent, so residual muscles that control related movements were selected for comparison. Across all the comparisons conducted with P2, implanted electrodes provided a 6 to 30-fold SNR improvement.

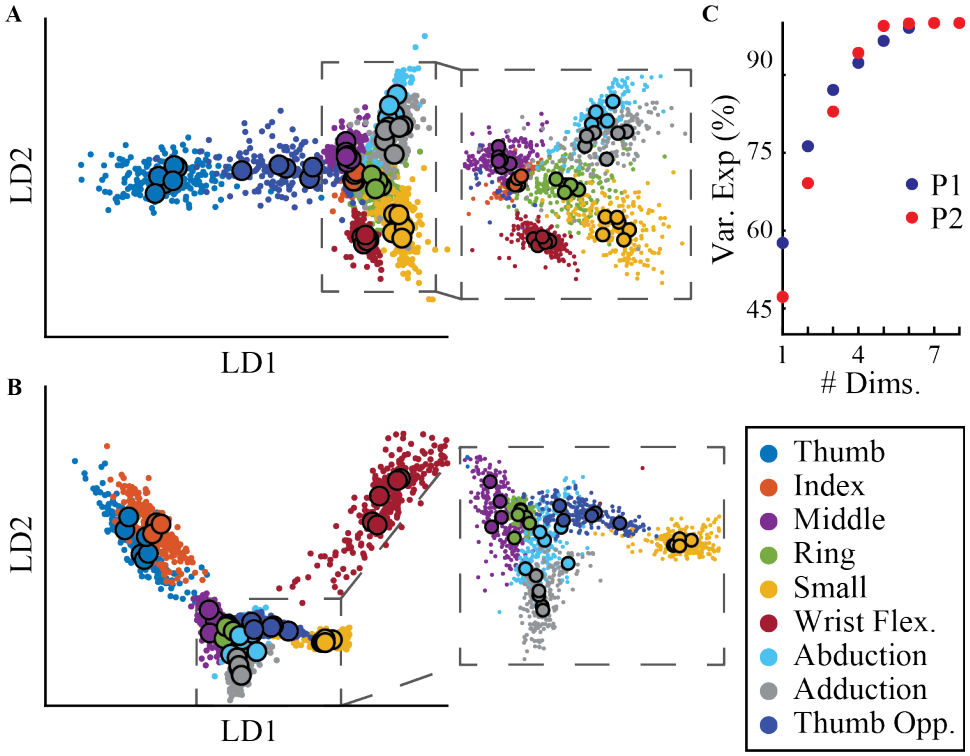

Figure 4.5 Dimensionality reduction to view posture separation. MAV from eight channels reduced to two discriminant dimensions found using LDA. Large outlined points indicate trial averages, while small dots represent individual timesteps during posture holds. Dashed boxes magnify separation of relatively close movements. **(A)** MAV for P1 was processed in non-overlapping 50 ms time bins. **(B)** MAV for P2 was processed in a sliding 200 ms window updated every 50ms. **(C)** Cumulative variance explained by additional dimensions.

A

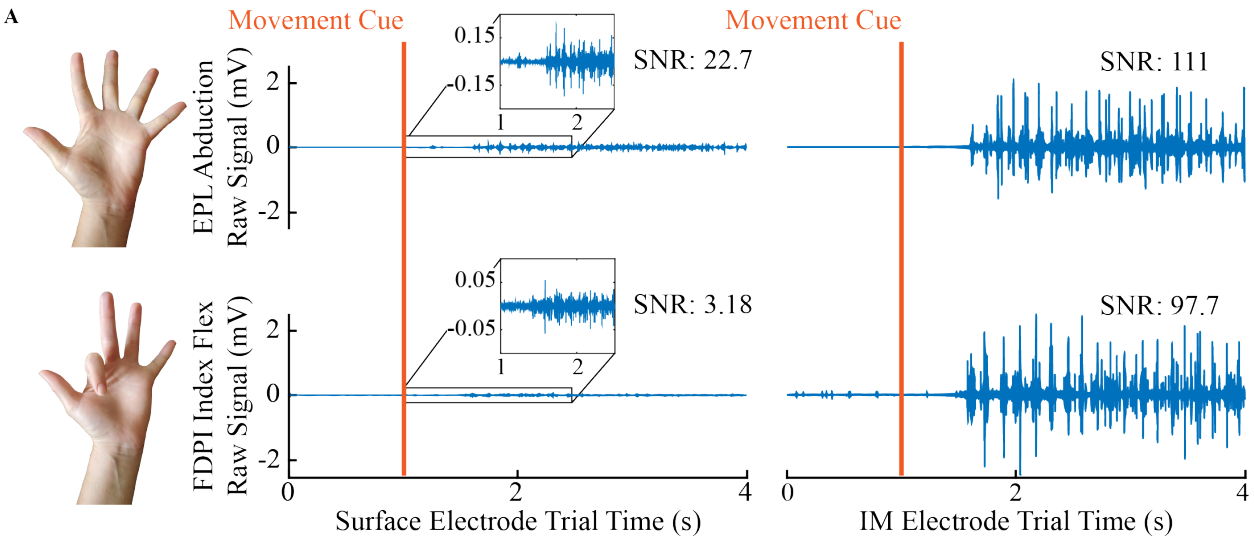

B

Movement	Thumb Flexion	Small Flexion	Index Flexion	Wrist Flexion	Finger Abduction
IM Channel	**Median RPNI**	**Ulnar RPNI**	**FDPI**	**FCR**	**EPL**
P1 IM SNR	251	54.1	56.4	88.5	77.2
P2 IM SNR	23.0	79.7	66.0	350	244
Surface Target	**FPL**	**FDPS**	**FDPI**	**FCR**	**EPL**
P2 Surface SNR	5.33	6.65	2.26	8.82	19.6

Figure 4.6 SNR of intramuscular and surface EMG for finger movements. Signal-to-Noise Ratios (SNR) from implanted (IM) electrodes from both subjects and simultaneous surface recordings from P2. **(A)** Example SNRs from individual movement trials with simultaneously recorded surface and implanted electrodes from P2. For both movements, the trial with the highest surface SNR was chosen. **(B)** SNRs were calculated for implanted channels by averaging the active and rest RMS voltages across 5 trials of the individual finger movement most relevant to the targeted muscle. For P2, simultaneous surface recordings were obtained by individually targeting implanted residual muscles. For RPNI comparisons (purple), appropriate residual muscles were selected based on the cued movement.

4.2.5 Alternate Classifier Simulations

The HMM-NB models underlying state transitions to rapidly issue accurate predictions. Classification stability and accuracy can also be improved by adding time history and additional informative features. Fig. 4.7 demonstrates the offline ability of the HMM-NB and a standard Naïve Bayes (NB) classifier as well as three alternate classifiers distinguishing the 1 of 10 posture set. The alternate classifiers used 5-time domain features and 6th order auto-regressive coefficients to characterize EMG from each channel. Increasing window length did not create multiple time

points for input, preventing alternate classifiers from modelling EMG patterns over time. P1's alternate classifiers yielded improvements in combination with larger processing windows, however this difference was not robust for P2 across four training sessions. Overall, the performance difference between NB using only MAV and each alternate classifier was not significant for implanted electrodes ($p > 0.2$, paired t-test, $n = 35$ window lengths across 5 datasets). However, additional features proved beneficial when applied to P2's surface EMG, which NB could not well distinguish from only MAV. Adding features increased P2's surface performance by 17.8±10% (mean±s.t.d.) across all window lengths without changing the classification model. By comparison, additional features did not significantly impact NB performance with the implanted electrodes ($p > 0.5$, paired t-test, $n = 35$ window lengths across 5 datasets). The HMM-NB consistently improved simulated performance over NB, and overall outperformed each alternate classifier ($p < 0.01$, paired t-test, $n = 42$ window lengths across 6 datasets). The HMM-NB most noticeably improved performance for smaller processing windows. These results indicate that algorithms modelling state transitions or EMG dynamics can improve accuracy and remain robust to smaller processing windows. This potentially benefits real-time control applications by reducing a trade-off between responsiveness and stability. An online comparison between the NB classifier and the HMM-NB is detailed in Supplementary Materials and Methods. Both participants used the NB classifier to complete the 1 of 10 posture switching task with average online accuracy of 85.8% and latency of 328 ms. These results are promising for situations that demand simplicity or are highly sensitive to computational workload.

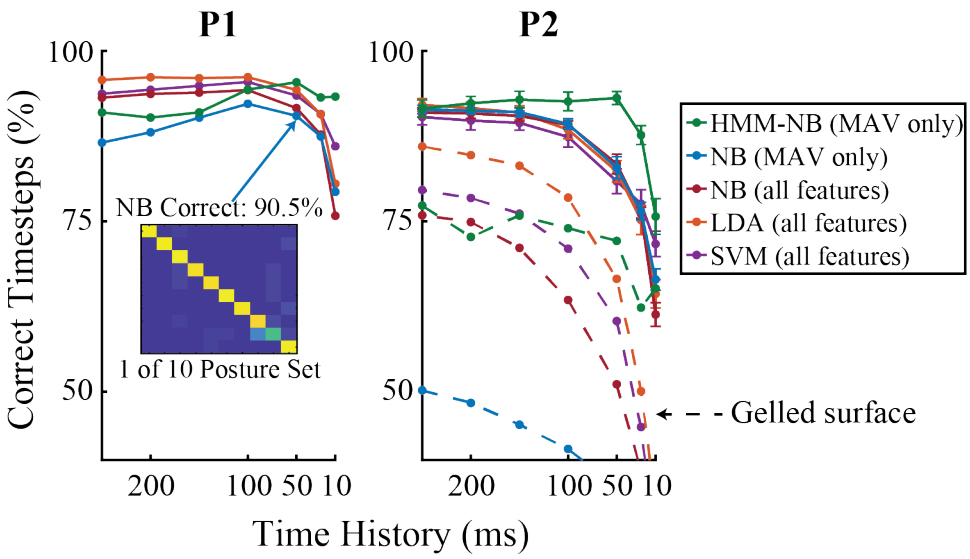

Figure 4.7 Offline alternate classifier simulations. Offline performance of different algorithms evaluated across 7 increasing window lengths on the 1 of 10 posture set for P1 and P2. The Hidden Markov Model (HMM-NB) and a standard Naïve Bayes classifier (NB), used only mean absolute value (MAV) as an input feature. An alternate NB implementation, linear discriminant analysis (LDA), and a support vector machine (SVM) used five time domain features and 6th order auto-regressive coefficients per channel. Classifiers were evaluated across individual timesteps during hold and rest periods using 5-fold cross validation. Dashed lines for P2 represent performance using EMG recorded from eight bipolar gelled adhesive surface electrodes. Performance with P2's implanted electrodes (mean±s.e.m) was evaluated for simultaneously recorded intramuscular EMG and three calibration sessions used for real-time control experiments.

4.3 Discussion

In this study, we have demonstrated that implanted electrodes record high-quality EMG signals from RPNIs and residual innervated forearm muscles in two persons with transradial amputations. Both participants were implanted with electrodes targeting the same individual finger movements and were able to control a virtual hand to distinguish the same posture sets which included individual finger, intrinsic, and compound hand movements. The posture switching task tested real-time control capabilities of the high speed pattern recognition system, allowing users to directly switch between postures and rest. The speed and accuracy of our pattern recognition system with implanted electrodes, to distinguish finger movements, exceeds earlier work which quantified real-time performance in virtual environments (Table A.2.1). In a controlled environment, the HMM-NB also distinguished a smaller set of functional postures in novel static

arm positions. P2's performance was consistent across the majority of the workspace, which we attribute to the stability of signals from the implanted electrodes. Finally, we demonstrated that participants could use the high speed pattern recognition system to control advanced robotic prostheses, eliminating the need for time consuming grip triggers or selection schemes. The LUKE arm came equipped with real-time research software that allowed P1 to achieve functional control similar to the virtual environment. He was able to activate grasps without a perceived delay and seamlessly switch between postures. P1 leveraged this capability to use the pinch and fist grasps to manipulate the SHAP sphere. For P2, our pattern recognition system was adapted to work with commercially available grip selection software, similar to previous work (Kanitz et al., 2018; Krasoulis et al., 2020; Kuiken et al., 2009). Enforcing a grip entry/exit structure can improve stability, however it increases the effort required to correct erroneous outputs. Furthermore, the ability to move directly between hand postures has been shown to improve functional performance (Piazza et al., 2020). Regardless of the hand interface, implementing proportional control will be beneficial for more precise tasks. The specificity of the indwelling electrodes offers the ability to directly map muscle activations to individual fingers. Different mappings can be explored to either improve precision within i-Limb grips or increase dexterity of the LUKE arm during object manipulations.

Pattern recognition is just one approach being considered for intuitive grasp control, although it may be the most practical and immediately applicable technique, because it pairs well with commercially available hand software. Furthermore, classifiers can be computationally inexpensive and remain accurate when increasing the number of predicted movements relative to the number of input channels (Kanitz et al., 2018; Krasoulis et al., 2020; Li et al., 2010). For example, in Vu et al., P1 was able to activate rest and four finger postures using only two EMG

channels (Vu et al., 2020). However, it can be challenging for classifiers to generalize to new contexts. In both participants, arm movements occasionally produced unintentional extensor activity. Ignoring unreliable channels was a quick and effective solution for this study, but could limit the number of predictable grasps compared to more robust classifiers (Betthauser et al., 2018). Changing EMG patterns during object interactions also led to some misclassifications when P1 pressed the timer button with the point grasp. Similar phenomena have been noted in other research applications (de Luca, 1979; Hudgins et al., 1993) and could be a natural product of the motor system (Alaerts et al., 2012; Downey et al., 2018; Krasoulis et al., 2019). Regression algorithms are being explored in combination with implantable electrodes for multiple DOF hand control (Dewald et al., 2019; Davis, et al., 2020; Vu et al., 2020). In addition to increased dexterity, regressors may be more robust to changing contexts (Hahne et al., 2018). However, there are limitations on the number of DOF that can be simultaneously and independently activated. Biomechanical control strategies are also being developed that use a principled musculoskeletal model to provide robust estimates of intended joint kinematics and torques (Kapelner et al., 2020; Sartori et al., 2018). In order to be effective, regression and biomechanical techniques require the prosthetic hand to allow precise and simultaneous control of individual fingers. The ability to incorporate an active wrist is also an important consideration for algorithm development, as it allows for more natural body movements (Gates et al., 2016). Ultimately, the signal quality and strength of implanted electrodes is relevant to any EMG control paradigm. Our signal processing and feature extraction provide a stable proxy for local motor unit activity for residual muscles or the peripheral nervous system via RPNIs (Vu et al., 2018, 2020). Signals from implanted electrodes can be stable for months to years (Dewald et al., 2019; Vu et al., 2020), which is

advantageous for pattern recognition and regression algorithms as large calibration datasets can readily be assembled.

Our experimental system used indwelling electrodes that exited the skin and were connected to a computer. While we have found these signals stable over years, this is not a viable long-term solution for most users. The signal processing chain can readily be adapted to a low-power architecture (Irwin et al., 2016), however many other system features need to be considered. Multi-channel percutaneous electrical connectors have been developed (Mooney et al., 1974), but risks of complication and infection have limited their use to temporary or life-saving medical devices (Koch et al., 2019). Osseointegration is a hardware innovation that improves the mechanical linkage between user and prosthesis. In our study, we observed unintentional muscle activations during some arm movements and reduced performance at the extremes of P2's range of motion. For some patients, osseointegration may mitigate these issues and improve controller reliability by reducing the effects of prosthesis weight. It also has the benefit of creating a direct physical feed-through for intramuscular electrodes (Boni et al., 2018; OrtizCatalan et al., 2020). However, it is limited to patients that meet anatomical criteria such as residual limb length. Fully implantable wireless devices have gained traction for neuromodulation therapies (Coffey, 2009; Verrills et al., 2016). By modifying these approved neuromodulation systems, development and certification costs can be reduced by utilizing shared platforms across the industry (B. Smith et al., 2005).

This study focused on expanding the capabilities of pattern recognition algorithms to extract hand motor commands reflective of user intent. However, a lack of sensory feedback and proprioception can limit the benefits of myoelectric devices. For example, even though thumb opposition and finger abduction were accurately predicted offline, P2 had difficulty activating

these postures during real-time control. P2 reported limitations on proprioceptive feedback in her phantom limb, notably including her thumb metacarpal phalangeal joint. Additional practice (Krasoulis et al., 2019) or enhanced training strategies (Nam et al., 2017) could potentially resolve this issue. However, improved feedback mechanisms (D'Anna et al., 2019; George et al., 2019; Srinivasan et al., 2017; Tan et al., 2014) may be necessary for some patients to realize the full potential of improved motor control. Increasing the responsiveness, precision, and sensory feedback can provide additional benefits for prosthetic users such as increased trust (OrtizCatalan et al., 2020), increased embodiment or reduced phantom limb pain in some users (Page et al., 2018). Regardless of the specific algorithm or control strategy, the stable and highly specific EMG afforded by indwelling electrodes can play a significant role in improving prosthetic control and user satisfaction in the coming years.

4.4 Materials and Methods

4.4.1 Signal Processing and Experiment Set-Up

The two participants with RPNIs and indwelling electrodes labelled P1 and P2 for this study, were respectively labelled P3 and P4 in Vu et al. (Vu et al., 2020). Detailed anatomical information is also present in Supplementary Materials and Methods. Briefly, both participants had bipolar electrode pairs (Synapse Biomedical, Oberlin, OH) chronically implanted into their ulnar and median RPNIs along with the following residual muscles targeting finger and wrist functions: Flexor Pollicis Longus (FPL), Flexor Digitorum Profundus - Index Finger (FDPI), Extensor Pollicis Longus (EPL), Extensor Digitorum Communis (EDC), and Flexor Carpi Radialis (FCR). P1 also had an electrode pair implanted in Flexor Digitorum Profundus - Small Finger (FDPS). EMG from the implanted electrode contacts was amplified, sampled at 30kSps, and

referenced with a Cerebus Neural Signal Processor (Blackrock Microsystems, Salt Lake City, UT). The Cerebus simultaneously recorded and sent referenced EMG to a Matlab xPC (Mathworks, Natick, MA) for real-time processing. Fig. 4.8D shows the signal processing chain on the xPC for online decoding. The xPC applied the 100-500Hz band-pass filter and down-sampled EMG to 1 kSps, from which mean absolute value (MAV) was the only feature extracted for online decoding. The xPC sent UDP packets to manipulate two virtual hands (Kumar & Todorov, 2015) which were presented to the subject on an external laptop. A lead hand to cue postures was positioned in the foreground, while a secondary hand which the subjects could control was positioned in the background. The xPC's real-time guarantee ensured that EMG was processed and time-synced with behavioral data and decoders executed within one millisecond.

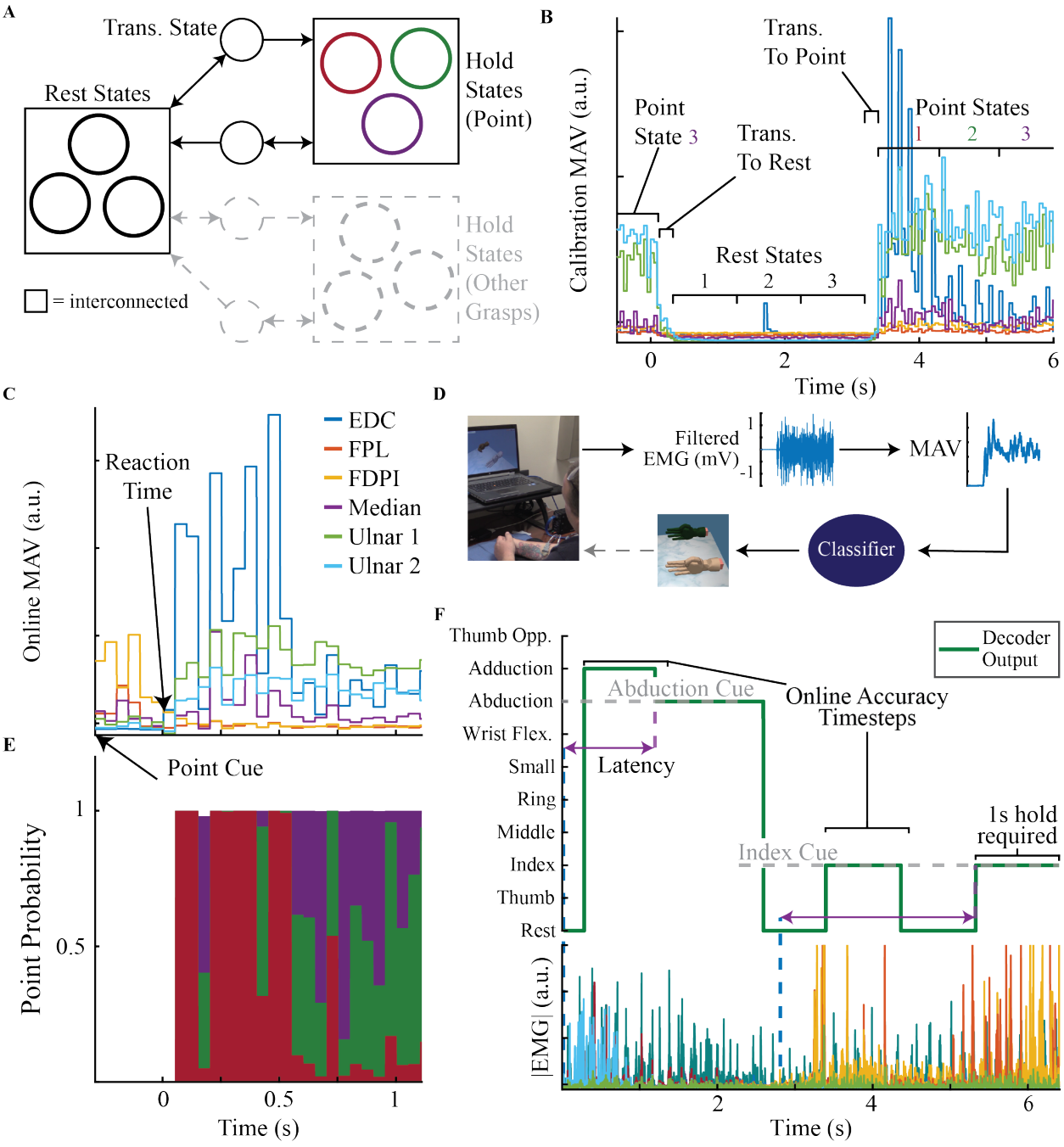

Figure 4.8 Details of posture switching task and HMM architecture. **(A)** The HMM-NB contained three interconnected states for rest and posture holds with one transition state to and from rest. Point highlighted for example. The probability of a posture was determined by summing the probabilities of the rest and hold states. **(B)** An expectation-maximization unsupervised learner was carefully initialized by placing rest and hold states sequentially along active hold periods with transition states in between. Mean absolute value (MAV) was the EMG feature used for online decoding. **(C)** P2's online activity during a switch to point posture. **(D)** Participants controlled a secondary hand (background) with visual feedback to match posture cues (foreground). **(E)** Optimized latent states of the online decoder capture EMG dynamics in C. One state (red) reflects a sharp increase in EDC activity while two states (green and purple) capture continued hold of the Ulnar RPNIs. **(F)** Participants were required to hold the cued posture for one second continuously before the next cue was presented. Decoder latency measured classifier responsiveness as the time difference between new EMG activity and a successful hold. Online accuracy was evaluated across individual timesteps for the first second of transition to the cued posture. 1 of 10 posture set with errors shown for example.

4.4.2 Hidden Markov Model for Real-Time Control

Many EMG classification algorithms are error prone when users move between postures or during extended holds. This is because they characterize postures as an average point in feature space and have no knowledge of the prior state or capability to model transitions. Common methods to improve performance are to increase the length of the processing window for stability or add additional output filters to reduce transition errors. These methods are effective, but they automatically introduce a compromise between classifier stability and responsiveness (Smith et al., 2011). Here, we explore a more principled solution. The Hidden Markov Model (HMM-NB) models transitions between latent states and closely resembled previous work (Kemere et al., 2008). The probability of a latent state occurring is determined both by the observed EMG inputs as well as the occurrence of previous states. A linear transition matrix determined the likelihood of moving from one latent state to another and optimally smoothed transitions. A Naive Bayes model represented three interconnected "hold" states per posture which can capture dynamic EMG patterns. The model also contained "transition" states going to and from rest as shown in Fig. 4.8A. State models were carefully initialized by splitting the active period or rest periods of the training data into thirds Fig. 4.8B. Active periods were automatically marked in training data per trial by retroactively finding active channels and selecting the starting point of when their MAV exceeded 4 times the standard deviation of the trial's rest data for at least 200ms. The transition matrix for “hold” and “rest” states was initialized with an equal probability of remaining in or moving to another connected state. “Transition” states were initialized with a 0.9 probability of remaining in the state. We limited the expectation-maximization algorithm (Rabiner, 1989) to five iterations and selected parameters from the iteration with the highest likelihood on held out test data. During online decoding, the probability of a given posture or rest was taken as the sum of the three “hold”

or “rest” state probabilities as shown in Fig. 4.8E. The “transition” states were not selected for output because they represented the beginning of activations from rest, while participants could directly switch between grasps during real-time control. Fig. 4.8C shows an example of P2 initiating a point during online control. The solution found by the HMM-NB captures her changing EMG patterns, as shown in Fig 4.8E. The inclusion of multiple latent states per posture increases modeling capabilities and the ability to model transitions allow the HMM-NB to operate with less time history than steady-state classifiers. Performance comparison to a standard NB classifier and analysis are included in Supplementary Materials and Methods.

4.4.3 Virtual Posture Switching Task

Table A.2.2 shows the posture sets explored in this study. MAV from all eight channels and calculated with 50 ms of time history, was used to control the virtual hand for both the 1 of 10 and grasps posture sets. P1 had significant time constraints during the course of the study. He performed one session of the virtual posture switching task for both the 1 of 10 and grasps posture sets. P2 completed three sessions for both posture sets. To calibrate the HMM-NB, participants matched the virtual cue hand with their phantom hand to the best of their ability. Participants faced the external laptop while resting their arm on the table in a neutral and comfortable position. Calibration runs involved participants holding each of the desired postures 5-7 times for 2.5-3 seconds with an equal length rest period in between each hold. Where possible, calibration runs were completed on the same day before online control runs. Even though the total routine was relatively quick (approximately five minutes or less), older calibrations – 18 days for P1’s 1of 10 posture switching task and 16 days for P2’s arm position test – were used twice to save time and effort. During online real-time control, participants actively controlled the secondary hand and attempted to match the cue hand. Participants used a free running classifier, meaning the decoder

output was never automatically reset to rest or a particular posture. The secondary hand turned green when the decoder output matched the cued posture as an additional success indicator. Participants were required to match the cued posture for one second without interruption. If the participants failed to achieve a one second hold within 10 seconds, the trail was considered a failure. A five second timeout was used for P2's arm position test. After a successful hold or failure, a new posture was immediately cued in a pseudo-random order. This task encourages participants to directly switch between postures at a faster pace than the training procedure. The requirement of a continuous hold ensures that successful algorithms must be both stable and responsive. In summary, the posture switching task was designed to be indicative of a classifier's capability to actively control prostheses in real-time.

Fig. 4.8F highlights two of P2's real-time control trials with errors to demonstrate the analysis metrics for the posture switching task. Online classification accuracy was evaluated across individual timesteps for the first second of transitions to the cued posture. Perfect accuracy required the classifier to switch and maintain a one second successful hold without any error. The one second hold length was chosen to be similar to the selection period in previous work (Kuiken et al., 2009; Li et al., 2010). Sometimes, participants would pause before attempting the cued posture, possibly due to physical or mental fatigue. Rest outputs under those circumstances were ignored, however moving from the cue to rest was penalized. Decoder latency measured classifier responsiveness and controllability. Latency was calculated as the time difference between the onset of new muscle activity and the beginning of a successful hold. EMG onset was determined visually by viewing the filtered and rectified EMG for each trial and marking the beginning of a new EMG pattern. EMG onset approximates reaction time and averaged 604.9±268.8 ms for P1 and 517.8±281.6 ms for P2 (mean±s.t.d.). Latency was not calculated for trials without a distinct EMG

change or when the pseudo-random order produced a duplicate. These were rare occurrences, accounting for 3.5% of all trials. Failed trials were marked with a 10 second latency to reflect task timeout. Median and i.q.r. were used to characterize latency since the distributions did not have a normal shape.

4.4.4 Functional Testing

The functional posture set was used to test decoder stability across arm positions and to complete the SHAP inspired task. P2 completed one arm position session quantified with virtual posture switching task described above. Both participants performed the SHAP-inspired task in one session. The functional posture set matched the direct control strategy for robotic prostheses which used rest to open the hand. We did not employ a distinct hand open state because the robotic hand interface was sensitive to instabilities. We observed instances of unintentional extensor activity during arm movements, which could erroneously trigger finger abduction predictions. Incorporating an active hand open signal for proportional control is a consideration for future studies. P2's functional decoder used MAV from her RPNIs, FPL, FDPI, and EDC. EPL was observed to activate unintentionally during arm movements and held out. FCR was not observed to cause any issues but was removed as a precaution since it was not necessary to distinguish grasps. P1 used a decoder that received MAV only from his RPNIs, FPL, FDPI, and FDPS electrodes. Alternate channel combinations were not explored due to time constraints.

Both participants donned myoelectric prostheses to perform the SHAP-inspired tasks. Participants relied solely on their robotic prostheses for visual feedback of the pattern recognition system. Durplex sockets were fabricated for each participant's residual limb at the University of Michigan Orthotics and Prosthetics center by a certified prosthetist. To control physical prostheses, the xPC sent commands via serial connection to a custom circuit board which issued the

appropriate CAN messages for each hand. The software interface controlled robotic prostheses by directly translating predicted postures to closed grasps while rest commands opened the hand. For P1, the internal controller on the LUKE arm operated in position control mode. Finger positions corresponding to the endpoints of the current predicted posture were sent to the LUKE arm, which processed updates every 10ms. For P2, a state machine was coded to interface between the xPC and i-Limb which closed and opened selected grips. The i-Limb interface introduced a hardware delay due to the time to process a grip change. However, the compact form factor of the extra small i-Limb Quantum was greatly preferred for P2, who could not lift the LUKE arm. The SHAP-inspired task was evaluated by trial time and two qualitative metrics. A sub-task was counted as complete if it was performed in a single attempt. It was possible to complete tasks without using the instructed grasp. The number of sub-tasks where the correct grasp was achieved without multiple activation attempts was also counted.

4.5 Acknowledgements

The following colleagues contributed to this work: Philip Vu, Cynthia Chestek, and Deanna Gates helped design the study. Philip Vu, Naia North, and Alicia Davis helped gather data and develop analysis techniques. Paul Cederna and Theodore Kung. developed and performed the surgical implantation procedure. Alicia Davis fabricated and fit the prototype sockets. Christina Lee collected range of motion measurements and assisting during experiments. Kelsey Ebbs managed regulatory compliance and clinical trial coordination. Michael Gonzalez built a socket adapter for the LUKE arm, and John Busch helped develop the RS232-CAN interface for the LUKE arm. This work was supported by the Defense Advanced Research Projects Agency (DARPA) Biological Technologies Office (BTO) Hand Proprioception and Touch Interfaces

(HAPTIX) program through the DARPA Contracts Management Office grant/contract no. N66001-16-1-4006 and by the National Institute Of Neurological Disorders And Stroke of the National Institutes of Health under Award Number R01NS105132. Philip Vu was supported by the National Science Foundation Graduate Research Fellowship Program under Award Number DGE 1256260.

Chapter 5 Dexterous Hand Control with Peripheral Interfaces

These results were submitted as an abstract to the Myoelectric Controls Symposium 2020. However, the conference was postponed due to COVID-19. This thesis expands on those results with additional details, analysis, and discussion.

5.1 Introduction

Pattern recognition systems can allow prostheses users to intuitively activate different grips of multiarticulating hands. In Chapter 4, we demonstrated that intramuscular electrodes and a high-speed pattern recognition system can may increase the number of movements that can reliably be activated. However, other challenges associated with grasp control remain unresolved by commercial technologies. First, since individual flexor activity cannot reliably be measured via surface EMG, a global proportional control signal is often applied across all grips. Specifically, rectified EMG is integrated over time, averaged across all input channels, and then thresholds and gains are tuned per user preference (Kuiken et al., 2016). This requires users to learn how to modulate grips with a uniform contraction instead of directly controlling active fingers. Second, most multi-articulating hands require a return to a fully open position before activating a new grip. This prevents users from being able to manipulate or handle objects, which may limit the practical benefits of grasp distinction (Piazza et al., 2020).

At a minimum, multi-articulating hands have two motors to support actuation of power and precision functions. Most commercial devices have a single motor per finger and an additional motor for thumb opposition. Independent control of these motors is technically feasible but rarely used due to a lack of independent control signals. RPNIs and other intramuscular recording

electrodes now provide more movement-specific signals (Vu et al., 2020). As a result, hand manufacturers will likely support individual finger control as these technologies move closer to clinical practice. In addition to specificity, intramuscular electrodes have also been shown to improve the precision of proportional control (OrtizCatalan et al., 2020). Previous work with RPNIs in able-bodied primates has shown accurate position tracking of digits with a linear Kalman Filter (KF) (Vu et al., 2018). In this study, we combine our high-speed movement classifier, the Hidden Markov Model (HMM), to predict movements in combination the linear KF. Both of our participants with transradial amputations and indwelling electrodes used this system to control 2 DOF simultaneously. Performance was measured using a virtual target task that required participants to match positions of the index and middle-ring-small (MRS) fingers.

5.2 Results

For each patient, Kalman Filters were trained to model individual and combined flexion of the index and MRS fingers, rest, and a combined finger extension. A Hidden Markov Model (HMM) switched between the five movement states and loaded control parameters specific to individual and combined finger movements (Wu et al., 2004; Yu et al., 2007). The switching architecture prevented unintended coactivations by freezing inactive fingers. Decoder parameters were trained by cueing each patient to follow a virtual hand as it fully flexed or extended different movements. The online target task required patients to simultaneously move both fingers to full and partial position targets within a tolerance. To approximate task difficulty, an able-bodied subject also completed the task with a data glove as shown in Table 5.1. P1 successfully navigated to 99% of the presented targets. He was able to approach performance of the able-bodied subject, but with reduced path efficiency and increased orbiting time. This indicates minor issues

stabilizing finger positions and a few unintentional state activations. P2 was still able to successfully reach 91% percent of the targets within the timeout period. However, she had more difficulty stabilizing around the targets and activating the correct fingers. Eliminating extension movements from the kinematic space greatly improved her performance.

	Trials (n)	Success Rate (%)	Acquisition Time (ms)	Orbiting Time (ms)	Bit Rate (bps)	Path Efficiency (%)
P1	101	99	872±77	191±72	1.79±0.08	73.8±2.5
P2	64	91	1772±233	510±156	1.15±0.10	53.7±4.2
P2 (flex only)	109	99	1026±82	141±51	1.52±0.10	61.8±2.5
AB (glove)	109	100	721±31	50±21	1.80±0.06	86.8±1.5

Table 5.1 Performance metrics for the 2-DOF target task with peripheral interfaces. The task was performed by P1, P2, and an able-bodied (AB) subject. P1 and P2 controlled the virtual hand with their EMG using switching Kalman filter (SKF), while the able-bodied subject used a data glove that tracked his finger positions in real-time. P2 also completed one session where the decoder was only required to move to flexion targets from rest.

The differences in classifier performance between P1 and P2 was reflective of their overall task performance as shown in Figure 5.1. This task required distinction between a similar number of movements as Chapter 4. However, from the perspective of both the user and decoder, it was more difficult because it spanned several movement conditions including full activations, subtle movements, and fine adjustments of two continuous DOF. The HMM accurately tracked P1's movements to both full and intermediate targets. Across both subjects, we did not observe large differences in classifier accuracy between partial and full movements during real-time control, even though the decoders were only trained on full target distances. For P2, the HMM did not perform as well, often confusing rest with extension and all finger flexion with index only flexion. The latter was still noticed when extension movements were removed, although overall performance improved. Figure 5.2 shows that P1's online behavior was consistent, and his decoder robust to differences between his calibration. P2's behavior was less consistent and shows remaining extensor activity from previous trials, possibly from effort to stabilize her decoder.

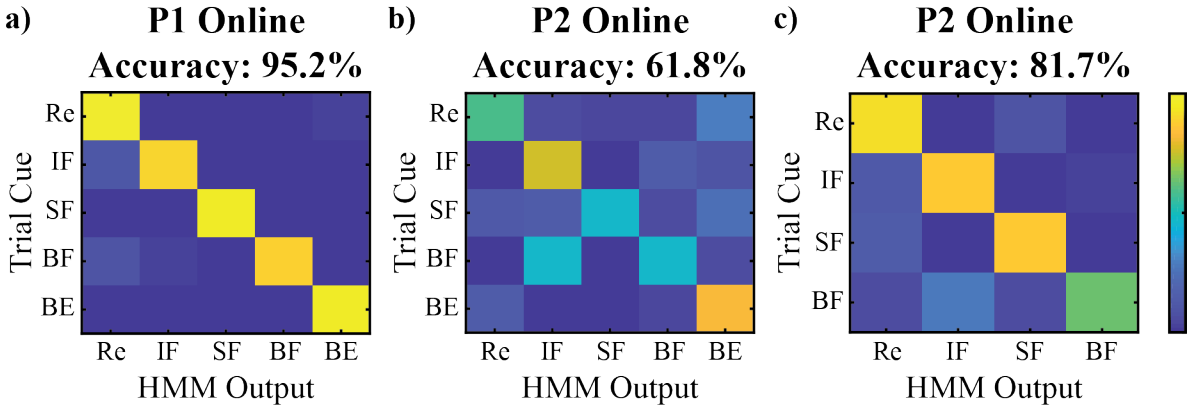

Figure 5.1 : Classifier accuracy during online continuous control. **a)** P1 classifier accuracy for rest targets (Re) and partial and full movement targets for index flexion (IF), MRS flexion (SF), flexion of all four fingers (BF), and extension of all four fingers (BE). **b)** same for P2. **c)** P2's classifier accuracy improved when only flexion movements were considered.

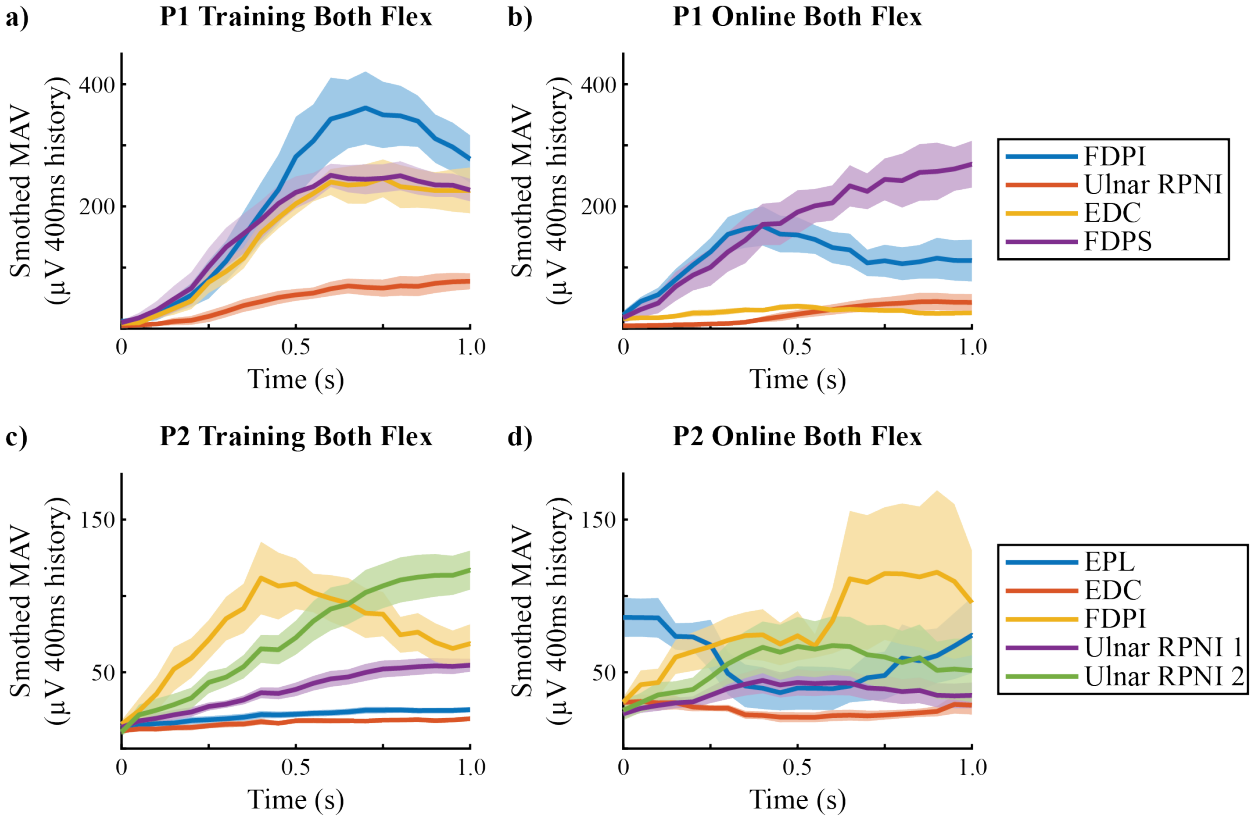

Figure 5.2 EMG envelopes during calibration and online control. **a)** Smoothed EMG envelopes (mean±s.e.m.) for training cues where P1 fully flexed both his MRS and index fingers. **b)** activation envelopes of the same channels for similar targets during real-time control. Trials were time aligned such that time = 0s is the onset of EMG activity. **c,d)** same for P2.

5.3 Discussion

In this study, both participants were able to use a 2 DOF grasp controller to simultaneously match finger position targets at intermediate and end points of the range of motion. These results demonstrate that RPNIs and indwelling electrodes can restore some dexterous grasping functions in persons with amputations. An HMM was chosen to distinguish active finger movements for the SKF. This classifier was chosen based on the results of Chapter 4 and could track subtle as well as full finger movements. P1's performance with the SKF was almost as good as the able-bodied subject, although he did require more time to stabilize the decoder around targets. In addition to independence, this system may also improve movement precision compared to proportional controllers that use surface EMG as an input.

P1 and P2 completed the task with varying degrees of success. The example calibration data in Figure 5.2 suggests similar consistency during training for each participant. P2's inconsistencies during online control could be due to changes in control policy or individual skill level (Krasoulis et al., 2019). Alternatively, they could be in response to decoder errors, which were reduced by removing active extension from the task. Her SKF implementation output new state and position estimates every 100ms compared to 50ms processing bins for P1. The lengthier integration window may have reduced her ability to make fine adjustments (Cunningham et al., 2011). In Chapter 4, P2 was highly successful using a HMM with the same structure to perform discrete movements. A different model may have improved performance for graded movements, and trajectory smoothing may have made it easier for her to correct errors (Yu et al., 2007).

The SKF can be adapted to commercial multi-articulating hands by using the classifier to switch between pre-programmed grips. Most grip selection software is not designed to frequently switch between movement states. Therefore, a single-state classifier such as linear discriminant

analysis (LDA) could reduce computational overhead and may not noticeably impact performance. The regressor in the SKF would then improve modulation within grips compared to proportional controllers that do not specify a relationship between channels and individual DOF. Future wearable or implantable systems may have strict limits on channel counts. P1 and P2's SKF implementations used only four and five differentiated channels, respectively. Dexterous grasp control may then be achievable even when a portion of channels is reserved for wrist or arm functions. Including additional control signals could increase the number of DOF. Although the HMM predicted 11 discrete movements in Chapter 4, it may be difficult to scale to an increasing number of movement combinations for the SKF. The two DOF controller in this study would be sufficient to control precision and power synergies of the SoftHand Pro 2 (Piazza et al., 2020). Alternatively, multi-articulating hands can have grasp synergies programmed in software. Based on the results in Chapter 4, we expect performance to remain robust across different arm positions. However, it is unknown if participants will be able to use the SKF to handle and manipulate objects. Future work should explore the functional utility of dexterous hand control compared to grip-switching.

5.4 Methods

5.4.1 Target Matching Task

The virtual target matching task is shown in Figure 5.3a,b. In each trial the inner hand moved its fingers to a target position and subjects simultaneously moved the two finger groups on the outer hand to match. Trials were considered successful if the subject was able to remain within ±11% along each dimension for a continuous 1s hold time. To aid visualization of the task, the inner hand turned green when subjects were within the movement tolerance. Targets were

presented in a center-out order where every other target was a return to rest. Individual extension movements were not considered in this study. Future studies should include more and smaller targets to evaluate kinematic boundaries and precision.

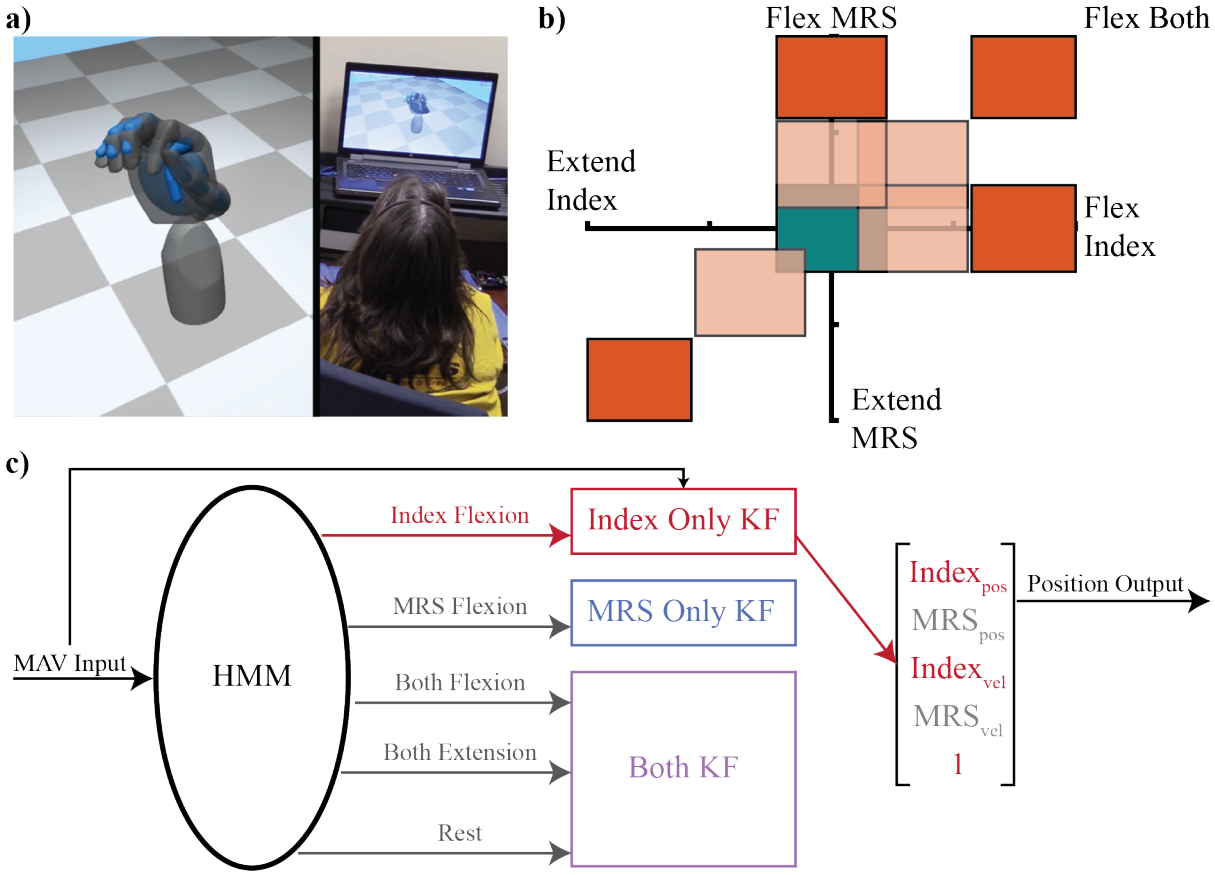

Figure 5.3 Details of the target matching task and SKF architecture. **a)** Target matching task showing an index flexion trial where P2 controlled the outer (grey) hand and was asked to match the position of the inner (blue) hand. **b)** Targets shown in a two dimensional plane. Decoders were trained on rest (green) and targets at the end of range of motion (orange). Intermediate (light) targets were only presented during real-time control. Trials where the decoder began in an overlapping region were ignored for analysis. **c)** A Switching Kalman Filter (SKF) decoded EMG into finger positions. Mean absolute value (MAV) was input into the SKF which used a Hidden-Markov Model (HMM) to select and recursively update only active finger kinematics. For example, index finger flexion shown in red. The "1" in the kinematic vector is a dummy variable used to model baseline EMG activity.

Success rate was defined as the number of trials with successful hold periods out of valid online trials. If the subject began a trial to an intermediate or rest target in the overlapping tolerance region, the trial was marked as invalid and discarded. Additional performance metrics were evaluated on successful trials and calculated similar to previous work (Vaskov et al., 2018). Acquisition time and orbiting time measured the total time required to begin a successful hold and time spent stabilizing around the target, respectively. Bit rate was calculated by considering the

underlying task as acquiring a single target in a two dimensional space (Thompson et al., 2014). Path efficiency measured movement quality and was sensitive to incorrect activations at the start of a trial. An ideal path was calculated per trial by projecting the point of first target contact onto a straight line between the start and end points of the trajectory. Efficiency was then calculated as the distance of the ideal path divided by actual distance taken to contact the target.

5.4.2 Switching Kalman Filter

P1 and P2 participated in this study while completing experiments for Chapter 4 which details the signal processing setup. For P1, mean absolute value (MAV) of Flexor Digitorum Profundus, index section (FDPI), Flexor Digitorum Profundus, small section (FDPS), Extensor Digitorum Communis (EDC), and his Ulnar RPNI were calculated in 50ms bins and input to the SKF. P2's decoder used MAV calculated in 100ms bins from her FDPI and EDC electrode pairs as well as Extensor Pollicis Longus (EPL), and both of her Ulnar RPNIs. Decoders were calibrated by asking patients to mimic the virtual hand with their phantom limb as it moved between rest and out targets. Intermediate targets (light orange in Figure 5.3b) were not included in the calibration routine but were presented during the online matching task. Each calibration trial began with a 300ms delay accounting for reaction time, followed by 750ms movement to and a 2s hold at each target. This procedure meant that kinematic relationships were determined around single movement speed. Although not ideal, this method is practical and has been successfully used in previous experiments with linear decoders (Vu et al., 2020).

In preliminary experiments, P1 was unable to complete this task with a two DOF Kalman filter and no switching architecture. Figure 5.3c details the structure of the SKF. A HMM that distinguished between rest, index flexion, MRS flexion, combined flexion, and combined extension was trained with the same iterative algorithm and latent state structure presented in

Chapter 4 (Vaskov et al., 2020). Two separate single DOF KFs were trained for each individual movement using procedures from previous work (Vaskov et al., 2018; Vu et al., 2018, 2020). The index only filter used MAV from extensors and FDPI as inputs and coefficients were determined from extension and index flexion trials. The MRS only filter used MAV from extensors, Ulnar RPNIs, and/or FDPS as inputs and coefficients were determined from extension and MRS flexion trials. An additional two DOF Kalman filter was trained using all decoder channels and all movement trials. Like Chapter 4, the HMM selected a new movement if it occurred with probability greater than 0.8. Since the KF is a recursive algorithm, the selected filter simply continued to update active finger states in the combined kinematic vector while the velocity of inactive fingers was set to 0 and the position unchanged. Trajectory blending schemes to smooth transitions could also be considered in future work (Yu et al., 2007).

5.5 Acknowledgements

The following colleagues contributed to these experiments: Philip Vu and Cynthia Chestek, helped design this study. Philip Vu helped design the switching Kalman Filter architecture and helped gather data. Paul Cederna and Theodore Kung. developed and performed the surgical implantation procedure. Kelsey Ebbs managed regulatory compliance and clinical trial coordination. This work was supported by the Defense Advanced Research Projects Agency (DARPA) Biological Technologies Office (BTO) Hand Proprioception and Touch Interfaces (HAPTIX) program through the DARPA Contracts Management Office grant/contract no. N66001-16-1-4006 and by the National Institute Of Neurological Disorders And Stroke of the National Institutes of Health under Award Number R01NS105132.

Chapter 6 Discussion

6.1 Brain-Machine Interfaces

The results of the non-human primate study discussed in Chapter 2 are clinically applicable to patients suffering from SCI or other motor degenerative conditions. In these populations, sensors that directly interface with the brain can be used to control prostheses that restore hand and arm functions. Clinical surveys suggest that many patients would be willing to adopt this technology provided the performance benefits outweigh surgical risks (Blabe et al., 2015; Lahr et al., 2015). Although a few laboratory systems have been cleared by the FDA for clinical research, animal models remain key to the development of novel recording electrodes and implantable electronics.

In Chapter 2 we demonstrated that individual finger movements can be distinguished based on motor cortex activity in two primates. Precise real-time control of each finger group was achieved using a state-of-the-art linear decoder (Gilja et al., 2012). In clinical studies, patients have used BMI to fully open or close grasps with a prostheses (Ajiboye et al., 2017; Bouton et al., 2016; Collinger et al., 2013). Chapter 2 demonstrates that re-calibration with a velocity-based intention estimation model could improve grasp precision across the complete range of finger motion. Previous work has documented strong connections between motor and sensory cortices relating to hand functions (Schroeder et al., 2017). Despite these connections, decoder performance remained consistent in the absence of physical hand movements and changes in tactile sensation. This could either be due to adaptation by the patient or the calibration process finding an ideal forward map (Orsborn et al., 2014b; Shenoy & Carmena, 2014).

In the future, the linear framework presented here and elsewhere may be expanded to accommodate simultaneous hand, wrist, and arm DOF. The selection of DOF will also be a function of prostheses availability. Kinematic decoders output predictions which can easily be sent as control inputs to robotic arms or exoskeletons, however these devices may be limited in their movement capabilities. Functional electrical stimulation can activate individual muscles or nerve synergies in a paralyzed limb, however precise control of these systems is still being researched (Ajiboye et al., 2017; Ciancibello et al., 2019). In both cases power management, either in terms of battery life or muscle fatigue, will need to be considered as portable platforms are developed for daily use. In a clinical setting, patients may find it more difficult to independently control increasing DOF (Wodlinger et al., 2015). Due to the complexity of the interface, extensive coaching or relying on patient adaptation may be difficult or impossible in many cases. Supervised sessions using intention estimation and adaptive calibration share the learning burden with the algorithm and may ease adoption for a broad segment of the patient population.

6.2 Peripheral Nerve Interfaces

In other cases, such as amputations, the peripheral nervous system remains intact up until the point of injury. In a clinical trial, electrodes implanted into RPNIs and residual muscles extracted high resolution motor commands to control robotic hands (Vu et al., 2020). Similar to other populations, surveys of people with amputations indicate that surgically implanted systems are likely to be adopted provided they can improve grasp control (Engdahl et al., 2015).

In Chapter 4 we presented a high-speed pattern recognition system that two patients used to activate up to 10 individual finger and wrist postures. In BMI studies, faster decoding rates have

been shown to improve online performance (Cunningham et al., 2011; Shanechi et al., 2017). This inspired us to implement a classifier that increased responsiveness without introducing instabilities. The "limb position effect" is a common problem with state-of-the-art pattern recognition systems (Betthauser et al., 2018; Teh & Hargrove, 2020). Surface EMG signals can be influenced by superficial muscle contractions, while bipolar indwelling electrodes captured muscle and RPNI activity specific to finger and thumb movements. Similar to other work, indwelling signals proved robust as decoding performance was not greatly affected by limb position (Dewald et al., 2019). In Chapter 5 we demonstrated that a regression algorithm could be used in combination with our pattern recognition framework to provide continuous position control of two grasp DOF. Dexterous grasp control may offer functional improvements by allowing patients to manipulate objects (Piazza et al., 2020). However, independent motor control is required for multi-articulating hands to take advantage of this capability.

We believe the implantation of RPNIs and indwelling electrodes can deliver improved motor control to a broad range of people with amputations. In Chapters 3 to 5, two individuals with transradial amputations had electrodes implanted to target the same hand and one wrist function. For future participants, additional wrist muscles may be implanted since simultaneous wrist control can improve functional performance (Sartori et al., 2018). In more proximal cases, nerves can be subdivided into multiple RPNIs to provide motor signals for wrist and hand functions (Vu et al., 2020). These otherwise lost control sites can improve grasp fidelity of systems with similar (Dantas et al., 2019; Dewald et al., 2019; Ortiz Catalan et al., 2020; Salminger et al., 2019) or even alternate sensing modalities (Dhawan et al., 2019). Fully implantable or portable systems may have limited channel counts (Salminger et al., 2019). The results in Chapter 5 were achieved using four and five input channels for P1 and P2. A first-generation system with eight bipolar EMG

channels could conceivably provide a patient with elbow flexion, wrist rotation, and a two DOF grasp.

Advances in sensing platforms will allow patients to realize high fidelity motor control. Osseointegration is a surgical intervention that improves mechanical coupling over a traditional socket and has the immediate benefit of creating a percutaneous feedthrough for electrodes (Ortiz Catalan et al., 2020). Patients that cannot or do not wish to undergo osseointegration will still benefit from this technology as wireless implantable devices are developed. First-generation systems could modify current FDA approved devices, such as implantable pulse generators or cochlear implants. In other systems, an external device both powers and receives data from multiple miniaturized sensors (Seo et al., 2016; Weir et al., 2009). One example, the IMES has been clinically tested and revised over the past decade (Pasquina et al., 2015; Salminger et al., 2019). These research systems may eventually reduce surgical complexity and make charging more convenient. The electrodes used in Chapters 3 to 5 only support one differentiated channel per RPNI, even though RPNIs can contain motor units intended for more than one muscle. Novel electrodes with multiple recording sites per RPNI combined with electronics that support high channel counts will be achieve better control of more DOF. Regression algorithms may then be used without a switching architecture, or biomechanical approaches may become common if torque control provides functional benefits over kinematic decoders.

The continued advancement of robotic hands and study of sensory feedback mechanisms are critical to the long-term goal of meaningfully restoring grasping functions for people with amputations. Future prosthetic hands can be designed with the expectation of multiple-DOF grasp control. Initially, this may be software changes to access individual motors. However, this would also allow manufacturers to consider the roles of specific DOF and design individual fingers to

support precision and power functions (Dalley et al., 2014). The studies in this thesis demonstrated a method to improve motor control of myoelectric prosthesis. However, a lack of sensory feedback is also a major issue to restoring grasp functions. Sensory feedback solutions can vary in resolution, type (electrical or mechanical) and location (evoked in the phantom limb or referred). Some recent studies have paired electrical nerve stimulation with intramuscular recording electrodes (George et al., 2019; OrtizCatalan et al., 2020). However, others are evaluated with low-resolution commercial controllers (D'Anna et al., 2019; Pena et al., 2019). Combined improvements to motor control and sensory feedback will provide more benefit than either can alone. As this technology progresses, outcomes-driven research is needed to evaluate different sensorimotor packages.

6.3 Future Directions

Based on the results of this thesis, I believe a clinical system using implantable electrodes and RPNIs is both presently viable and can deliver valuable functional improvements over state-of-the-art solutions to patients with major upper extremity amputations. Such a system may also expand the population of patients that use myoelectric devices, particularly multiarticulating hands. The development of miniaturized wireless sensors could also create viable clinical solutions for patients with partial hand amputations. Further development of implantable electronics will also be beneficial for prosthetics that require interfacing with the brain. In this application, validating the long-term safety of intracortical electrode arrays and developing power efficient systems that support higher channel counts are needed for clinical translation.

This thesis focused on sensing and reasoning approaches; however acting methods are critical for patients to realize benefits from neuroprosthetics. If peripheral nerve interfaces allow more patients to fully utilize robotic hands, these devices may then require improvements to

durability, power efficiency, and additional features to support sensory feedback. Functional electrical stimulation systems may be used to actuate grasps in patients with paretic hands. However, the development of compact exoskeletons may be required to support control of whole arm movements or augment grip strength. The ability to decode control signals from the brain and nervous systems will ultimately increase the demand for robotic solutions to improve the lives of patients.

Appendix

A.1 Supplementary Methods for Chapter 4

A.1.1 Hidden Markov Model Performance Analysis

The HMM-NB was compared to a standard Naïve Bayes (NB) classifier using the virtual task to switch between postures for the 1 of 10 and grasps sets (Table A.2.2). Parameters for each decoder are shown in Table A.2.3. For both participants, classifier parameters were selected by completing preliminary real-time control tests with larger window sizes and more conservative filtering and decreasing both parameters until instabilities prevented task completion. The output for the HMM-NB at each time step was updated if the sum of probabilities of hold or rest states exceeded 0.8. No additional output filters were applied to the HMM-NB, with the exception of P1's implementations with 10 ms updates. Both the NB and HMM used the same calibration data in each session. P1 completed one A-B session with the NB (A) and HMM-NB (B) classifiers for the 1 of 10 and Grasps posture sets. P2 completed three sessions for posture set: one A-B, one A-B-A, and one B-A-B session for 1 of 10 and three A-B-A sessions for Grasps. Fig. A.2.1 and Fig. A.2.2 show the results of the NB classifier which can be compared to the HMM-NB from Fig. 4.1 and Fig. 4.2. P1 completed the 1 of 10 posture set faster with the HMM-NB, achieving a latency of 159±237 ms compared to 258±313 ms (median±i.q.r.). However, the NB was more stable evidenced by a higher online accuracy, 95.9% compared to 93.0%, and fewer trials with a latency greater than one second. The HMM-NB outperformed NB in both online metrics for Grasps. NB

achieved a high offline Grasp accuracy for P1, but had a lower online accuracy of 83.7% compared to 99.5%. The increase in transition errors contributed to a higher median latency of 280±251 ms compared to 96±30 ms for the HMM-NB. For P2, the HMM improved performance of both posture sets. For 1 of 10, P2's NB classifier had a median latency of 398±1246 ms compared to 344±924 ms with the HMM-NB. Transition errors were worse overall as she achieved an online accuracy of 75.7% with NB compared to 80.0% with the HMM-NB. However, the NB classifier was able to return to rest more efficiently than the HMM-NB. For the Grasps posture set, the NB classifier was far less responsive with a latency of 355±1184 ms compared to 173±151 ms. Transition errors were also much worse with an online accuracy of 81.5% compared to 96.3% with the HMM-NB.

The HMM-NB particularly excelled in distinguishing the Grasp posture set. The ability to represent a posture as multiple states could be a greater advantage for predicting compound finger movements. The simplicity of the Naive Bayes assumption within the HMM-NB meant that latent states could not represent complex phenomena, but also meant the model was not as prone to over-fitting as more powerful techniques (Domingos & Pazzani, 1997). The incomplete selection of latent states for output was problematic for P2's 1 of 10 decoders which sometimes got stuck in transition states while returning to rest. Supervised learning with alternate output mappings could be explored to mitigate this issue. Expectation-Maximization algorithms can settle into local minima. Here, the low amount of training data, 5-7 movement repetitions, meant the HMM-NB was especially sensitive to state structure and initialization. Therefore, we cannot say the specific implementation chosen here was the best model, rather one that worked well. The number and structure of latent states per posture was driven by the computational requirements of the real-time system, ease of initialization, and success in prior applications (Kao et al., 2017; Kemere et al., 2008). Relaxing the state structure and initialization routine could allow the HMM-NB to converge

to more optimal solutions, although this would likely require more training data. As noted elsewhere, assembling large training data-sets is feasible due to the signal stability of implanted electrodes over time, which has been documented in other work (Dewald et al., 2019; Vu et al., 2020).

A.1.2 Offline Analysis and Signal Comparisons

The 1 of 10 posture set was chosen for alternate classifier simulations because it required classifiers to distinguish between the most movements. It also requires distinction between individual fingers, some of which were well represented by electrode placement and some of which were not. The algorithms used for real-time control were compared offline to a Naive Bayes (NB), linear discriminant analysis (LDA), and a multi-class support vector machine (SVM) using five time domain features (mean absolute value, waveform length, variance, slope sign changes, and zero crossings) along with coefficients from a 6th order auto-regressive model. Alternate classifiers assumed equal prior probabilities for each posture and used default Matlab 2018 built-ins for training and evaluation. LDA used a diagonal-regularized pooled covariance matrix. The multi-class SVM used a one-vs-one architecture with a linear kernel. Performance was evaluated on calibration data with different sized processing windows containing 10, 25, 50, 100, 150, 200, and 250ms of EMG history. P1's HMM-NB for comparison was updated in 10ms timesteps matching his online implementation (Table A.2.3). All other classifiers were updated every 50ms for lengthier processing windows.

P2 completed additional sessions to compare the performance between implanted and surface EMG. For the classifier simulation, eight pairs of adhesive electrodes were placed on P2's residual limb. Surface muscles corresponding to implanted electrode functions were targeted by feeling P2's forearm while asking her to perform movements with her phantom limb. The size of

adhesive electrodes resulted in the majority of her medial forearm being covered. EMG from both the surface and implanted electrodes was simultaneously recorded while P2 performed a calibration run for the 1 of 10 posture set. In a separate session we also precisely targeted FCR, FDPS, FPL and EPL using established techniques (Buschbacher, 2007). For targeted sessions, recordings were done individually to avoid space constraints. Before each recording, P2's forearm was cleaned with alcohol wipes and allowed to dry before applying the gelled electrodes. Signals from the corresponding implanted electrode pair were also recorded for the simultaneous comparison. The same calibration routine was used to instruct movement cues that corresponded to the muscles' motor functions. SNR's were calculated by averaging the RMS voltage of active periods and dividing by the averaged RMS of rest periods. Rest periods sometimes began with EMG settling activity from the previous trial. This was particularly noticeable for some of P2's surface channels as well as her FDPI and EPL implanted electrodes. SNR comparisons were conducted for surface and implanted channels targeting FDPI, EPL, and FCR. The SNR of RPNI electrodes was roughly compared to surface by targeting FPL and FDPS, residual muscles with similar motor functions. SNR analysis was performed on both the targeted and classifier calibration datasets. Settling activity was manually removed for all SNR analysis, but not for classifier training because it is important to the characterization of a rest intention. For each movement and muscle pair, the session with the better surface SNR was chosen for presentation in Fig. 4.6. For FCR and FPDS, the targeted sessions yielded better results, while EPL, FDPI, and FPL comparisons were taken from the classifier calibration dataset.

A.1.3 Participant Anatomy and Experiment Set-Up

RPNIs are created by suturing a small muscle graft to the end of severed nerve. In addition to preventing neuroma growth, RPNIs serve as bioamplifier for afferent motor signals and have

been demonstrated to produce stable functionally selective EMG in animal and human studies (Frost et al., 2018; Vu et al., 2018, 2020). P1 is a 30 year old male who sustained a right wrist disarticulation as the result of a traumatic hand injury. In 2015 he underwent surgery to resect neuromas on the median, ulnar, and radial nerves. A single RPNI was created on each nerve using free skeletal muscle grafts from his ipsilateral vastus lateralis. P1 is not a body powered user due to a shoulder injury. In March of 2018, P1 underwent an additional surgery to have eight pairs of bipolar intramuscular electrodes (Synapse Biomedical, Oberlin, OH) chronically implanted into the median and ulnar RPNIs and residual muscle corresponding to hand and wrist functions. P1 had the following residual muscles targeted for implantation: Flexor Pollicis Longus (FPL), Flexor Digitorum Profundus - Index Section (FDPI), Flexor Digitorum Profundus - Small Section (FDPS), Extensor Pollicis Longus (EPL), Extensor Digitorum Communis (EDC), and Flexor Carpi Radialis (FCR). P2 completed experiment sessions for this study between November 2018 and February 2019. The electrodes remained implanted for approximately one year and were partially explanted in March of 2019 by removing any exposed and subcutaneous wire lengths not embedded in muscle. In February 2020, P1 had his electrodes fully explanted from RPNIs and residual muscles.

P2 is a 53 year old female who, during treatment for septic shock and acute renal failure, suffered an intravenous extravasation of calcium into her right hand and forearm, which led to tissue necrosis and required a partial hand amputation. Her hand became contracted with extremely limited function and she underwent a voluntary transradial amputation in October of 2017. Single RPNIs were created on each of the median and radial nerves while an intraneural dissection was performed on the ulnar nerve to create two RPNIs. All RPNIs were creating using free muscle grafts from the ipsilateral vastus lateralis. P2 currently uses a body powered prostheses outside of

the study, although she reports to seldom use the open-close functionality. In October of 2018, P2 underwent chronic implantation of eight pairs of bipolar electrodes into the median and both ulnar RPNIs and five residual muscles. The same residual muscles were targeted for both patients with the exception of FDPS, which was only targeted for P1. P2 completed experiments for this study between and February 2019 and February 2020. At the time of writing, P2 remains implanted. P2's right passive elbow range of motion was recorded in clinic November 2017 to be 20 – 120° of flexion. Clinicians also noted limited ability to supinate her forearm with maximal supination in neutral at 0°. In August 2020, experimenters measured her passive right shoulder range of motion to be 160° shoulder flexion and 90° external rotation. We measured shoulder external rotation with the participant lying on her back, arm abducted to 90°, shoulder flexed to 90°, and forearm prone. In October 2020, her elbow range of motion was again measured by experimenters to be 20 – 125° of flexion.

The experiment set-up also differed slightly between subjects. P1 completed calibration runs with pseudo-randomly ordered cues and rest and hold periods of 2.5 seconds each. P2 preferred a slower pace and performed the calibration run with rest and hold periods of 3 seconds each and consecutively ordered cues. For the grasps posture set, P1's visual prompt showed finger extension instead of finger abduction. In preliminary calibration sessions, we found these two cues produced similar EMG responses. P1's prompt for point also resembled small finger flexion. This cue was consistent with other physical prostheses experiments P1 performed with the LUKE arm, which can only move its small finger in combination with the middle and ring fingers. A custom adapter was made to connect the LUKE arm to P1's socket, which was secured to his forearm with an Otto Bock silicone liner (Ottobock, Duderstadt, Germany). His socket also featured a window to allow access to the percutaneous electrode connectors on his

medial forearm. For P2, the i-Limb was connected to her socket with a quick wrist disconnect (QWD) that allowed manual wrist rotation. The QWD was embedded in a PVC adapter that connected to her socket which was secured to her forearm with an Iceross Upper-X liner (Ossur, Reykjavik, Iceland). Her percutaneous leads exited on her lateral bicep and did not interfere with her socket.

A.2 Supplementary Figures and Tables for Chapter 4

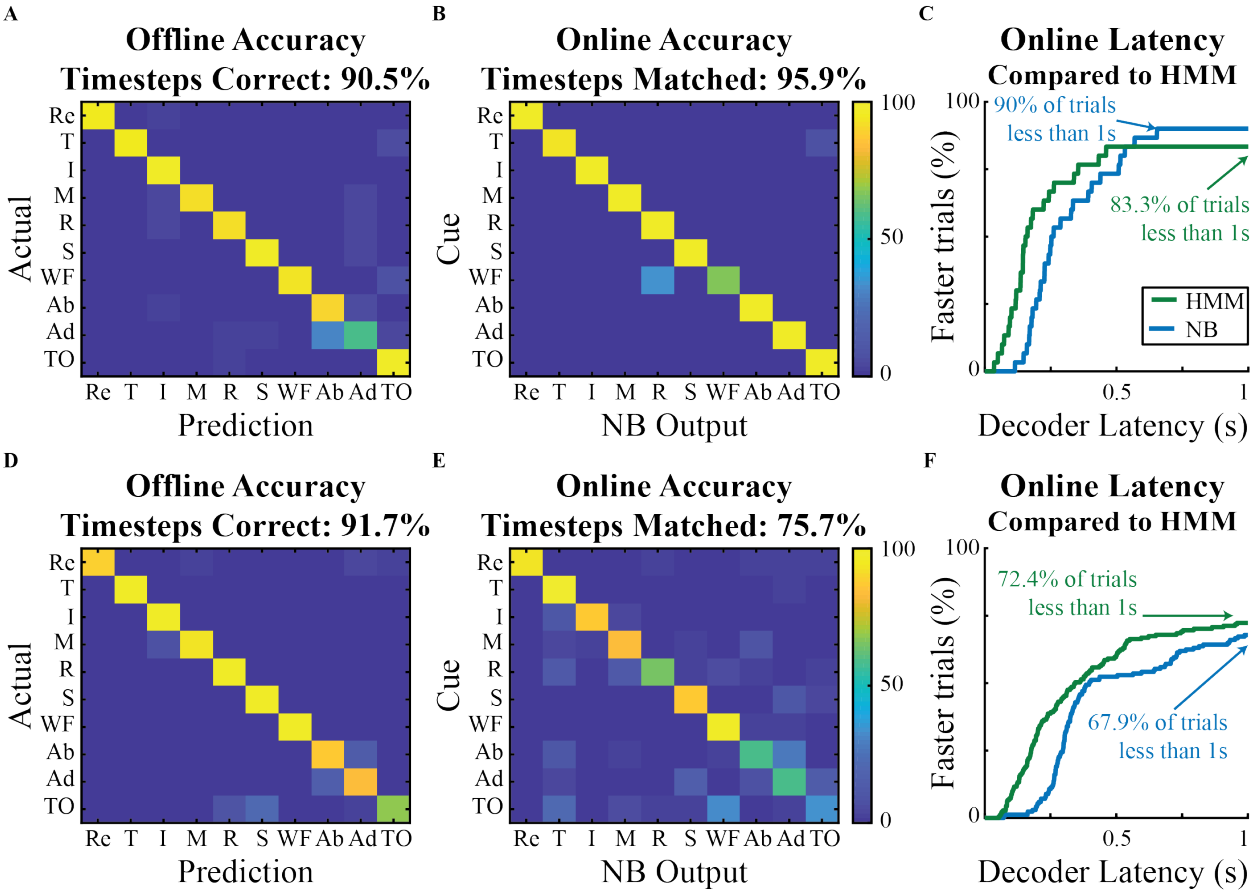

Figure A.2.1 HMM and Naïve Bayes comparison on the 1 of 10 posture set. **(A)** Offline classifier accuracy simulated on individual time bins during hold periods using 5-fold cross validation on P1's training data. **(B)** An output filter of three consecutive decodes was used for real-time control and P1 was able to achieve an online accuracy of 95.9%. **(C)** Cumulative latency lines are drawn so the y-axis indicates the percentage of trials with latency less than values on the x-axis (n = 30 trials, 27 shown). Results compared to the HMM results from Fig. 4.1 **(D,E)** P2's decoder used larger processing windows and a filter length of four consecutive decodes for real-time control. **(F)** Cumulative latency comparison for P2 (n = 168 trials, 114 shown).

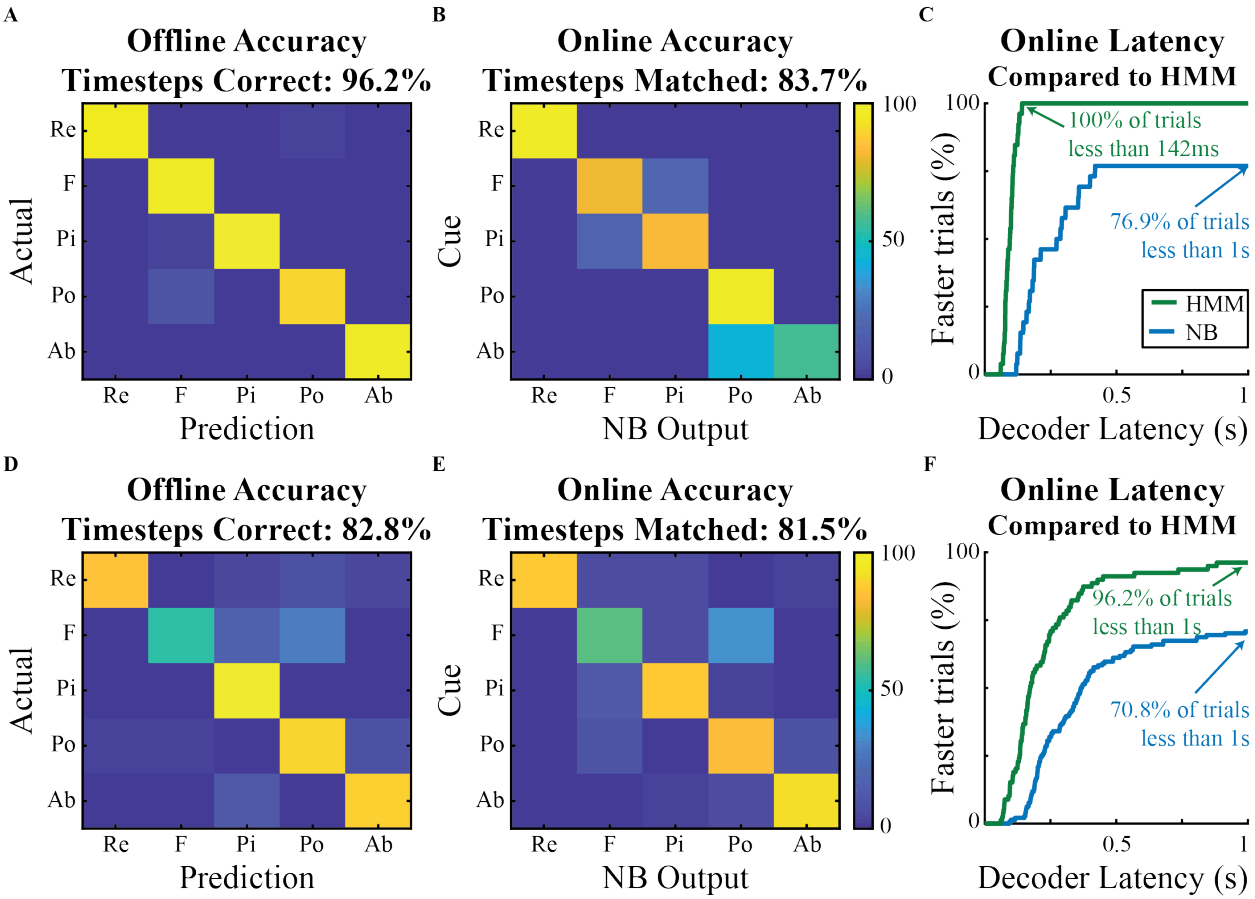

Figure A.2.2 HMM and Naïve Bayes comparison on the grasps posture set. **(A)** Offline classifier accuracy simulated on P1's training data. **(B)** An output filter of three consecutive decodes was again used for real-time control. **(C)** Cumulative latency comparison for P1 (n = 26 trials, 20 shown). Results compared to the HMM from Fig. 4.2. **(D,E)** P2's decoder again used larger processing windows and a filter length of four consecutive decodes for real-time control. **(F)** Cumulative latency comparison for P2 (n = 144 trials, 102 shown).

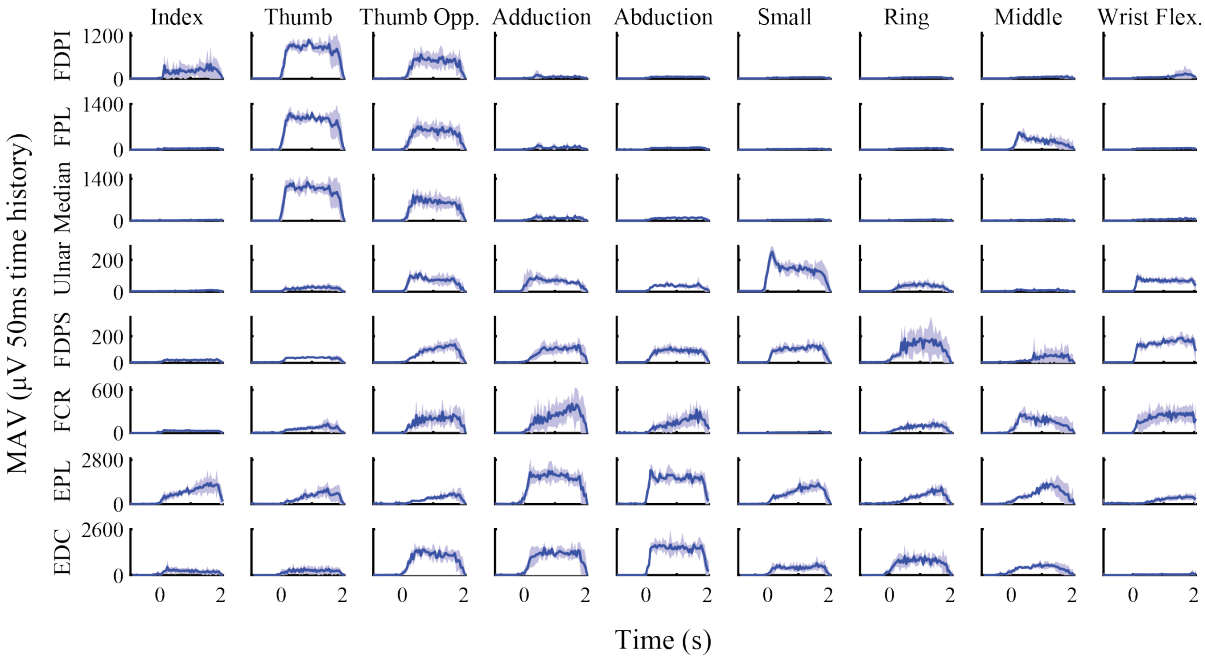

Figure A.2.3 P1 EMG envelopes during 1 of 10 calibration. Mean absolute value (MAV) traces of P1's EMG during the 1 of 10 posture set used for classifier training and clustering analysis. EMG was rectified and averaged in non-overlapping 50ms time bins from electrodes targeting flexor digitorum profundus, index section (FDPI), flexor pollicis longus (FPL), Median RPNI, Ulnar RPNI, flexor digitorum profundus, small section (FDPS), flexor carpi radialis (FCR), extensor pollicis longus (EPL), and extensor digitorum communis (EDC). Trials were time aligned to the start of the hold period and then averaged (mean±s.t.d. n = 5-6 trials).

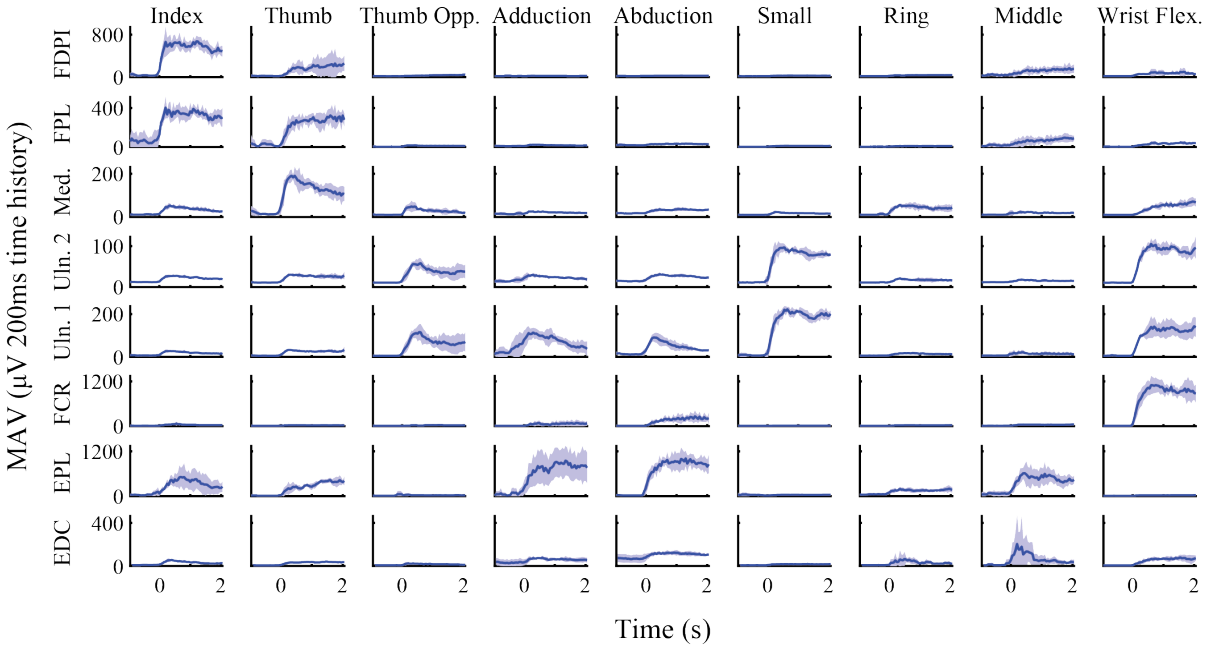

Figure A.2.4 P2 EMG envelopes during 1 of 10 calibration. Mean absolute value (MAV) traces of P2's EMG during the 1 of 10 posture set from the experiment session used for offline and clustering analysis. EMG was rectified and averaged in 200ms time bins with a 50ms update rate. Electrodes targeted flexor digitorum profundus, index section (FDPI), flexor pollicis longus (FPL), Median RPNI (Med.), Ulnar RPNI 1 (Uln. 1), Ulnar RPNI 2 (Uln. 2), flexor carpi radialis (FCR), extensor pollicis longus (EPL), and extensor digitorum communis (EDC). Trials were time aligned to the start of the hold period and then averaged (mean±s.t.d, n = five trials).

Study	Participants	EMG Channels	Hand Classes	Completion Delay (s)	Completion Rate (%)
Kuiken et al., 2009	3 SD, 2 TR	12 surface gelled	4	0.54±0.27	86.9±13.9
Li et al., 2010	5 TR	12 surface gelled	6	0.45±0.35	53.9±14.2
Cipriani et al., 2011	5 TR	8 surface gelled	7	0.86*	77*
Vaskov et al. 2020	2 TR	8 intra-muscular	8	0.26±0.09	96.3±5.3
			4	0.14±0.06	100±0.0

Table A.2.1 Comparison of the high-speed pattern recognition system to previous work. Three earlier studies quantified real-time classification including multiple hand (finger or grasp) movements for persons with shoulder disarticulations (SD), transhumeral (TH), or transradial (TR) amputations using similar randomized control tasks. Movement completion metrics for hand postures were calculated consistent with previous work. The task in those studies differed from the posture switching task in two ways: a rest period was presented in between cues and the requirement for completion was a cumulative selection rather than a continuous hold. Completion rate and time were defined as the percentage of trials and median time in which one second of the correct posture was cumulatively matched. Completion delay is presented as the difference between the reported completion time and the cumulative selection length, which differed amongst earlier studies. By nature, completion rate is greater than or equal to success rate and completion delay is less than or equal to latency. Metrics were averaged across subjects (mean±s.t.d.) *variance across subjects not reported.

Posture Set	No. of Classes	Classes
1 of 10	10	Thumb, Index, Middle, Ring, and Small Finger Flexion (T,I,M,R,S) Wrist Flexion (WF), Finger Abduction (Ab), Finger Adduction (Ad), Thumb Opposition (TO), Rest (Re)
Grasps	5	Fist (F), Pinch (Pi), Point (Po), Finger Abduction (Ab), Rest (Re)
Functional	4	Fist (F), Pinch (Pi), Point (Po), Rest (Re)

Table A.2.2 Posture sets used for virtual and physical tasks in Chapter 4. P2 performed three experiment sessions of the virtual task with the 1 of 10 and grasps posture sets, while P1 performed one session with each set. The functional posture set was used by both participants to control robotic prostheses and for the static arm position test performed by P2

Participant	Task	Decoder	Time History (ms)	Update Rate (ms)	Filter Length
P1	1 of 10	HMM	50	10	5
		NB	50	50	3
	Grasps	HMM	50	10	5
		NB	50	50	3
P2	1 of 10	HMM	50	50	1
		NB	200	50	4
	Grasps	HMM	50	50	1
		NB	200	50	4

Table A.2.3 Processing window and filtering parameters for decoders in Chapter 4. Time history refers to the length of the processing window to extract MAV from all eight bipolar electrode pairs, while update rate refers to the timestep features and decoders were updated. The filter length is the number of consecutive decodes required for a change to be sent to the virtual prostheses.

Bibliography

Aflalo, T., Kellis, S., Klaes, C., Lee, B., Shi, Y., Pejsa, K., Shanfield, K., Hayes-Jackson, S., Aisen, M., Heck, C., Liu, C. Y., & Andersen, R. A. (2015). Decoding motor imagery from the posterior parietal cortex of a tetraplegic human. *Science*, *348*(6237), 906–910. https://doi.org/10.1126/science.aaa5417

Aggarwal, V., Acharya, S., Tenore, F., Shin, H. C., Etienne-Cummings, R., Schieber, M. H., & Thakor, N. V. (2008). Asynchronous decoding of dexterous finger movements using M1 neurons. *IEEE Transactions on Neural Systems and Rehabilitation Engineering*, *16*(1), 3–14. https://doi.org/10.1109/TNSRE.2007.916289

Aggarwal, V., Mollazadeh, M., Davidson, A. G., Schieber, M. H., & Thakor, N. V. (2013). State-based decoding of hand and finger kinematics using neuronal ensemble and LFP activity during dexterous reach-to-grasp movements. *Journal of Neurophysiology*, *109*(12), 3067–3081. https://doi.org/10.1152/jn.01038.2011

Ajiboye, A. B., Willett, F. R., Young, D. R., Memberg, W. D., Murphy, B. A., Miller, J. P., Walter, B. L., Sweet, J. A., Hoyen, H. A., Keith, M. W., Peckham, P. H., Simeral, J. D., Donoghue, J. P., Hochberg, L. R., & Kirsch, R. F. (2017). Restoration of reaching and grasping movements through brain-controlled muscle stimulation in a person with tetraplegia: a proof-of-concept demonstration. *The Lancet*, *389*(10081), 1821–1830. https://doi.org/10.1016/S0140-6736(17)30601-3

Akhtar, A., Choi, K. Y., Fatina, M., Cornman, J., Wu, E., Sombeck, J., Yim, C., Slade, P., Lee, J., Moore, J., Gonzales, D., Wu, A., Anderson, G., Rotter, D., Shin, C., & Bretl, T. (2016). A low-cost, open-source, compliant hand for enabling sensorimotor control for people with transradial amputations. *Proceedings of the Annual International Conference of the IEEE Engineering in Medicine and Biology Society, EMBS*. https://doi.org/10.1109/EMBC.2016.7591762

Alaerts, K., de Beukelaar, T. T., Swinnen, S. P., & Wenderoth, N. (2012). Observing how others lift light or heavy objects: Time-dependent encoding of grip force in the primary motor cortex. *Psychological Research*. https://doi.org/10.1007/s00426-011-0380-1

Atzori, M., Cognolato, M., & Müller, H. (2016). Deep learning with convolutional neural networks applied to electromyography data: A resource for the classification of movements for prosthetic hands. *Frontiers in Neurorobotics*. https://doi.org/10.3389/fnbot.2016.00009

Atzori, M., & Müller, H. (2015). Control capabilities of myoelectric robotic prostheses by hand amputees: A scientific research and market overview. *Frontiers in Systems Neuroscience*. https://doi.org/10.3389/fnsys.2015.00162

Belter, J. T., Reynolds, B. C., & Dollar, A. M. (2014). Grasp and force based taxonomy of split-hook prosthetic terminal devices. *2014 36th Annual International Conference of the IEEE Engineering in Medicine and Biology Society, EMBC 2014*. https://doi.org/10.1109/EMBC.2014.6945144

Betthauser, J. L., Hunt, C. L., Osborn, L. E., Masters, M. R., Levay, G., Kaliki, R. R., & Thakor,

N. V. (2018). Limb Position Tolerant Pattern Recognition for Myoelectric Prosthesis Control with Adaptive Sparse Representations from Extreme Learning. *IEEE Transactions on Biomedical Engineering*. https://doi.org/10.1109/TBME.2017.2719400

Biddiss, E., Beaton, D., & Chau, T. (2007). Consumer design priorities for upper limb prosthetics. *Disability and Rehabilitation: Assistive Technology*. https://doi.org/10.1080/17483100701714733

Biddiss, E., & Chau, T. (2007). Upper-limb prosthetics: Critical factors in device abandonment. *American Journal of Physical Medicine and Rehabilitation*. https://doi.org/10.1097/PHM.0b013e3181587f6c

Birdwell, J. A., Hargrove, L. J., Weir, R. F. f., & Kuiken, T. A. (2015). Extrinsic Finger and Thumb Muscles Command a Virtual Hand to Allow Individual Finger and Grasp Control. *IEEE Transactions on Biomedical Engineering*, *62*(1), 218–226. https://doi.org/10.1109/TBME.2014.2344854

Blabe, C. H., Gilja, V., & Chestek, C. A. (2015). Assessment of brain – machine interfaces from the perspective of people with paralysis Assessment of brain – machine interfaces from the perspective of people with paralysis. *Journal of Neural Engineering*, *12*(August 2016), 43002. https://doi.org/10.1088/1741-2560/12/4/043002

Boni, I., Millenaar, J., Controzzi, M., & Ortiz-Catalan, M. (2018). Restoring Natural Forearm Rotation in Transradial Osseointegrated Amputees. *IEEE Transactions on Neural Systems and Rehabilitation Engineering*. https://doi.org/10.1109/TNSRE.2018.2880948

Bouton, C. E., Shaikhouni, A., Annetta, N. V., Bockbrader, M. A., Friedenberg, D. A., Nielson, D. M., Sharma, G., Sederberg, P. B., Glenn, B. C., Mysiw, W. J., Morgan, A. G., Deogaonkar, M., & Rezai, A. R. (2016). Restoring cortical control of functional movement in a human with quadriplegia. *Nature*, *533*, 247–250. https://doi.org/10.1038/nature17435

Buschbacher, R. M. (2007). Anatomical Guide for the Electromyographer: The Limbs and Trunk. *American Journal of Physical Medicine & Rehabilitation*. https://doi.org/10.1097/phm.0b013e31803217b1

Carmena, J. M., Lebedev, M. A., Crist, R. E., O'Doherty, J. E., Santucci, D. M., Dimitrov, D. F., Patil, P. G., Henriquez, C. S., & Nicolelis, M. A. L. (2003). Learning to control a brain-machine interface for reaching and grasping by primates. *PLoS Biology*, *1*(2). https://doi.org/10.1371/journal.pbio.0000042

Chadwell, A., Kenney, L. P. J., Howard, D., Ssekitoleko, R. T., Nakandi, B. T., & Head, J. (2020). Evaluating reachable workspace and user control over prehensor aperture for a body-powered prosthesis. *IEEE Transactions on Neural Systems and Rehabilitation Engineering*. https://doi.org/10.1109/tnsre.2020.3010625

Cheesborough, J. E., Smith, L. H., Kuiken, T. A., & Dumanian, G. A. (2015). Targeted muscle reinnervation and advanced prosthetic arms. *Seminars in Plastic Surgery*. https://doi.org/10.1055/s-0035-1544166

Chestek, C. A., Gilja, V., Blabe, C. H., Foster, B. L., Shenoy, K. V., Parvizi, J., & Henderson, J. M. (2013). Hand posture classification using electrocorticography signals in the gamma band over human sensorimotor brain areas. *Journal of Neural Engineering*, *10*(2). https://doi.org/10.1088/1741-2560/10/2/026002

Chestek, C. A., Gilja, V., Nuyujukian, P., Foster, J. D., Fan, J. M., Kaufman, M. T., Churchland, M. M., Rivera-Alvidrez, Z., Cunningham, J. P., Ryu, S. I., & Shenoy, K. V. (2011). Long-term stability of neural prosthetic control signals from silicon cortical arrays in rhesus macaque motor cortex. *Journal of Neural Engineering*. https://doi.org/10.1088/1741-

2560/8/4/045005
Christie, B. P., Tat, D. M., Irwin, Z. T., Gilja, V., Nuyujukian, P., Foster, J. D., Ryu, S. I., Shenoy, K. V., Thompson, D. E., & Chestek, C. A. (2015). Comparison of spike sorting and thresholding of voltage waveforms for intracortical brain-machine interface performance. *Journal of Neural Engineering*, *12*(1), 16009. https://doi.org/10.1088/1741-2560/12/1/016009
Ciancibello, J. G., King, K., Meghrazi, M. A., Padmanaban, S., Levy, T., Ramdeo, R., Straka, M., & Bouton, C. E. (2019). Closed-loop neuromuscular electrical stimulation using feedforward-feedback control and textile electrodes to regulate grasp force in quadriplegia. *Bioelectronic Medicine*, *5*(1), 19. https://doi.org/10.1186/s42234-019-0034-y
Cipriani, C., Antfolk, C., Controzzi, M., Lundborg, G., Rosen, B., Carrozza, M. C., & Sebelius, F. (2011). Online myoelectric control of a dexterous hand prosthesis by transradial amputees. *IEEE Transactions on Neural Systems and Rehabilitation Engineering*. https://doi.org/10.1109/TNSRE.2011.2108667
Coffey, R. J. (2009). Deep brain stimulation devices: A brief technical history and review. In *Artificial Organs*. https://doi.org/10.1111/j.1525-1594.2008.00620.x
Colachis, S. C., Bockbrader, M. A., Zhang, M., Friedenberg, D. A., Annetta, N. V., Schwemmer, M. A., Skomrock, N. D., Mysiw, W. J., Rezai, A. R., Bresler, H. S., & Sharma, G. (2018). Dexterous control of seven functional hand movements using cortically-controlled transcutaneous muscle stimulation in a person with tetraplegia. In *Frontiers in Neuroscience* (Vol. 12, Issue APR, p. 208). https://doi.org/10.3389/fnins.2018.00208
Collinger, J. L., Wodlinger, B., Downey, J. E., Wang, W., Tyler-Kabara, E. C., Weber, D. J., McMorland, A. J. C., Velliste, M., Boninger, M. L., & Schwartz, A. B. (2013). High-performance neuroprosthetic control by an individual with tetraplegia. *The Lancet*, *381*(9866), 557–564. https://doi.org/10.1016/S0140-6736(12)61816-9
Cunningham, J. P., Nuyujukian, P., Gilja, V., Chestek, C. A., Ryu, S. I., & Shenoy, K. V. (2011). A closed-loop human simulator for investigating the role of feedback control in brain-machine interfaces. *Journal of Neurophysiology*, *105*(4), 1932–1949. https://doi.org/10.1152/jn.00503.2010
D'Anna, E., Valle, G., Mazzoni, A., Strauss, I., Iberite, F., Patton, J., Petrini, F. M., Raspopovic, S., Granata, G., Iorio, R. Di, Controzzi, M., Cipriani, C., Stieglitz, T., Rossini, P. M., & Micera, S. (2019). A closed-loop hand prosthesis with simultaneous intraneural tactile and position feedback. *Science Robotics*. https://doi.org/10.1126/scirobotics.aau8892
Dalley, S. A., Bennett, D. A., & Goldfarb, M. (2014). Functional assessment of the Vanderbilt Multigrasp myoelectric hand: a continuing case study. *Annual International Conference of the IEEE Engineering in Medicine and Biology Society. IEEE Engineering in Medicine and Biology Society. Annual International Conference*, *2014*, 6195–6198. https://doi.org/10.1109/EMBC.2014.6945044
Dangi, S., Orsborn, A. L., Moorman, H. G., & Carmena, J. M. (2013). Design and analysis of closed-loop decoder adaptation algorithms for brain-machine interfaces. *Neural Computation*, *25*(7), 1693–1731. https://doi.org/10.1162/NECO_a_00460
Dantas, H., Warren, D. J., Wendelken, S., Davis, T. S., Clark, G. A., & Mathews, V. J. (2019). Deep Learning Movement Intent Decoders Trained with Dataset Aggregation for Prosthetic Limb Control. *IEEE Transactions on Biomedical Engineering*, *PP*(JANUARY), 1–1. https://doi.org/10.1109/tbme.2019.2901882
Davis, T. S., Wark, H. A. C., Hutchinson, D. T., Warren, D. J., O'Neill, K., Scheinblum, T.,

Clark, G. A., Normann, R. A., & Greger, B. (2016). Restoring motor control and sensory feedback in people with upper extremity amputations using arrays of 96 microelectrodes implanted in the median and ulnar nerves. *Journal of Neural Engineering*. https://doi.org/10.1088/1741-2560/13/3/036001

Davoodi, R., Urata, C., Hauschild, M., Khachani, M., & Loeb, G. E. (2007). Model-based development of neural prostheses for movement. *IEEE Transactions on Biomedical Engineering*, *54*(11), 1909–1918. https://doi.org/10.1109/TBME.2007.902252

de Luca, C. J. (1979). Physiology and Mathematics of Myoelectric Signals. *IEEE Transactions on Biomedical Engineering*. https://doi.org/10.1109/TBME.1979.326534

Deeny, S., Chicoine, C., Hargrove, L., Parrish, T., & Jayaraman, A. (2014). A Simple ERP Method for Quantitative Analysis of Cognitive Workload in Myoelectric Prosthesis Control and Human-Machine Interaction. *PLOS ONE*, *9*(11), e112091. https://doi.org/10.1371/journal.pone.0112091

Dewald, H. A., Lukyanenko, P., Lambrecht, J. M., Anderson, J. R., Tyler, D. J., Kirsch, R. F., & Williams, M. R. (2019). Stable, three degree-of-freedom myoelectric prosthetic control via chronic bipolar intramuscular electrodes: A case study. *Journal of NeuroEngineering and Rehabilitation*. https://doi.org/10.1186/s12984-019-0607-8

Dhawan, A. S., Mukherjee, B., Patwardhan, S., Akhlaghi, N., Diao, G., Levay, G., Holley, R., Joiner, W. M., Harris-Love, M., & Sikdar, S. (2019). Proprioceptive Sonomyographic Control: A novel method for intuitive and proportional control of multiple degrees-of-freedom for individuals with upper extremity limb loss. *Scientific Reports*. https://doi.org/10.1038/s41598-019-45459-7

Domingos, P., & Pazzani, M. (1997). On the Optimality of the Simple Bayesian Classifier under Zero-One Loss. *Machine Learning*. https://doi.org/10.1023/A:1007413511361

Downey, J. E., Weiss, J. M., Flesher, S. N., Thumser, Z. C., Marasco, P. D., Boninger, M. L., Gaunt, R. A., & Collinger, J. L. (2018). Implicit Grasp Force Representation in Human Motor Cortical Recordings. *Frontiers in Neuroscience*. https://doi.org/10.3389/fnins.2018.00801

Downey, J. E., Weiss, J. M., Muelling, K., Venkatraman, A., Valois, J. S., Hebert, M., Bagnell, J. A., Schwartz, A. B., & Collinger, J. L. (2016). Blending of brain-machine interface and vision-guided autonomous robotics improves neuroprosthetic arm performance during grasping. *Journal of NeuroEngineering and Rehabilitation*, *13*(1), 28. https://doi.org/10.1186/s12984-016-0134-9

Engdahl, S. M., Christie, B. P., Kelly, B., Davis, A. J., Chestek, C. A., & Gates, D. H. (2015). Surveying the interest of individuals with upper limb loss in novel prosthetic control techniques. *Journal of NeuroEngineering and Rehabilitation*. https://doi.org/10.1186/s12984-015-0044-2

Ethier, C., Acuna, D., Solla, S. A., & Miller, L. E. (2016). Adaptive neuron-to-EMG decoder training for FES neuroprostheses. *Journal of Neural Engineering*, *13*(4), 46009. https://doi.org/10.1088/1741-2560/13/4/046009

Fan, J. M., Nuyujukian, P., Kao, J. C., Chestek, C. A., Ryu, S. I., & Shenoy, K. V. (2014). Intention estimation in brain-machine interfaces. *Journal of Neural Engineering*, *11*(1), 16004. https://doi.org/10.1088/1741-2560/11/1/016004

Farina, D., Jiang, N., Rehbaum, H., Holobar, A., Graimann, B., Dietl, H., & Aszmann, O. C. (2014). The extraction of neural information from the surface EMG for the control of upper-limb prostheses: Emerging avenues and challenges. *IEEE Transactions on Neural Systems*

and Rehabilitation Engineering. https://doi.org/10.1109/TNSRE.2014.2305111
Farina, D., Vujaklija, I., Sartori, M., Kapelner, T., Negro, F., Jiang, N., Bergmeister, K. D., Andalib, A., Principe, J., & Aszmann, O. C. (2017). Man/machine interface based on the discharge timings of spinal motor neurons after targeted muscle reinnervation. *Nature Biomedical Engineering*, *1*. https://doi.org/10.1038/s41551-016-0025
Flesher, S. N., Collinger, J. L., Foldes, S. T., Weiss, J. M., Downey, J. E., Tyler-Kabara, E. C., Bensmaia, S. J., Schwartz, A. B., Boninger, M. L., & Gaunt, R. A. (2016). Intracortical microstimulation of human somatosensory cortex. *Science Translational Medicine*, *8*(361), 361ra141--361ra141. https://doi.org/10.1126/scitranslmed.aaf8083
Franzke, A. W., Kristoffersen, M. B., Bongers, R. M., Murgia, A., Pobatschnig, B., Unglaube, F., & Van Der Sluis, C. K. (2019). Users' and therapists' perceptions of myoelectric multi-function upper limb prostheses with conventional and pattern recognition control. *PLoS ONE*. https://doi.org/10.1371/journal.pone.0220899
Fraser, G. W., Chase, S. M., Whitford, A., & Schwartz, A. B. (2009). Control of a brain-computer interface without spike sorting. *Journal of Neural Engineering*. https://doi.org/10.1088/1741-2560/6/5/055004
Frost, C. M., Ursu, D. C., Flattery, S. M., Nedic, A., Hassett, C. A., Moon, J. D., Buchanan, P. J., Gillespie, R. B., Kung, T. A., Kemp, S. W. P., Cederna, P. S., & Urbanchek, M. G. (2018). Regenerative peripheral nerve interfaces for real-time, proportional control of a Neuroprosthetic hand. *Journal of NeuroEngineering and Rehabilitation*. https://doi.org/10.1186/s12984-018-0452-1
Ganguly, K., & Carmena, J. M. (2010). Neural correlates of skill acquisition with a cortical brain-machine interface. *Journal of Motor Behavior*, *42*(6), 355–360. https://doi.org/10.1080/00222895.2010.526457
Gao, Y., Archer, E., Paninski, L., & Cunningham, J. P. (2016). Linear dynamical neural population models through nonlinear embeddings. In D. D. Lee, M. Sugiyama, U. V Luxburg, I. Guyon, & R. Garnett (Eds.), *Neural Information Processing Systems (NIPS)* (pp. 163–171). Curran Associates, Inc. http://arxiv.org/abs/1605.08454
Gates, D. H., Walters, L. S., Cowley, J., Wilken, J. M., & Resnik, L. (2016). Range of motion requirements for upper-limb activities of daily living. *American Journal of Occupational Therapy*. https://doi.org/10.5014/ajot.2016.015487
George, J. A., Brinton, M. R., Duncan, C. C., Hutchinson, D. T., & Clark, G. A. (2018). Improved Training Paradigms and Motor-decode Algorithms: Results from Intact Individuals and a Recent Transradial Amputee with Prior Complex Regional Pain Syndrome. *Proceedings of the Annual International Conference of the IEEE Engineering in Medicine and Biology Society, EMBS*, *2018-July*, 3782–3787. https://doi.org/10.1109/EMBC.2018.8513342
George, J. A., Davis, T. S., Brinton, M. R., & Clark, G. A. (2020). Intuitive neuromyoelectric control of a dexterous bionic arm using a modified Kalman filter. In *Journal of Neuroscience Methods*. https://doi.org/10.1016/j.jneumeth.2019.108462
George, J. A., Kluger, D. T., Davis, T. S., Wendelken, S. M., Okorokova, E. V., He, Q., Duncan, C. C., Hutchinson, D. T., Thumser, Z. C., Beckler, D. T., Marasco, P. D., Bensmaia, S. J., & Clark, G. A. (2019). Biomimetic sensory feedback through peripheral nerve stimulation improves dexterous use of a bionic hand. *Science Robotics*, *4*(32), eaax2352. https://doi.org/10.1126/scirobotics.aax2352
George, J. A., Tully, T. N., Colgan, P. C., & Clark, G. A. (2020). Bilaterally Mirrored

Movements Improve the Accuracy and Precision of Training Data for Supervised Learning of Neural or Myoelectric Prosthetic Control. *Proceedings of the Annual International Conference of the IEEE Engineering in Medicine and Biology Society, EMBS*. https://doi.org/10.1109/EMBC44109.2020.9175388

Georgopoulos, A. P., Schwartz, A. B., & Kettner, R. E. (1986). Neuronal population coding of movement direction. *Science*, *233*(4771), 1416–1419. https://doi.org/10.1126/science.3749885

Gilja, V., Nuyujukian, P., Chestek, C. A., Cunningham, J. P., Yu, B. M., Fan, J. M., Churchland, M. M., Kaufman, M. T., Kao, J. C., Ryu, S. I., & Shenoy, K. V. (2012). A high-performance neural prosthesis enabled by control algorithm design. *Nature Neuroscience*, *15*(12), 1752–1757. https://doi.org/10.1038/nn.3265

Gilja, V., Nuyujukian, P., Chestek, C. A., Cunningham, J. P., Yu, B. M., Fan, J. M., Ryu, S. I., & Shenoy, K. V. (2012). A brain machine interface control algorithm designed from a feedback control perspective. *2012 Annual International Conference of the IEEE Engineering in Medicine and Biology Society*, 1318–1322. https://doi.org/10.1109/EMBC.2012.6346180

Guido, K., Clavijo, A., Zhu, K., Ding, X., & Ma, K. (2020). Strategies to Improve Neural Electrode Performance. In *Neural Interface Engineering*. https://doi.org/10.1007/978-3-030-41854-0_7

Hahne, J. M., Schweisfurth, M. A., Koppe, M., & Farina, D. (2018). Simultaneous control of multiple functions of bionic hand prostheses: Performance and robustness in end users. *Science Robotics*. https://doi.org/10.1126/scirobotics.aat3630

Hamed, S. B., Schieber, M. H., & Pouget, A. (2007). Decoding M1 Neurons During Multiple Finger Movements. *Journal of Neurophysiology*, *98*(1), 327–333. https://doi.org/10.1152/jn.00760.2006

Hichert, M., Vardy, A. N., & Plettenburg, D. (2018). Fatigue-free operation of most body-powered prostheses not feasible for majority of users with trans-radial deficiency. *Prosthetics and Orthotics International*. https://doi.org/10.1177/0309364617708651

Hochberg, L. R., Bacher, D., Jarosiewicz, B., Masse, N. Y., Simeral, J. D., Vogel, J., Haddadin, S., Liu, J., Cash, S. S., Van Der Smagt, P., & Donoghue, J. P. (2012). Reach and grasp by people with tetraplegia using a neurally controlled robotic arm. *Nature*, *485*(7398), 372–375. https://doi.org/10.1038/nature11076

Hotson, G., McMullen, D. P., Fifer, M. S., Johannes, M. S., Katyal, K. D., Para, M. P., Armiger, R., Anderson, W. S., Thakor, N. V., Wester, B. A., & Crone, N. E. (2016). Individual finger control of a modular prosthetic limb using high-density electrocorticography in a human subject. *Journal of Neural Engineering*, *13*(2), 26017. https://doi.org/10.1088/1741-2560/13/2/026017

Hudgins, B., Parker, P., & Scott, R. N. (1993). A New Strategy for Multifunction Myoelectric Control. *IEEE Transactions on Biomedical Engineering*. https://doi.org/10.1109/10.204774

Irwin, Z. T., Schroeder, K. E., Vu, P. P., Bullard, A. J., Tat, D. M., Nu, C. S., Vaskov, A. K., Nason, S. R., Thompson, D. E., Bentley, J. N., Patil, P. G., & Chestek, C. A. (2017). Neural control of finger movement via intracortical brain-machine interface. *Journal of Neural Engineering*, *14*(6). https://doi.org/10.1088/1741-2552/aa80bd

Irwin, Z. T., Thompson, D. E., Schroeder, K. E., Tat, D. M., Hassani, A., Bullard, A. J., Woo, S. L., Urbanchek, M. G., Sachs, A. J., Cederna, P. S., Stacey, W. C., Patil, P. G., & Chestek, C. A. (2016). Enabling Low-Power, Multi-Modal Neural Interfaces Through a Common,

Low-Bandwidth Feature Space. *IEEE Transactions on Neural Systems and Rehabilitation Engineering*, *24*(5), 521–531. https://doi.org/10.1109/TNSRE.2015.2501752
Kanitz, G., Cipriani, C., & Edin, B. B. (2018). Classification of transient myoelectric signals for the control of multi-grasp hand prostheses. *IEEE Transactions on Neural Systems and Rehabilitation Engineering*. https://doi.org/10.1109/TNSRE.2018.2861465
Kao, J. C., Nuyujukian, P., Ryu, S. I., & Shenoy, K. V. (2017). A High-Performance Neural Prosthesis Incorporating Discrete State Selection with Hidden Markov Models. *IEEE Transactions on Biomedical Engineering*, *64*(4), 935–945. https://doi.org/10.1109/TBME.2016.2582691
Kapelner, T., Sartori, M., Negro, F., & Farina, D. (2020). Neuro-Musculoskeletal Mapping for Man-Machine Interfacing. *Scientific Reports*. https://doi.org/10.1038/s41598-020-62773-7
Kemere, C., Santhanam, G., Yu, B. M., Afshar, A., Ryu, S. I., Meng, T. H., & Shenoy, K. V. (2008). Neural-State Transitions Using Hidden Markov Models for Motor Cortical Prostheses. *Journal of Neurophysiology*, *100*, 2441–2452. https://doi.org/10.1152/jn.00924.2007.
Kennedy, S. D., & Schwartz, A. B. (2019). Distributed processing of movement signaling. *Proceedings of the National Academy of Sciences of the United States of America*. https://doi.org/10.1073/pnas.1902296116
Khushaba, R. N., Kodagoda, S., Takruri, M., & Dissanayake, G. (2012). Toward improved control of prosthetic fingers using surface electromyogram (EMG) signals. *Expert Systems with Applications*. https://doi.org/10.1016/j.eswa.2012.02.192
Kilgore, K. L., Hoyen, H. A., Bryden, A. M., Hart, R. L., Keith, M. W., & Peckham, P. H. (2008). An Implanted Upper-Extremity Neuroprosthesis Using Myoelectric Control. *Journal of Hand Surgery*, *33*(4), 539–550. https://doi.org/10.1016/j.jhsa.2008.01.007
Kim, S. P., Simeral, J. D., Hochberg, L. R., Donoghue, J. P., & Black, M. J. (2008). Neural control of computer cursor velocity by decoding motor cortical spiking activity in humans with tetraplegia. *Journal of Neural Engineering*, *5*(4), 455–476. https://doi.org/10.1088/1741-2560/5/4/010
Koch, J., Schuettler, M., Pasluosta, C., & Stieglitz, T. (2019). Electrical connectors for neural implants: Design, state of the art and future challenges of an underestimated component. In *Journal of Neural Engineering*. https://doi.org/10.1088/1741-2552/ab36df
Krasoulis, A., Vijayakumar, S., & Nazarpour, K. (2019). Effect of User Practice on Prosthetic Finger Control With an Intuitive Myoelectric Decoder. *Frontiers in Neuroscience*. https://doi.org/10.3389/fnins.2019.00891
Krasoulis, A., Vijayakumar, S., & Nazarpour, K. (2020). Multi-Grip Classification-Based Prosthesis Control with Two EMG-IMU Sensors. *IEEE Transactions on Neural Systems and Rehabilitation Engineering*. https://doi.org/10.1109/TNSRE.2019.2959243
Kubiak, C. A., Kemp, S. W. P., Cederna, P. S., & Kung, T. A. (2019). Prophylactic Regenerative Peripheral Nerve Interfaces to Prevent Postamputation Pain. *Plastic and Reconstructive Surgery*. https://doi.org/10.1097/PRS.0000000000005922
Kuiken, T. A., Li, G., Lock, B. A., Lipschutz, R. D., Miller, L. A., Stubblefield, K. A., & Englehart, K. B. (2009). Targeted muscle reinnervation for real-time myoelectric control of multifunction artificial arms. *JAMA - Journal of the American Medical Association*. https://doi.org/10.1001/jama.2009.116
Kuiken, T. A., Miller, L. A., Turner, K., & Hargrove, L. J. (2016). A Comparison of Pattern Recognition Control and Direct Control of a Multiple Degree-of-Freedom Transradial

Prosthesis. *IEEE Journal of Translational Engineering in Health and Medicine*. https://doi.org/10.1109/JTEHM.2016.2616123

Kumar, V., & Todorov, E. (2015). MuJoCo HAPTIX: A virtual reality system for hand manipulation. *IEEE-RAS International Conference on Humanoid Robots*. https://doi.org/10.1109/HUMANOIDS.2015.7363441

Lahr, J., Schwartz, C., Heimbach, B., Aertsen, A., Rickert, J., & Ball, T. (2015). Invasive brain-machine interfaces: A survey of paralyzed patients' attitudes, knowledge and methods of information retrieval. *Journal of Neural Engineering*. https://doi.org/10.1088/1741-2560/12/4/043001

Lebedev, M. A. (2005). Cortical Ensemble Adaptation to Represent Velocity of an Artificial Actuator Controlled by a Brain-Machine Interface. *Journal of Neuroscience*, *25*(19), 4681–4693. https://doi.org/10.1523/JNEUROSCI.4088-04.2005

Li, G., Schultz, A. E., & Kuiken, T. A. (2010). Quantifying pattern recognition- based myoelectric control of multifunctional transradial prostheses. *IEEE Transactions on Neural Systems and Rehabilitation Engineering*. https://doi.org/10.1109/TNSRE.2009.2039619

Ludwig, K. A., Miriani, R. M., Langhals, N. B., Joseph, M. D., Anderson, D. J., & Kipke, D. R. (2009). Using a Common Average Reference to Improve Cortical Neuron Recordings From Microelectrode Arrays. *Journal of Neurophysiology*, *101*(3), 1679–1689. https://doi.org/10.1152/jn.90989.2008

Marathe, A. R., & Taylor, D. M. (2011). Decoding position, velocity, or goal: Does it matter for brain-machine interfaces? *Journal of Neural Engineering*. https://doi.org/10.1088/1741-2560/8/2/025016

Mendez-Balbuena, I., Manjarrez, E., Schulte-Monting, J., Huethe, F., Tapia, J. A., Hepp-Reymond, M.-C., & Kristeva, R. (2012). Improved Sensorimotor Performance via Stochastic Resonance. *Journal of Neuroscience*, *32*(36), 12612–12618. https://doi.org/10.1523/JNEUROSCI.0680-12.2012

Menz, V. K., Schaffelhofer, S., & Scherberger, H. (2015). Representation of continuous hand and arm movements in macaque areas M1, F5, and AIP: A comparative decoding study. *Journal of Neural Engineering*, *12*(5), 56016. https://doi.org/10.1088/1741-2560/12/5/056016

Mollazadeh, M., Aggarwal, V., Thakor, N. V., & Schieber, M. H. (2014). Principal components of hand kinematics and neurophysiological signals in motor cortex during reach to grasp movements. *Journal of Neurophysiology*, *112*(8), 1857–1870. https://doi.org/10.1152/jn.00481.2013

Mooney, V., Hartmann, D. B., Mcneal, D., & Benson, J. (1974). The Use of Pure Carbon for Permanent Percutaneous Electrical Connector Systems. *Archives of Surgery*. https://doi.org/10.1001/archsurg.1974.01350260012003

Nam, H. S., Koh, S., Beom, J., Kim, Y. J., Park, J. W., Koh, E. S., Chung, S. G., & Kim, S. (2017). Recovery of proprioception in the upper extremity by robotic mirror therapy: A clinical pilot study for proof of concept. *Journal of Korean Medical Science*. https://doi.org/10.3346/jkms.2017.32.10.1568

Nason, S. R., Vaskov, A. K., Willsey, M. S., Welle, E. J., An, H., Vu, P. P., Bullard, A. J., Nu, C. S., Kao, J. C., Shenoy, K. V., Jang, T., Kim, J. S., Blaauw, D., Patil, P. G., & Chestek, C. A. (2020). A low-power band of neuronal spiking activity dominated by local single units improves the performance of brain–machine interfaces. *Nature Biomedical Engineering*. https://doi.org/10.1038/s41551-020-0591-0

Nazarpour, K., Ethier, C., Paninski, L., Rebesco, J. M., Miall, R. C., & Miller, L. E. (2012). EMG prediction from motor cortical recordings via a nonnegative point-process filter. *IEEE Transactions on Biomedical Engineering*, *59*(7), 1829–1838. https://doi.org/10.1109/TBME.2011.2159115

Nunez, P. L. (1988). Methods to improve spatial resolution of EEG. *IEEE/Engineering in Medicine and Biology Society Annual Conference*. https://doi.org/10.1109/iembs.1988.95290

Nunez, P. L., & Srinivasan, R. (2006). Electric Fields of the Brain : The neurophysics of EEG Abstract and Keywords 1 A Window on the Mind. In *interactions*.

Oby, E. R., Ethier, C., & Miller, L. E. (2013). Movement representation in the primary motor cortex and its contribution to generalizable EMG predictions. *Journal of Neurophysiology*, *109*(3), 666–678. https://doi.org/10.1152/jn.00331.2012

Orsborn, A. L., Dangi, S., Moorman, H. G., & Carmena, J. M. (2012). Closed-loop decoder adaptation on intermediate time-scales facilitates rapid BMI performance improvements independent of decoder initialization conditions. *IEEE Transactions on Neural Systems and Rehabilitation Engineering*, *20*(4), 468–477. https://doi.org/10.1109/TNSRE.2012.2185066

Orsborn, A. L., Moorman, H. G., Overduin, S. A., Shanechi, M. M., Dimitrov, D. F., & Carmena, J. M. (2014a). Closed-loop decoder adaptation shapes neural plasticity for skillful neuroprosthetic control. *Neuron*, *82*(6), 1380–1393. https://doi.org/10.1016/j.neuron.2014.04.048

Orsborn, A. L., Moorman, H. G., Overduin, S. A., Shanechi, M. M., Dimitrov, D. F., & Carmena, J. M. (2014b). Closed-loop decoder adaptation shapes neural plasticity for skillful neuroprosthetic control. *Neuron*. https://doi.org/10.1016/j.neuron.2014.04.048

OrtizCatalan, M., Mastinu, E., Sassu, P., Aszmann, O. C., & Brånemark, R. (2020). Self-contained neuromusculoskeletal arm prostheses. *New England Journal of Medicine*. https://doi.org/10.1056/NEJMoa1917537

Østlie, K., Lesjø, I. M., Franklin, R. J., Garfelt, B., Skjeldal, O. H., & Magnus, P. (2012). Prosthesis rejection in acquired major upper-limb amputees: a population-based survey. *Disability and Rehabilitation: Assistive Technology*, *7*(4), 294–303. https://doi.org/10.3109/17483107.2011.635405

Page, D. M., George, J. A., Kluger, D. T., Duncan, C., Wendelken, S., Davis, T., Hutchinson, D. T., & Clark, G. A. (2018). Motor Control and Sensory Feedback Enhance Prosthesis Embodiment and Reduce Phantom Pain After Long-Term Hand Amputation. *Frontiers in Human Neuroscience*, *12*(September), 1–16. https://doi.org/10.3389/fnhum.2018.00352

Pandarinath, C., Nuyujukian, P., Blabe, C. H., Sorice, B. L., Saab, J., Willett, F. R., Hochberg, L. R., Shenoy, K. V., & Henderson, J. M. (2017). High performance communication by people with paralysis using an intracortical brain-computer interface. *ELife*, *6*, 18554. https://doi.org/10.7554/eLife.18554

Pasquina, P. F., Evangelista, M., Carvalho, A. J., Lockhart, J., Griffin, S., Nanos, G., McKay, P., Hansen, M., Ipsen, D., Vandersea, J., Butkus, J., Miller, M., Murphy, I., & Hankin, D. (2015). First-in-man demonstration of a fully implanted myoelectric sensors system to control an advanced electromechanical prosthetic hand. *Journal of Neuroscience Methods*, *244*, 85–93. https://doi.org/10.1016/j.jneumeth.2014.07.016

Patel, P. R., Zhang, H., Robbins, M. T., Nofar, J. B., Marshall, S. P., Kobylarek, M. J., Kozai, T. D. Y., Kotov, N. A., & Chestek, C. A. (2016). Chronic in vivo stability assessment of carbon fiber microelectrode arrays. *Journal of Neural Engineering*.

https://doi.org/10.1088/1741-2560/13/6/066002
Pena, A. E., Rincon-Gonzalez, L., Abbas, J. J., & Jung, R. (2019). Effects of vibrotactile feedback and grasp interface compliance on perception and control of a sensorized myoelectric hand. *PLOS ONE*, *14*(1), e0210956. https://doi.org/10.1371/journal.pone.0210956
Perel, S., Sadtler, P. T., Godlove, J. M., Ryu, S. I., Wang, W., Batista, A. P., & Chase, S. M. (2013). Direction and speed tuning of motor-cortex multi-unit activity and local field potentials during reaching movements. *Proceedings of the Annual International Conference of the IEEE Engineering in Medicine and Biology Society, EMBS*. https://doi.org/10.1109/EMBC.2013.6609496
Piazza, C., Simon, A. M., Turner, K. L., Miller, L. A., Catalano, M. G., Bicchi, A., & Hargrove, L. J. (2020). Exploring augmented grasping capabilities in a multi-synergistic soft bionic hand. *Journal of Neuroengineering and Rehabilitation*. https://doi.org/10.1186/s12984-020-00741-y
Rabiner, L. R. (1989). A Tutorial on Hidden Markov Models and Selected Applications in Speech Recognition. *Proceedings of the IEEE*. https://doi.org/10.1109/5.18626
Rastogi, A., Vargas-Irwin, C. E., Willett, F. R., Abreu, J., Crowder, D. C., Murphy, B. A., Memberg, W. D., Miller, J. P., Sweet, J. A., Walter, B. L., Cash, S. S., Rezaii, P. G., Franco, B., Saab, J., Stavisky, S. D., Shenoy, K. V., Henderson, J. M., Hochberg, L. R., Kirsch, R. F., & Ajiboye, A. B. (2020). Neural Representation of Observed, Imagined, and Attempted Grasping Force in Motor Cortex of Individuals with Chronic Tetraplegia. *Scientific Reports*. https://doi.org/10.1038/s41598-020-58097-1
Resnik, L., Klinger, S. L., & Etter, K. (2014). The DEKA Arm: Its features, functionality, and evolution during the veterans affairs study to optimize the DEKA Arm. *Prosthetics and Orthotics International*. https://doi.org/10.1177/0309364613506913
Romm, S. (1989). Arms by design: From antiquity to the renaissance. *Plastic and Reconstructive Surgery*. https://doi.org/10.1097/00006534-198907000-00029
Rouse, A. G. (2016). A four-dimensional virtual hand brain-machine interface using active dimension selection. *Journal of Neural Engineering*, *13*(3), 36021. https://doi.org/10.1088/1741-2560/13/3/036021
Rouse, A. G., & Schieber, M. H. (2015). Advancing brain-machine interfaces: moving beyond linear state space models. *Frontiers in Systems Neuroscience*, *9*(108). https://doi.org/10.3389/fnsys.2015.00108
Sachs, N. A., Ruiz-Torres, R., Perreault, E. J., & Miller, L. E. (2015). Brain-state classification and a dual-state decoder dramatically improve the control of cursor movement through a brain-machine interface. *Journal of Neural Engineering*, *13*(1), 16009. https://doi.org/10.1088/1741-2560/13/1/016009
Salminger, S., Sturma, A., Hofer, C., Evangelista, M., Perrin, M., Bergmeister, K. D., Roche, A. D., Hasenoehrl, T., Dietl, H., Farina, D., & Aszmann, O. C. (2019). Long-term implant of intramuscular sensors and nerve transfers for wireless control of robotic arms in above-elbow amputees. *Science Robotics*. https://doi.org/10.1126/scirobotics.aaw6306
Santosa, K. B., Oliver, J. D., Cederna, P. S., & Kung, T. A. (2020). Regenerative Peripheral Nerve Interfaces for Prevention and Management of Neuromas. In *Clinics in Plastic Surgery*. https://doi.org/10.1016/j.cps.2020.01.004
Sartori, M., Durandau, G., Došen, S., & Farina, D. (2018). Robust simultaneous myoelectric control of multiple degrees of freedom in wrist-hand prostheses by real-time

neuromusculoskeletal modeling. *Journal of Neural Engineering*. https://doi.org/10.1088/1741-2552/aae26b

Schaffelhofer, S., Agudelo-Toro, A., & Scherberger, H. (2015). Decoding a Wide Range of Hand Configurations from Macaque Motor, Premotor, and Parietal Cortices. *Journal of Neuroscience*, *35*(3), 1068–1081. https://doi.org/10.1523/JNEUROSCI.3594-14.2015

Schroeder, K. E., Irwin, Z. T., Bullard, A. J., Thompson, D. E., Bentley, J. N., Stacey, W. C., Patil, P. G., & Chestek, C. A. (2017). Robust tactile sensory responses in finger area of primate motor cortex relevant to prosthetic control. *Journal of Neural Engineering*, *14*(4), 46016. https://doi.org/10.1088/1741-2552/aa7329

Scott, S., & Kalaska, J. (1997). Reaching movements with similar hand paths but different arm orientations. {I}. {A}ctivity of individual cells in motor cortex. *Journal of Neurophysiology*. https://doi.org/10.1152/jn.1997.77.2.826

Seo, D., Neely, R. M., Shen, K., Singhal, U., Alon, E., Rabaey, J. M., Carmena, J. M., & Maharbiz, M. M. (2016). Wireless Recording in the Peripheral Nervous System with Ultrasonic Neural Dust. *Neuron*, *91*(3), 529–539. https://doi.org/10.1016/j.neuron.2016.06.034

Serruya, M., Hatsopoulos, N. G., Fellows, M. R., Paninski, L., & Donoghue, J. P. (2003). Robustness of neuroprosthetic decoding algorithms. *Biological Cybernetics*, *88*(3), 219–228. https://doi.org/10.1007/s00422-002-0374-6

Shanechi, M. M., Orsborn, A. L., Moorman, H. G., Gowda, S., Dangi, S., & Carmena, J. M. (2017). Rapid control and feedback rates enhance neuroprosthetic control. *Nature Communications*, *8*, 1–10. https://doi.org/10.1038/ncomms13825

Shenoy, K. V., & Carmena, J. M. (2014). Combining decoder design and neural adaptation in brain-machine interfaces. *Neuron*, *84*(4), 665–680. https://doi.org/10.1016/j.neuron.2014.08.038

Simeral, J. D., Kim, S. P., Black, M. J., Donoghue, J. P., & Hochberg, L. R. (2011). Neural control of cursor trajectory and click by a human with tetraplegia 1000 days after implant of an intracortical microelectrode array. *Journal of Neural Engineering*, *8*(2), 25027. https://doi.org/10.1088/1741-2560/8/2/025027

Smit, G., Bongers, R. M., Van der Sluis, C. K., & Plettenburg, D. H. (2012). Efficiency of voluntary opening hand and hook prosthetic devices: 24 years of development? *Journal of Rehabilitation Research and Development*. https://doi.org/10.1682/JRRD.2011.07.0125

Smith, B., Crish, T. J., Buckett, J. R., Kilgore, K. L., & Peckham, P. H. (2005). Development of an implantable networked neuroprosthesis. *2nd International IEEE EMBS Conference on Neural Engineering*. https://doi.org/10.1109/CNE.2005.1419657

Smith, L. H., Hargrove, L. J., Lock, B. A., & Kuiken, T. A. (2011). Determining the optimal window length for pattern recognition-based myoelectric control: Balancing the competing effects of classification error and controller delay. *IEEE Transactions on Neural Systems and Rehabilitation Engineering*. https://doi.org/10.1109/TNSRE.2010.2100828

Srinivasan, S., Carty, M. J., Calvaresi, P. W., Clites, T. R., Maimon, B. E., Taylor, C. R., Zorzos, A. N., & Herr, H. (2017). On prosthetic control: A regenerative agonist-antagonist myoneural interface. *Science Robotics*. https://doi.org/10.1126/scirobotics.aan2971

Stark, E., & Abeles, M. (2007). Predicting Movement from Multiunit Activity. *Journal of Neuroscience*, *27*(31), 8387–8394. https://doi.org/10.1523/JNEUROSCI.1321-07.2007

Suner, S., Fellows, M. R., Vargas-Irwin, C., Nakata, G. K., & Donoghue, J. P. (2005). Reliability of signals from a chronically implanted, silicon-based electrode array in non-human primate

primary motor cortex. *IEEE Transactions on Neural Systems and Rehabilitation Engineering*. https://doi.org/10.1109/TNSRE.2005.857687

Sussillo, D., Nuyujukian, P., Fan, J. M., Kao, J. C., Stavisky, S. D., Ryu, S. I., & Shenoy, K. V. (2012). A recurrent neural network for closed-loop intracortical brain-machine interface decoders. *Journal of Neural Engineering*, *9*(2), 26027. https://doi.org/10.1088/1741-2560/9/2/026027

Sussillo, D., Stavisky, S. D., Kao, J. C., Ryu, S. I., & Shenoy, K. V. (2016). Making brain-machine interfaces robust to future neural variability. *Nature Communications*, *7*, 1–12. https://doi.org/10.1038/ncomms13749

Tan, D. W., Schiefer, M. A., Keith, M. W., Anderson, J. R., Tyler, J., & Tyler, D. J. (2014). A neural interface provides long-term stable natural touch perception. *Science Translational Medicine*, *6*(257). https://doi.org/10.1126/scitranslmed.3008669

Taylor, D. M., Tillery, S. I. H., & Schwartz, A. B. (2002). Direct Cortical Control of 3D Neuroprosthetic Devices. *Science*, *296*(5574), 1829–1832. https://doi.org/10.1126/science.1070291

Teh, Y., & Hargrove, L. J. (2020). Understanding Limb Position and External Load Effects on Real-Time Pattern Recognition Control in Amputees. *IEEE Transactions on Neural Systems and Rehabilitation Engineering*. https://doi.org/10.1109/TNSRE.2020.2991643

Thompson, D. E., Quitadamo, L. R., Mainardi, L., Laghari, K. U. R., Gao, S., Kindermans, P. J., Simeral, J. D., Fazel-Rezai, R., Matteucci, M., Falk, T. H., Bianchi, L., Chestek, C. A., & Huggins, J. E. (2014). Performance measurement for brain-computer or brain-machine interfaces: A tutorial. *Journal of Neural Engineering*, *11*(3), 35001. https://doi.org/10.1088/1741-2560/11/3/035001

Todorova, S., Sadtler, P., Batista, A. P., Chase, S. M., & Ventura, V. (2014). To sort or not to sort: The impact of spike-sorting on neural decoding performance. *Journal of Neural Engineering*. https://doi.org/10.1088/1741-2560/11/5/056005

Vargas-Irwin, C. E., Shakhnarovich, G., Yadollahpour, P., Mislow, J. M. K., Black, M. J., & Donoghue, J. P. (2010). Decoding Complete Reach and Grasp Actions from Local Primary Motor Cortex Populations. *Journal of Neuroscience*, *30*(29), 9659–9669. https://doi.org/10.1523/JNEUROSCI.5443-09.2010

Vaskov, A. K., Irwin, Z. T., Nason, S. R., Vu, P. P., Nu, C. S., Bullard, A. J., Hill, M., North, N., Patil, P. G., & Chestek, C. A. (2018). Cortical decoding of individual finger group motions using ReFIT Kalman filter. *Frontiers in Neuroscience*, *12*(NOV). https://doi.org/10.3389/fnins.2018.00751

Vaskov, A. K., Vu, P. P., North, N., Davis, A. J., Kung, T. A., Gates, D. H., Cederna, P. S., & Chestek, C. A. (2020). Surgically Implanted Electrodes Enable Real-Time Finger and Grasp Pattern Recognition for Prosthetic Hands. *MedRxiv*, 2020.10.28.20217273. https://doi.org/10.1101/2020.10.28.20217273

Velliste, M., Perel, S., Spalding, M. C., Whitford, A. S., & Schwartz, A. B. (2008). Cortical control of a prosthetic arm for self-feeding. *Nature*, *453*(7198), 1098–1101. https://doi.org/10.1038/nature06996

Verrills, P., Sinclair, C., & Barnard, A. (2016). A review of spinal cord stimulation systems for chronic pain. In *Journal of Pain Research*. https://doi.org/10.2147/JPR.S108884

Volkova, K., Lebedev, M. A., Kaplan, A., & Ossadtchi, A. (2019). Decoding Movement From Electrocorticographic Activity: A Review. In *Frontiers in Neuroinformatics*. https://doi.org/10.3389/fninf.2019.00074

Vu, P. P., Irwin, Z. T., Bullard, A. J., Ambani, S. W., Sando, I. C., Urbanchek, M. G., Cederna, P. S., & Chestek, C. A. (2018). Closed-Loop Continuous Hand Control via Chronic Recording of Regenerative Peripheral Nerve Interfaces. *IEEE Transactions on Neural Systems and Rehabilitation Engineering*. https://doi.org/10.1109/TNSRE.2017.2772961

Vu, P. P., Vaskov, A. K., Irwin, Z. T., Henning, P. T., Lueders, D. R., Laidlaw, A. T., Davis, A. J., Nu, C. S., Gates, D. H., Gillespie, R. B., Kemp, S. W. P., Kung, T. A., Chestek, C. A., & Cederna, P. S. (2020). A regenerative peripheral nerve interface allows real-time control of an artificial hand in upper limb amputees. *Science Translational Medicine*. https://doi.org/10.1126/scitranslmed.aay2857

Wahnoun, R., He, J., & Helms Tillery, S. I. (2006). Selection and parameterization of cortical neurons for neuroprosthetic control. *Journal of Neural Engineering*, *3*(2), 162–171. https://doi.org/10.1088/1741-2560/3/2/010

Weir, R. F., Troyk, P. R., DeMichele, G. A., Kerns, D. A., Schorsch, J. F., & Maas, H. (2009). Implantable myoelectric sensors (IMESs) for intramuscular electromyogram recording. *IEEE Transactions on Biomedical Engineering*. https://doi.org/10.1109/TBME.2008.2005942

Welle, E. J., Patel, P. R., Woods, J. E., Petrossians, A., Della Valle, E., Vega-Medina, A., Richie, J. M., Cai, D., Weiland, J. D., & Chestek, C. A. (2020). Ultra-small carbon fiber electrode recording site optimization and improved in vivo chronic recording yield. *Journal of Neural Engineering*. https://doi.org/10.1088/1741-2552/ab8343

Willett, F. R., Pandarinath, C., Jarosiewicz, B., Murphy, B. A., Memberg, W. D., Blabe, C. H., Saab, J., Walter, B. L., Sweet, J. A., Miller, J. P., Henderson, J. M., Shenoy, K. V., Simeral, J. D., Hochberg, L. R., Kirsch, R. F., & Ajiboye, A. B. (2017). Feedback control policies employed by people using intracortical brain-computer interfaces. *Journal of Neural Engineering*, *14*(1), 16001. https://doi.org/10.1088/1741-2560/14/1/016001

Wodlinger, B., Downey, J. E., Tyler-Kabara, E. C., Schwartz, A. B., Boninger, M. L., & Collinger, J. L. (2015). Ten-dimensional anthropomorphic arm control in a human brain-machine interface: Difficulties, solutions, and limitations. *Journal of Neural Engineering*, *12*(1), 16011. https://doi.org/10.1088/1741-2560/12/1/016011

Woo, S. L., Kung, T. A., Brown, D. L., Leonard, J. A., Kelly, B., & Cederna, P. S. (2016). Regenerative peripheral nerve interfaces for the treatment of postamputation neuroma pain: A pilot study. *Plastic and Reconstructive Surgery - Global Open*. https://doi.org/10.1097/GOX.0000000000001038

Wu, W., Black, M. J., Mumford, D., Gao, Y., Bienenstock, E., & Donoghue, J. P. (2004). Modeling and decoding motor cortical activity using a switching Kalman filter. *IEEE Transactions on Biomedical Engineering*. https://doi.org/10.1109/TBME.2004.826666

Wurth, S. M., & Hargrove, L. J. (2014). A real-time comparison between direct control, sequential pattern recognition control and simultaneous pattern recognition control using a Fitts' law style assessment procedure. *Journal of NeuroEngineering and Rehabilitation*, *11*(1), 91. https://doi.org/10.1186/1743-0003-11-91

Young, A. J., Smith, L. H., Rouse, E. J., & Hargrove, L. J. (2014). A comparison of the real-time controllability of pattern recognition to conventional myoelectric control for discrete and simultaneous movements. *Journal of NeuroEngineering and Rehabilitation*, *11*(1), 5. https://doi.org/10.1186/1743-0003-11-5

Yu, B. M., Kemere, C., Santhanam, G., Afshar, A., Ryu, S. I., Meng, T. H., Sahani, M., & Shenoy, K. V. (2007). Mixture of Trajectory Models for Neural Decoding of Goal-Directed

Movements. *Journal of Neurophysiology*, *97*(5), 3763–3780. https://doi.org/10.1152/jn.00482.2006

Zhang, Y., & Chase, S. M. (2015). Recasting brain-machine interface design from a physical control system perspective. In *Journal of Computational Neuroscience*. https://doi.org/10.1007/s10827-015-0566-4

Zhou, P., Lowery, M., & Englehart, K. B. (2007). Decoding a new neural machine interface for control of artificial limbs. *Journal of Neurophysiology*, *98*, 2974–2982. https://doi.org/10.1152/jn.00178.2007.